



8-2001

An experimental study of labyrinth seal flow

Michael Andrew Michaud

Follow this and additional works at: https://trace.tennessee.edu/utk_gradthes

Recommended Citation

Michaud, Michael Andrew, "An experimental study of labyrinth seal flow. " Master's Thesis, University of Tennessee, 2001.

https://trace.tennessee.edu/utk_gradthes/9683

This Thesis is brought to you for free and open access by the Graduate School at TRACE: Tennessee Research and Creative Exchange. It has been accepted for inclusion in Masters Theses by an authorized administrator of TRACE: Tennessee Research and Creative Exchange. For more information, please contact trace@utk.edu.

To the Graduate Council:

I am submitting herewith a thesis written by Michael Andrew Michaud entitled "An experimental study of labyrinth seal flow." I have examined the final electronic copy of this thesis for form and content and recommend that it be accepted in partial fulfillment of the requirements for the degree of Master of Science, with a major in Aerospace Engineering.

Ahmad D. Vakili, Major Professor

We have read this thesis and recommend its acceptance:

Accepted for the Council:

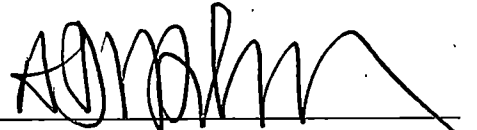
Carolyn R. Hodges

Vice Provost and Dean of the Graduate School

(Original signatures are on file with official student records.)

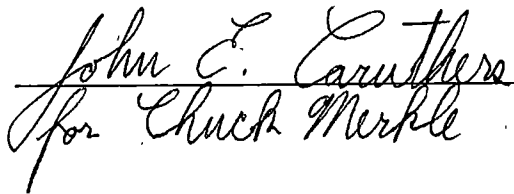
To the Graduate Council:

I am submitting herewith a thesis written by Michael A. Michaud entitled "An Experimental Study of Labyrinth Seal Flow." I have examined the final copy of this thesis for form and content and recommend that it be accepted in partial fulfillment of the requirements for the degree of Master of Science, with a major in Aerospace Engineering.

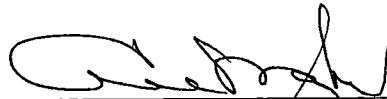


Ahmad D. Vakili, Major Professor

We have read this thesis
and recommend its acceptance:



Accepted for the Council:



Interim Vice Provost and
Dean of The Graduate School

**AN EXPERIMENTAL STUDY OF
LABYRINTH SEAL FLOW**

A Thesis
Presented for the
Master of Science
Degree
The University of Tennessee, Knoxville

Michael Andrew Michaud

August 2001

DEDICATION

This thesis is dedicated in loving memory of my Father, Howard Michaud, who passed away on 29 May, 2001 as this work was nearing completion. I miss you, Dad.

ACKNOWLEDGEMENTS

The successful completion of this research effort was due in no small part to the support, participation and dedication of several people, without whom this work would not have been nearly the memorable experience that it has been.

My faculty advisor and friend, Dr. Ahmad Vakili, has been inspirational throughout my work at UTSI, both in terms of the breadth of his knowledge, and his boundless enthusiasm. His work ethic and infectious drive to understand the underlying physics of any engineering problem at hand have made me a better engineer. The staff at the UTSI laboratories, including Jim Goodman, Keith Walker, and Gary Payne, has my gratitude for their patience, perseverance, and “can-do” attitude. They continuously managed to turn our ideas into a functional form; I can safely say that in some respects, a great deal of my education at UTSI was absorbed during my lab time. As well, my office-mates at UTSI, Sekhar Radhakrishnan and Abraham Meganathan have been indispensable for their ideas, help and willingness to “brainstorm” aspects of this project. Jim Terrel and Robert Zielke from TVA were extremely helpful throughout with their vast experience of the practical aspects of steam turbine operation.

My parents and sisters have been incredibly supportive throughout this endeavor and indeed throughout my life; my sincere thanks to them.

My deepest appreciation is for Julie McKenzie, my wife, best friend, and partner in all that I do. Her confidence in me consistently outweighs my confidence in myself, and I owe all of my achievements over our 15 years together to her optimism, good humor and patience.

Finally, I must thank my two beautiful daughters, Emily, and Anne-Marie; they are three years old and 10 months old respectively at the time of this writing. They have unwittingly maintained my perspective on the important aspects of life over these busy last two years and I love them dearly.

ABSTRACT

The leakage flow in a stationary stepped labyrinth seal is investigated by means of flow visualization, pressure field measurements and Particle Image Velocimetry (PIV). The basis of the investigation is a generic stepped labyrinth seal currently used by the Tennessee Valley Authority (TVA) in their steam turbine generators. Geometric and flow parameters were varied in order to examine their influence on leakage through the seal.

Following a brief theoretical development that details the physical mechanisms that cause flow energy loss and therefore leakage reduction in a single orifice, the discussion is extended to cover the current theory describing labyrinth seals.

Flow visualization results are presented for the baseline configuration, which was tested as a ten times scale water tunnel model at three different axial step locations. The observations made during these tests confirm the basic mechanisms of energy loss in labyrinth seals including turbulence induced viscous losses, chamber vortex generation, flow stagnation and increased flow streamline curvature.

A 5 times scale 2-D airflow measurement stepped labyrinth seal model was constructed and tested over a range of seal pressure ratios from 1:1 to 10:1. Tested model configurations included the baseline stepped labyrinth seal and six additional variants of this basic design that were obtained by varying step height and knife angle. Results show that with relatively minor changes in geometry based on the physics of the flow through the seal, leakage reductions of up to 17% can be achieved. Finally, PIV measurements were carried out on the 2-D airflow seal models including both the five times scale baseline seal model and the improved design seal five times scale model which incorporates an increased step height and inclined long knives. Results show that the reduced leakage occurs due to an increased amount of flow stagnation and streamline curvature within the improved seal.

TABLE OF CONTENTS

CHAPTER 1	1
INTRODUCTION	1
Background	1
Experimental objectives	4
CHAPTER 2	6
BACKGROUND AND THEORETICAL CONSIDERATIONS	6
Ideal flow through a single orifice	6
Viscous Effects	7
Compressibility Effects	9
Application of Orifice Theory to Labyrinth Seals	11
Data representation	18
Seal Discharge Coefficient	18
Flow Parameter	19
Labyrinth Flow Coefficient	19
Total Pressure Loss	20
Dimensional Analysis	20
EXPERIMENTAL SET-UP	22
Computer model	22
2-D Flow Visualization	24
2-D Flow Measurements	25
Particle Image Velocimetry	31
Overall Experimental Study	34
Experimental Configurations	34

Flow Visualization	34
2-D Flow Measurements	36
Particle Image Velocimetry	41
CHAPTER 4	42
EXPERIMENTAL RESULTS AND DISCUSSION.....	42
Flow Visualization.....	42
Flow Measurements In The 2-D Air Model	51
Configuration A – Baseline	51
Configuration B – High Step	54
Configuration C – 15 Degree Slant Knives.....	58
Configuration D – 30 Degree Slant Knives	62
Configuration E – Hybrid, 30 Degree Slant Short Knives and Straight Long Knives	65
Configuration F – Hybrid, High Steps and 15 Degree Slant Long Knives	68
Configuration G – Hybrid, High Steps and 30 Degree Slant Long Knives.....	71
Configuration Comparison	74
Particle Image Velocimetry.....	74
CHAPTER 5	88
CONCLUSIONS AND RECOMENDATIONS	88
Conclusions.....	88
Recommendations	89
REFERENCES.....	91
APPENDICES	94
APPENDIX A: DETAILED EXPERIMENTAL RESULTS.....	95

APPENDIX B: SAMPLE MATHCAD™ CALCULATIONS FOR EGLI, MARTIN, KEARTON & KEH AND MIYAKE & DUH METHODS.....	125
VITA.....	133

LIST OF TABLES

Table 2-1 – Non-Dimensional Groupings.....	21
Table 3-1 - Flow Visualization Configurations.....	35
Table 3-1 – 2D Flow Measurement Model Configurations	37

LIST OF FIGURES

Figure 1-1 - Straight Through Labyrinth Seal Arrangement.....	2
Figure 1-2 - Staggered Labyrinth Seal Arrangement.....	3
Figure 1-3 - Stepped Labyrinth Seal Arrangement.....	3
Figure 2-1 - Orifice Exposed to a Pressure Differential.....	7
Figure 2-2 - Flow Through a Sharp Edged Orifice.....	8
Figure 2-3 - Stepped Labyrinth Seal Nomenclature.....	12
Figure 2-4 - Martin's Expansion Function, Φ_{Martin}	15
Figure 3-1 - Labyrinth Seal Computer Model (Model Scale).....	23
Figure 3-2 - Labyrinth Seal Computer Model (Full Scale).....	23
Figure 3-3 - Labyrinth Seal Flow Visualization Model.....	24
Figure 3-4 - Water Tunnel Seal Model Installation.....	26
Figure 3-5 - Water Tunnel Laser Installation.....	26
Figure 3-6 - 2D Airflow Measurement Pressure Tap Locations.....	27
Figure 3-7 - 2D Airflow Measurement Model.....	28
Figure 3-8 - 2D Airflow Measurement Model Installation.....	28
Figure 3-9 - Instrumentation Screen View.....	30
Figure 3-10 - PIV Laser Sheet Orientation.....	32
Figure 3-11 - PIV Camera and Laser Arrangement.....	33
Figure 3-12 - PIV Seed Particle Injection Point.....	33
Figure 3-13 - Flow Visualization Model Configuration.....	35
Figure 3-14 - Configuration "A" (Baseline).....	36
Figure 3-15 - Configuration "B" (High Step).....	38
Figure 3-16 - Configuration "C" (15 ° Slant Knife).....	38
Figure 3-17 - Configuration "D" (30 ° Slant Knife).....	39
Figure 3-18 - Configuration "E" (30 ° Short Knives/Straight Long Knives).....	39
Figure 3-19 - Configuration "F" (15 ° Long Knives/High Step).....	40

Figure 3-20 - Configuration "G" (Hybrid 15 ° Long Knives/High Step).....	40
Figure 4-1 - Flow Visualization, $x/L = -0.190$, $Re = 6000$, View 1.....	43
Figure 4-2 - Flow Visualization, $x/L = -0.190$, $Re = 6000$, View 2.....	43
Figure 4-3 - Flow Visualization, $x/L = -0.190$, $Re = 6000$, View 3.....	44
Figure 4-4 - Flow Visualization, $x/L = -0.190$, $Re = 6000$, View 4.....	45
Figure 4-5 - Flow Visualization, $x/L = 0$, $Re = 6000$	46
Figure 4-6 - Flow Visualization, $x/L = 0.213$, $Re = 6000$, View 1	47
Figure 4-7 - Flow Visualization, $x/L = 0.213$, $Re = 6000$, View 2.....	47
Figure 4-8 - Flow Visualization, $x/L = 0.425$, $Re = 6000$, View 1.....	49
Figure 4-9 - Flow Visualization, $x/L = 0.425$, $Re = 6000$, View 2	49
Figure 4-10 - Sketch of Main Labyrinth Flow Features.....	50
Figure 4-11 - Flow Parameter (Configuration "A")	51
Figure 4-12 - Seal Discharge Coefficient (Configuration "A").....	52
Figure 4-13 - Measured Non-Dimensional Pressure Loss (Configuration "A").....	52
Figure 4-14 - Calculated Exit Mach Number (Configuration "A")	53
Figure 4-15 - Seal Static Pressure Distribution (Configuration "A").....	53
Figure 4-16 - Comparison with Models (Configuration "A")	55
Figure 4-17 - Flow Parameter (Configuration "B").....	55
Figure 4-18 - Seal Discharge Coefficient (Configuration "B").....	56
Figure 4-19 - Measured Non-Dimensional Pressure Loss (Configuration "B").....	56
Figure 4-20 - Calculated Exit Mach Number (Configuration "B").....	57
Figure 4-21 - Seal Static Pressure Distribution (Configuration "B").....	57
Figure 4-22 - Flow Parameter - (Configuration "C")	59
Figure 4-23 - Seal Discharge Coefficient (Configuration "C").....	59
Figure 4-24 - Measured Non-Dimensional Pressure Loss (Configuration "C").....	60
Figure 4-25 - Calculated Exit Mach Number (Configuration "C").....	60
Figure 4-26 - Seal Static Pressure Distribution (Configuration "C").....	61
Figure 4-27 - Flow Parameter (Configuration "D").....	62

Figure 4-28 - Seal Discharge Coefficient (Configuration "D").....	63
Figure 4-29 – Measured Non-Dimensional Pressure Loss (Configuration "D").....	63
Figure 4-30 – Calculated Exit Mach Number (Configuration "D")	64
Figure 4-31 - Seal Static Pressure Distribution (Configuration "D")	64
Figure 4-32 – Flow Parameter – (Configuration "E")	65
Figure 4-33 - Seal Discharge Coefficient (Configuration "E").....	66
Figure 4-34 – Measured Non-Dimensional Pressure Loss (Configuration "E")	66
Figure 4-35 – Calculated Exit Mach Number (Configuration "E").....	67
Figure 4-36 - Seal Static Pressure Distribution (Configuration "E").....	67
Figure 4-37 - Flow Parameter (Configuration "F").....	68
Figure 4-38 – Seal Discharge Coefficient (Configuration "F").....	69
Figure 4-39 – Measured Non-Dimensional Pressure Loss (Configuration "F").....	69
Figure 4-40 – Calculated Exit Mach Number (Configuration "F").....	70
Figure 4-41 - Seal Static Pressure Distribution (Configuration "F").....	70
Figure 4-42 - Flow Parameter (Configuration "G")	71
Figure 4-43 - Seal Discharge Coefficient (Configuration "G").....	72
Figure 4-44 – Measured Non-Dimensional Pressure Loss (Configuration "G").....	72
Figure 4-45 – Calculated Exit Mach Number (Configuration "G")	73
Figure 4-46 - Seal Static Pressure Distribution (Configuration "G")	73
Figure 4-47 - Flow Parameter Comparison ($x/L = 0.043$)	75
Figure 4-48 – Average Leakage Reduction ($x/L = 0.043$).....	75
Figure 4-49 - Flow Parameter Comparison ($x/L = 0.128$)	76
Figure 4-50 - Average Leakage Reduction ($x/L = 0.128$).....	76
Figure 4-51 - Flow Parameter Comparison ($x/L = 0.383$)	77
Figure 4-52 - Average Leakage Reduction ($x/L = 0.383$).....	77
Figure 4-53 - Flow Parameter Comparison ($x/L = 0.511$)	78
Figure 4-54 - Average Leakage Reduction ($x/L = 0.511$).....	78
Figure 4-55 – PIV Test Area (Configuration "A").....	79

Figure 4-56 - PIV Test Area (Configuration "G").....	80
Figure 4-57 - Configuration "A" Speed Contour ($P_1/P_7 = 7.58$).....	80
Figure 4-58 - Configuration "A" Vorticity Contour ($P_1/P_7 = 7.58$).....	81
Figure 4-59 - Configuration "A" Streamlines ($P_1/P_7 = 7.58$).....	81
Figure 4-60 - Configuration "A" Speed Contour ($P_1/P_7 = 7.87$).....	82
Figure 4-61 - Configuration "A" Vorticity Contour ($P_1/P_7 = 7.87$).....	83
Figure 4-62 - Configuration "A" Streamlines ($P_1/P_7 = 7.87$).....	83
Figure 4-63 - Configuration "G" Speed Contour ($P_1/P_7 = 7.87$).....	84
Figure 4-64 - Configuration "G" Vorticity Contour ($P_1/P_7 = 7.87$).....	85
Figure 4-65 - Configuration "G" Streamlines ($P_1/P_7 = 7.87$).....	85
Figure 4-66 - Configuration "G" Speed Contour ($P_1/P_7 = 7.69$).....	86
Figure 4-67 - Configuration "G" Vorticity Contour ($P_1/P_7 = 7.69$).....	87
Figure 4-68 - Configuration "G" Streamlines ($P_1/P_7 = 7.69$).....	87

NOMENCLATURE

A	seal clearance area (in ²)
a	speed of sound (ft/sec)
C_d	discharge coefficient
cl	throttling clearance (in)
DTC	distance to contact (in)
k	ratio of specific heats
$K\theta$	knife angle (Figure 2-3)
Kh	knife height (Figure 2-3)
Kn	number of throttlings
Kp	knife pitch (Figure 2-3)
k_r	knife tip radius of curvature (in)
k_t	knife tip thickness (in)
M	Mach Number
\dot{m}	mass flow rate (lb/sec)
P_n	static pressure (psi)
P_0	stagnation pressure (psi)
Re	Reynolds Number
Sh	step height
T_0	total temperature (°R)
V	velocity (ft/sec)
μ	absolute viscosity (poise)
ν	kinematic viscosity (in ² /sec)
ρ	density (slug/ft ³)
α	flow coefficient

$\alpha_{labyrinth}$	labyrinth flow coefficient
Φ	flow parameter
ϕ_0	ideal labyrinth function
$\phi_{labyrinth}$	labyrinth function
ϕ_{Martin}	Martin labyrinth function
ϕ_{Miyake}	Miyake labyrinth function
$\phi_{Orifice}$	Orifice loss function

Chapter 1

INTRODUCTION

BACKGROUND

Leakage in turbo-machinery is an inherent problem that has assumed greater importance as typical operating pressures have increased over the years. In any turbine or compressor, leakage between pressure zones results in a reduction of work accomplished for a given energy input thereby decreasing efficiency. The labyrinth seal is a non-contacting type shaft seal that has been in widespread use for many decades in a variety of applications. It is typically used as a shaft seal in steam¹ and gas turbines², compressors, turbo-chargers and various other applications^{3,4,5} where a robust yet relatively simple seal is required between two zones of different pressures. Labyrinth seals provide numerous benefits including:

- (a) low maintenance;
- (b) negligible running torque;
- (c) simplicity; and
- (d) reduced particulate contamination.

However, the typical labyrinth seal has an innate tendency to leak, given its lack of a mechanical seal between the two areas of differing pressures. Although other contacting types of seals have been devised that provide better leakage characteristics, their reliance on a contact area between a rotating and non-rotating surface leads to unacceptable levels of wear. In the typical contact type design, the contact area is usually provided by some type of abradable material that can be replaced as necessary; for many large industrial applications, this level of required maintenance is clearly unacceptable. Other interesting seal types include the viscoseal⁶ and the brush seal⁷. In the viscoseal, a continuous helical groove is scribed into the shaft; as the shaft rotates relative to the housing, the groove is essentially a screw that drives the fluid in a direction

opposite to the direction of leakage. This type of seal is typically used in applications where the working fluid has a relatively high viscosity. In the brush seal, the mechanism for leakage reduction is provided by a series of finely interleaved brushes that provide an obstruction to the flow path. This type of seal, which provides substantial leakage reductions as compared to a traditional labyrinth design, is becoming more common as advances in material science allow for the manufacture of heat resistant and robust brushes.

There are three types of traditional labyrinth seals: straight through, staggered, and stepped. Typical arrangements of these types of seals are shown in Figures 1-1, 1-2 and 1-3 respectively. The straight-through type has the advantage of being relatively easy to manufacture compared to the other arrangements. However, as will be described later in this report, the staggered and stepped types are generally more effective in reducing leakage through the seal.

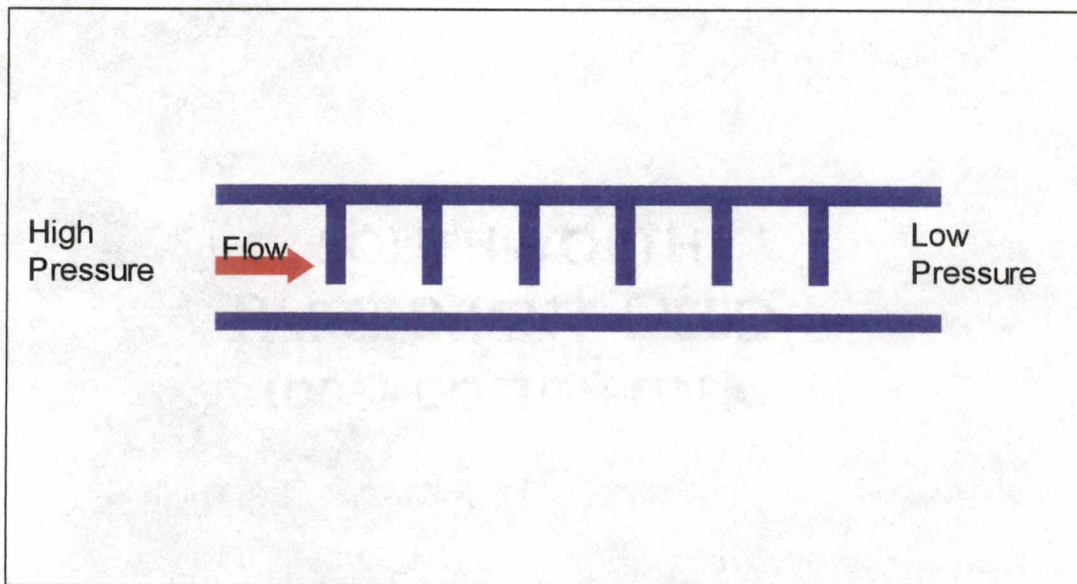


Figure 1-1 - Straight Through Labyrinth Seal Arrangement

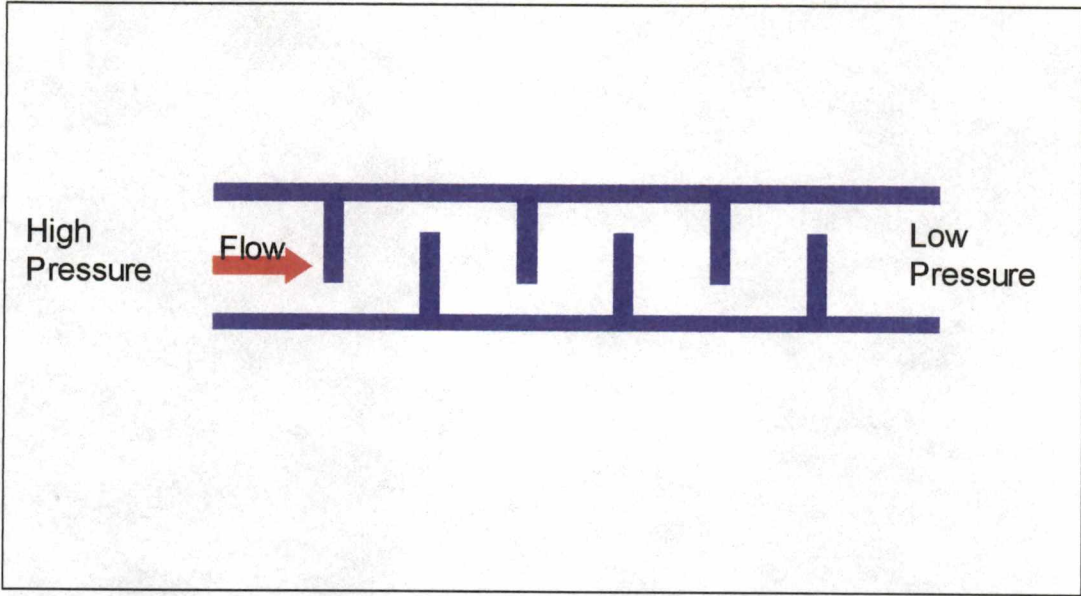


Figure 1-2 - Staggered Labyrinth Seal Arrangement

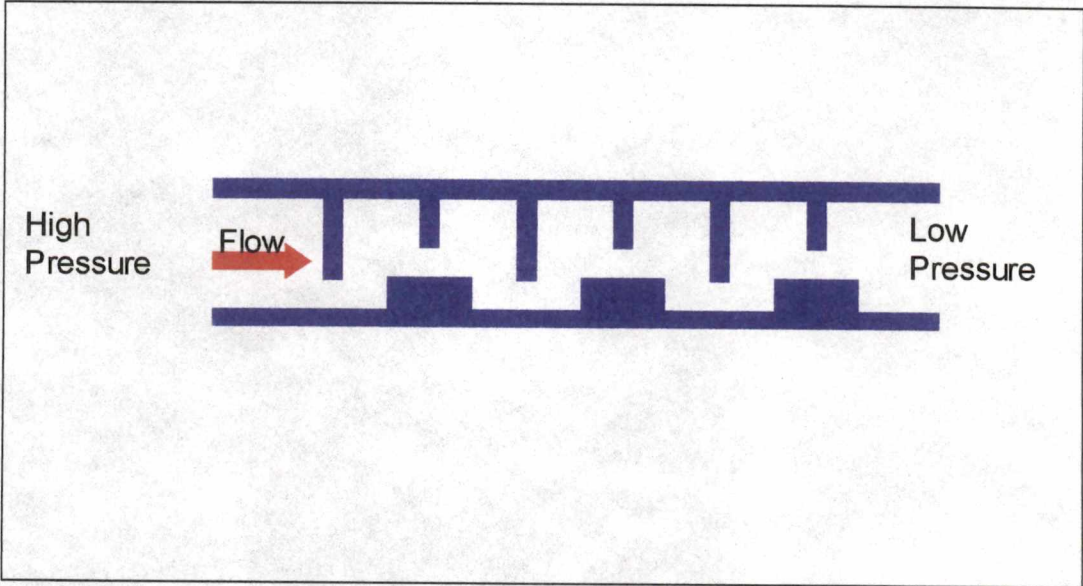


Figure 1-3 - Stepped Labyrinth Seal Arrangement

The benefits of reducing leakage in turbo-machinery (without an increase in required maintenance) cannot be overstated. Stocker² estimated that every 1% decrease in leakage flow through a high-pressure turbine seal would result in a 0.4% decrease in specific fuel consumption. Considering the vast number of high-pressure turbo-machinery devices in operation today, it can easily be seen that reducing seal leakage in these devices would produce enormous fuel savings. For example, using Stocker's methodology, which was predicated on an achievable leakage reduction of 25%, and jet fuel consumption figures⁸ in the US for 1998 would yield a fuel savings of approximately 16 million barrels a year of jet fuel alone.

EXPERIMENTAL OBJECTIVES

The experimental study outlined in this thesis has several objectives:

- (a) to provide a detailed physical understanding of the nature of flow leakage through a stepped labyrinth seal;
- (b) to provide quantitative data on the dependence of flow leakage on various relevant parameters;
- (c) to establish baseline leakage data for a particular labyrinth seal configuration currently in use by the Tennessee Valley Authority;
- (d) to provide an experimental set up that can be used to test various other types of seal designs;
- (e) to provide data for validating Computational Fluid Dynamics (CFD) calculations of shaft seal leakage flows; and
- (f) to attempt some limited modifications to the baseline configuration in order to improve leakage performance.

The overall goal of the research described in this thesis is to provide a fundamental understanding of the mechanism of leakage flows through a typical turbine stepped labyrinth seal. This knowledge, along with information gleaned from a survey of available literature, may then be used to design improvements that retain the desirable characteristics of the classic labyrinth seal, i.e. robustness and simplicity, while providing improved leakage attributes.

BACKGROUND AND THEORETICAL CONSIDERATIONS

IDEAL FLOW THROUGH A SINGLE ORIFICE

In order to analyze the leakage flow through a labyrinth seal, it is useful to first examine an ideal flow through a single orifice exposed to a pressure differential. This provides an understanding of the basic physical mechanisms which underlie the design of labyrinth seals. Many of the seminal analytical approaches used to analyze labyrinth seals were built upon this simplified analysis; examples include work by Martin⁹, and Egli¹. For an orifice in a duct, as shown in Figure 2-1, and the assumption that the fluid is an ideal gas undergoing an isentropic pressure change, the ideal mass flow can be derived using the first law of thermodynamics and the principle of continuity¹⁰:

$$\dot{m}_{isen} = A_2 \left\{ \frac{\frac{2k}{(k-1)} P_1 \rho_1 \left(\frac{P_2}{P_1}\right)^{\frac{2}{k}} \left[1 - \left(\frac{P_2}{P_1}\right)^{\frac{k-1}{k}} \right]}{1 - \left(\frac{P_2}{P_1}\right)^{\frac{2}{k}} \left(\frac{A_2}{A_1}\right)^2} \right\}^{\frac{1}{2}} \quad (1)$$

If the orifice area, A_2 , is much smaller than the duct area, A_1 , Eq. (1) simplifies to

$$\dot{m}_{isen} = A_2 \left\{ \frac{2k}{(k-1)} P_1 \rho_1 \left(\frac{P_2}{P_1}\right)^{\frac{2}{k}} \left[1 - \left(\frac{P_2}{P_1}\right)^{\frac{k-1}{k}} \right] \right\}^{\frac{1}{2}} \quad (2)$$

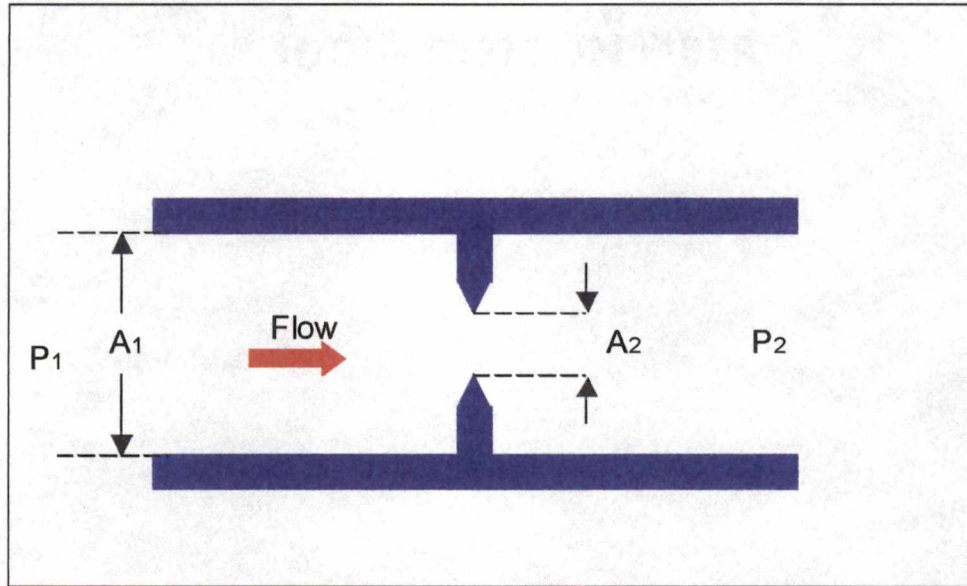


Figure 2-1 - Orifice Exposed to a Pressure Differential

Equation (2) is a reformation of the basic equation used in the analyses of Egli, Martin and others to establish the ideal flow through a single orifice exposed to a pressure differential. However, in actuality the pressure driven flow through the orifice shown in Figure 2-1 is subject to physical effects that require corrections to the flow assumed under the isentropic and one-dimensional model.

VISCOUS EFFECTS

The viscosity of any fluid causes losses that are not accounted for in an idealized isentropic model. Figure 2-2¹¹ shows an actual flow through a sharp edged orifice in a closed duct. Numerous authors including Rouse¹¹ describe the nature of the flow through a sharp edged orifice. Upstream of the restriction, areas of stagnation form in the corners, characterized by relatively weak recirculation.

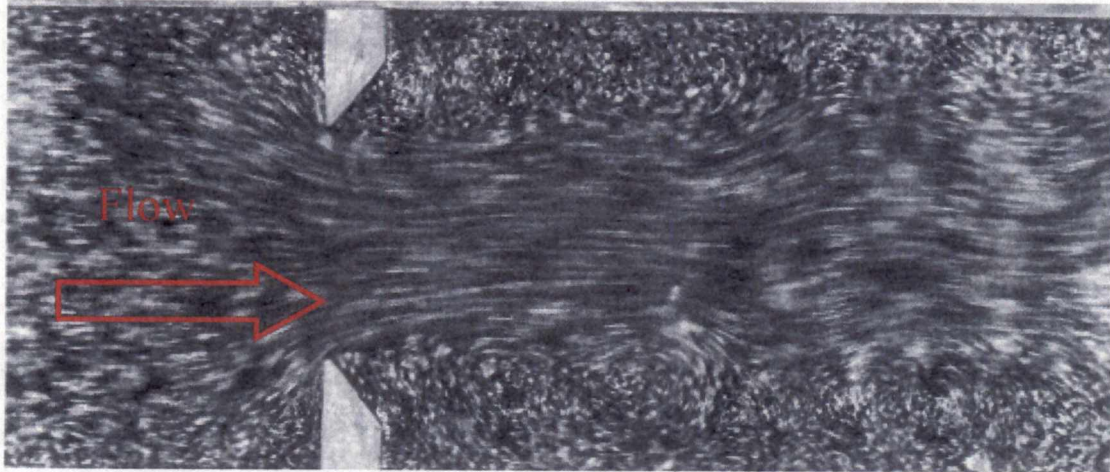


Figure 2-2 - Flow Through a Sharp Edged Orifice

After the restriction, the rapid deceleration caused by the sudden expansion causes expansion causes a highly turbulent area of flow reversal to form as shown in Figure 2-2. In this chaotic turbulent area, the viscous effects will cause total pressure dissipation in the form of heat. In a conduit flow, this turbulence will gradually be dissipated further downstream by viscous shear effects, if sufficient length is available. Note that this mechanism does not exist in the labyrinth seal where the distance to the next throttling is relatively small. In addition, viscous losses occur in the larger eddies shown in Figure 2-2 and all along the surfaces of the knife and the wall of the duct. However, since frictional losses are directly related to fluid velocity, the relatively slow rotating vortices near the duct and knife surfaces likely contribute less to overall energy loss through the orifice. The energy loss entailed in the production and dissipation of turbulence at the restriction is the fundamental mechanism of loss in the flow through an orifice in a closed duct. Any method of increasing the turbulence and therefore the energy dissipation at such an orifice will result in a decrease in total pressure; leakage through the orifice is reduced.

The amount that the flow through an orifice is reduced by the loss mechanism described above is described by a discharge coefficient, C_d , which is typically obtained from empirical data.

The discharge coefficient can be used in incompressible flow situations as shown in equation (3); C_d represents the ratio of actual flow to ideal flow through the orifice.

$$\dot{m} = C_d A_2 (2\rho(P_1 - P_2))^{1/2} \quad (3)$$

COMPRESSIBILITY EFFECTS

The compressibility of a real fluid may become a significant loss mechanism if the fluid is flowing in a regime where the velocity is greater than approximately 0.3 of the sonic velocity at the flow conditions or if there is strong heat transfer. When a compressible fluid flows through an orifice of the type described above, the fluid density does not remain constant. At low Mach numbers, some energy is expended as the fluid is compressed and expanded through the throttling but this is generally much less significant than the viscous losses. As the pressure difference across the orifice is increased, the Mach number at the minimum area reaches a value of 1. Theoretically, at this operating condition the orifice is said to be *choked* in that no further increase in mass flow is possible without changing the conditions upstream. If the pressure difference is increased further across the orifice, the Mach number at the minimum area point will remain equal to 1, although the axial location of this minimum area may shift; however the local Mach number beyond the minimum area point can reach supersonic velocities with Mach number greater than 1. At some point downstream of the minimum area point a shock (or series of shocks) can form. There can be a significant loss in total pressure across this shock(s) and therefore energy is again dissipated.

Typically, the flow equation shown above is based on the upstream density and the calculated flow is corrected by an expansion factor Y . For a sharp-edged obstruction, compressibility effects decrease the effective area and therefore the energy losses for given conditions¹². Therefore, the flow of a compressible fluid through an orifice can be calculated as:

$$\dot{m}_{orifice} = A_2 Y C_d (P_1 \rho_1)^{\frac{1}{2}} \left\{ \frac{2k}{(k-1)} \left(\frac{P_2}{P_1} \right)^{\frac{2}{k}} \left[1 - \left(\frac{P_2}{P_1} \right)^{\frac{k-1}{k}} \right] \right\}^{\frac{1}{2}} \quad (4)$$

Or, combining terms and using the ideal gas law, (4) can be re-written in the form:

$$\dot{m}_{orifice} = A_2 \phi_{Orifice} \frac{P_1}{\sqrt{RT_1}} \quad (5)$$

where,

$$\phi_{Orifice} = Y C_d \left\{ \frac{2k}{(k-1)} \left(\frac{P_2}{P_1} \right)^{\frac{2}{k}} \left[1 - \left(\frac{P_2}{P_1} \right)^{\frac{k-1}{k}} \right] \right\}^{\frac{1}{2}} \quad (6)$$

The parameter $\phi_{Orifice}$ therefore represents the correction in mass flow through the orifice from the ideal flow case. Note that the discharge coefficient, C_d , is often modified to account for geometrically related changes in approach velocity of the fluid to the orifice; in this context it is termed a flow coefficient, α .

APPLICATION OF ORIFICE THEORY TO LABYRINTH SEALS

The flow through a labyrinth seal can be considered as a flow through a series of orifice type restrictions. In a global sense, the losses caused by these individual restrictions combine in some manner to provide a net energy loss to the system. Referring to Figure 2-1 and Figure 2-3, the flow through a labyrinth seal can be described as follows: the fluid, driven by the pressure differential between P_{n-1} and P_n , is forced through a restricted orifice. As the fluid passes through the restriction, it undergoes an increase in velocity and a corresponding decrease in pressure. At some point after the orifice, the fluid expands to the pressure in the next chamber. During this process, some of the kinetic energy of the fluid is recovered as a pressure rise and some is lost as heat. The remaining kinetic and potential energies provide the fluid with a means to enter the next section of the seal.

In a labyrinth seal, the net result is a loss of total energy available to drive the flow towards the next throttling. Ideally, the kinetic energy of the fluid resulting from the previous stage of throttling will be dissipated before the fluid enters the next stage^{1,13}. In this manner, by the time the fluid has traveled through all of the stages of the seal, its kinetic energy is greatly reduced, and there is negligible leakage flow through the seal (ideally).

Static pressure measurement in various chambers in a labyrinth seal model provides indications of the local level of losses, although these results are inherently less informative a measure of losses than they would be in a regular duct. In a labyrinth seal, the flow changes direction and speed rapidly as it negotiates a path through the seal. Total pressure is lost continuously through the seal, but there may be local rises in static pressure due to local stagnation points and sudden expansions as the fluid flows into a chamber of the seal.

Tipton, Scott and Vogel¹⁵ noted that analyses of labyrinth seal leakage could be classified into two main categories, global models, and knife-to-knife models. Knife-to-knife models treat

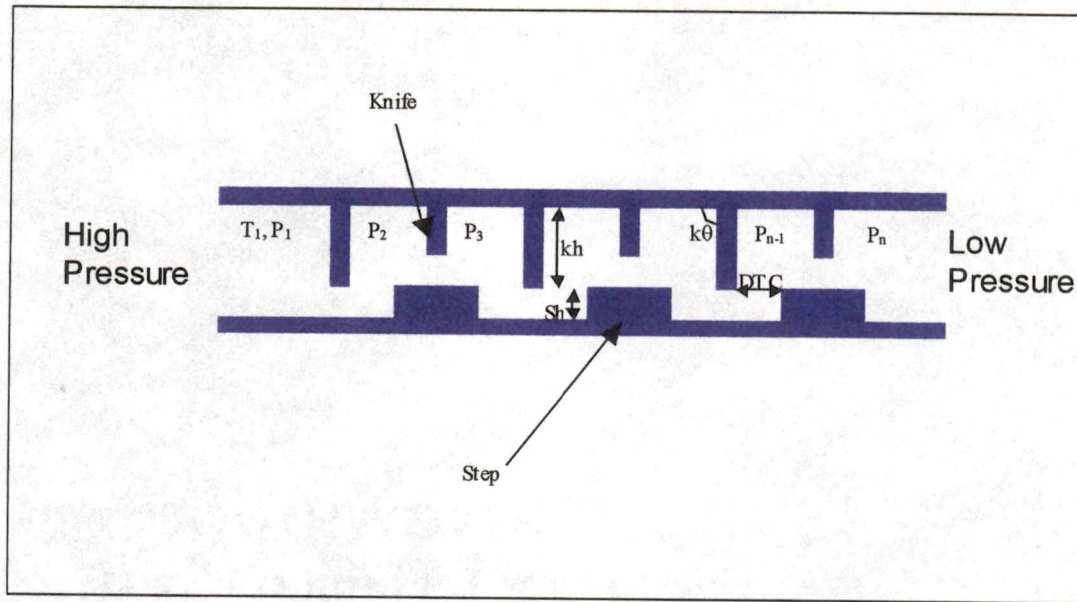


Figure 2-3 - Stepped Labyrinth Seal Nomenclature

the internal flow through a seal by calculating relevant physical parameters as they change at various points internal to the seal.

Although computationally intensive, this method allows for changes in flow behavior at each throttling within the seal. Global models characterize the labyrinth seal either by the net effect of a series of throttlings or as a rough pipe model with uniformly distributed wall friction.

While either of these approaches can yield good empirical correlations, the rough pipe model provides little information to the seal designer in terms of physically relevant design parameters. Series of restriction global models provide good results, but encounter difficulty calculating kinetic energy carry over. Additionally, problems are encountered predicting seal behavior in choked flow regimes¹⁵. All of the methods described above typically employ a combination of theoretical formulation and empirical corrections. The flow through a labyrinth seal is complex and is extremely dependent upon the specifics of the application. For the global series of throttlings methods, the reduction in flow from the ideal case is represented in a manner

analogous to the single orifice case as shown by equation (7):

$$\dot{m}_{labyrinth} = A_{cl} \alpha \varepsilon \phi_0 \frac{P_1}{\sqrt{RT_1}} \quad (7)$$

The function ϕ_0 is a dimensionless parameter often referred to as a leakage function¹, expansion function², or as the ideal labyrinth function¹⁷. The parameter ε is often included to account for kinetic energy carry over between throttlings in the seal¹⁸. The seal flow coefficient, α is primarily dependent on the sharpness and the tip thickness of the seal knives¹⁹. Since these three dimensionless parameters are not easily separated when analyzing experimental data, they can be combined to form $\phi_{Labyrinth}$, hereafter referred to as the labyrinth function. Komotori and Miyake²⁰ use a similar rationale. Therefore, (7) becomes:

$$\dot{m}_{labyrinth} = A_{cl} \phi_{Labyrinth} \frac{P_1}{\sqrt{RT_1}} \quad (8)$$

In 1908, Martin modeled leakage flow of a compressible fluid through labyrinth seals as an idealized process with the entire flow process being that of an ideal gas undergoing a series of isothermal expansions and compressions. Neglecting the effects of rotation and kinetic energy carry over, he developed an expression for leakage prediction in a labyrinth seal having n throttlings:

$$\dot{m} = A_{cl} \alpha \phi_{Martin} \frac{P_1}{\sqrt{RT_1}} \quad (9)$$

where,

$$\phi_{Martin} = \sqrt{\frac{1 - \left(\frac{P_n}{P_1}\right)^2}{n + \frac{2}{k} \ln\left(\frac{P_1}{P_n}\right)}} \quad (10)$$

Martin's development assumes that the flow coefficient, α , remains constant for each throttling within the seal and also that all kinetic energy is dissipated between throttlings. Figure 2-4 shows a plot of Martin's expansion function ϕ_{Martin} , for various values of n . Note that as shown in Figure 2-4, a labyrinth seal will in fact assume the characteristic "choked" condition of a nozzle operating at its critical pressure ratio¹⁶. Once this critical pressure ratio for the seal is reached, sonic velocity exists at one of the throttlings and no further increase in mass flow is possible without a change in the upstream conditions. Later investigations, as reported by Lowrie and Meyer¹⁴, detailed shortcomings in Martin's formula. For example, there is kinetic energy carry-over in labyrinth seals. Straight through labyrinth seals allow the most carry over, while stepped and staggered seals are designed to reduce this¹.

Egli's development¹ was based on an isentropic expansion of a fluid through a sharp edged orifice, using this result to derive an equation for a labyrinth seal with n throttlings. As a refinement to Martin's approach, Egli gave some consideration to the effects of kinetic energy carry over and provided some experimental results to support his method. Egli included a kinetic energy carry over factor for use in the analysis of straight through labyrinth seals. He hypothesized that stepped seals were almost entirely effective at removing carry over, and could therefore be reasonably modeled using Martin's equation. Further work in the field revealed that the global models of Martin and Egli were extremely useful as first estimates of leakage, but inherently neglected the complicated internal flow of a labyrinth seal.

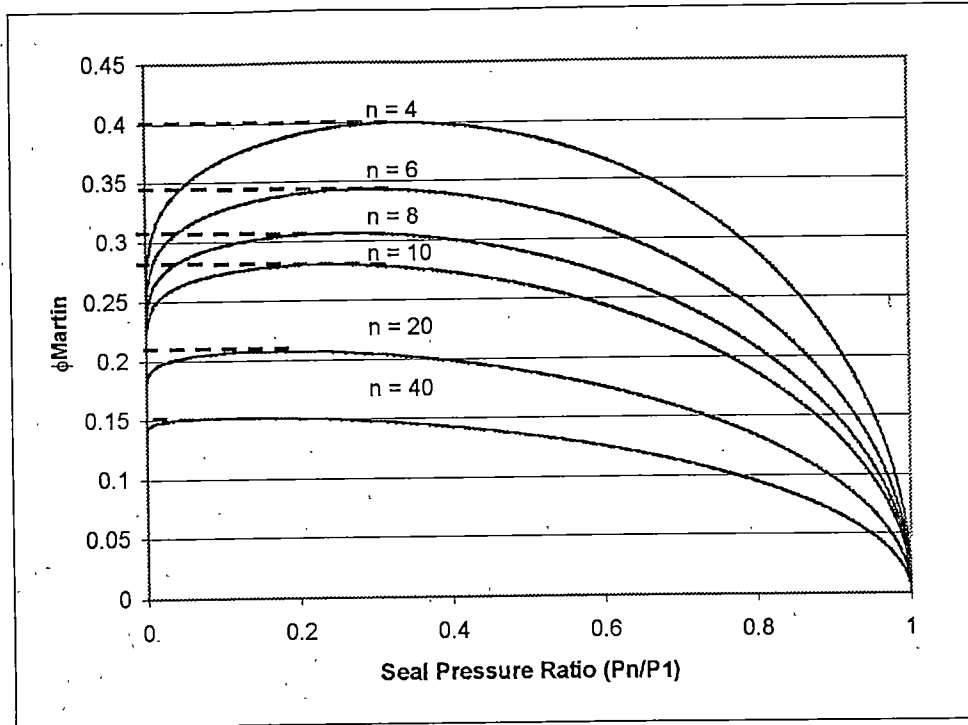


Figure 2-4 - Martin's Expansion Function, ϕ_{Martin}

In particular, the assumption of a constant flow coefficient at each throttling in the seal was shown by Meyer and Lowrie¹⁴ to be inaccurate for straight and slant seals. Stepped seals in particular presented complex paths for the fluid and the assumptions of zero carry over and constant flow coefficient were noted to be in error. Numerous studies were undertaken to further develop an understanding of labyrinth seal leakage. As noted by Yizhang and Feng¹⁷, because of the numerous factors involved, the most effective approach involves using a combination of theoretical method and experimental data.

Based on a review of the open literature, there is clearly a deficiency in available information detail on the behavior of stepped labyrinth seals. Greater success has been obtained analyzing and predicting the leakage of straight through labyrinth seals due to the relative simplicity of the internal flow, and the wide availability of experimental results¹⁸.

Miyake and Duh carried out a substantial study of leakage in both straight and stepped labyrinth seals¹⁹. They provide an empirical formula for calculation of a labyrinth function as used in equation (8).

$$\phi_{Miyake} = 117 \sqrt{\text{Re}^{\frac{-0.8}{1.2}} - 6.14 \text{Re}^{\frac{-1}{1.2}}} \cdot \left(\frac{DTC}{Kp} \right)^{0.3} \cdot n^{-0.55} \quad (10)$$

Note that in this formulation, Reynolds number, Re is defined as:

$$\text{Re} = \frac{Kp}{\nu} \sqrt{\frac{P_1 - P_n}{\rho}} \quad (11)$$

Equation (10) was formulated based on experimental work carried out by Miyake and Duh¹⁹ on various stepped labyrinth seals; they also provide design guidelines for stepped labyrinth seals:

- (a) A step height, Sh, of 2.0 to 2.5 times the clearance area is recommended;
- (b) The best sealing effect is obtained when the throttle is situated at the middle point of the step(s); and
- (c) The optimum ratio of depth of expansion chamber to knife pitch, K_p is ~0.6.

Kearon and Keh¹³ examine two particular cases in studying the flow of air through a staggered type labyrinth seal of n stages. Morrison et al¹⁸ suggest that since both staggered and stepped seals limit carry over effects and have similar flow paths, flow coefficients derived by analyzing a staggered type seal may be useful in predicting the leakage in a stepped seal design.

However it must be noted that these authors acknowledge that insufficient data is available to confirm this hypothesis¹⁸. The Kearton and Keh analysis is built on three assumptions:

- (a) that the leakage air flow process is isentropic;
- (b) that all kinetic energy of the flow is converted into heat at constant pressure at each stage of the seal; and
- (c) that there is no heat transfer to or from the seal.

In their paper, Kearton and Keh show that, with the assumptions above, a critical pressure ratio across the seal that will result in the flow being choked, i.e. acoustic velocity reached at a limiting point. Thus, they classify compressible flow through labyrinth seals into two cases:

- (a) the pressure differential across the seal, and the number of stages in the seal are such that the pressure drop at each stage of the seal is relatively small, and is always less than the critical pressure ratio; and
- (b) the pressure differential across the seal, and the number of stages in the seal are such that the pressure drop at the final restriction of the seal exceeds the critical, i.e. the flow is choked. In this case, the pressure differential across the preceding stages of the seal are still relatively small; only the pressure ratio across the last stage is equal to or lower than the critical ratio, i.e. 0.528 for air.

Based on data obtained from numerous tests of staggered labyrinth seals and single orifices, Kearton and Keh recommend the following formula for the subcritical (i.e. unchoked flow) case:

$$\dot{m} = A_{cl} C_{d1} \sqrt{\frac{Fg(P_1^2 - P_n^2)}{nRT_1}} \quad (12)$$

For the choked flow case, the authors also provide:

$$\dot{m} = \frac{3.873 A_{cl} C_{d2} P_{n-1}}{\sqrt{RT_1}} \quad (13)$$

Kearton and Keh provide data curves for their discharge coefficients, C_{d1} , and C_{d2} ; also, charts and calculation methods for the non-dimensional correction factor F are included.

DATA REPRESENTATION

Leakage flow through the system can be quantified in terms of various parameters.

Seal Discharge Coefficient

A particularly useful representation is the seal discharge coefficient, $C_{d_{seal}}$:

$$C_{d_{seal}} = \frac{\text{massflow}_{actual}}{\text{massflow}_{ideal}} \quad (14)$$

As described by Washka et al²¹, the ideal flow is calculated (for the sub-critical flow case) using equation (2), repeated here for clarity: the labyrinth clearance area is used as the cross sectional area of a hypothetical nozzle, and the seal overall pressure ratio as the nozzle pressure ratio.

$$\dot{m}_{ideal} = A_{cl} \left\{ \frac{2k}{(k-1)} P_1 \rho_1 \left(\frac{P_2}{P_1} \right)^{\frac{2}{k}} \left[1 - \left(\frac{P_2}{P_1} \right)^{\frac{k-1}{k}} \right] \right\}^{\frac{1}{2}} \quad (15)$$

For supercritical seal pressure ratios, the value of mass flow is equal to that obtained when the critical pressure ratio is obtained, i.e. for air:

$$\frac{P_2}{P_1} = \left(\frac{2}{k+1} \right)^{\frac{k}{k-1}} = 0.528 \quad (16)$$

Flow Parameter

A dimensional parameter is used by Stocker²² to correlate leakage performance of a labyrinth seal. This parameter can be derived from the relation shown in (8) using the ideal gas law:

$$\dot{m} = \frac{\Phi P_1 A_{cl}}{\sqrt{T_1}} \quad (17)$$

where, Φ has units of

$$\frac{\text{lbm} \cdot \text{°R}^{\frac{1}{2}}}{\text{lb} \cdot \text{sec}}$$

Labyrinth Flow Coefficient

Considering Martin's development, Equations (9) and (10), the labyrinth flow coefficient for a given seal/operating condition can be calculated from measurements. This coefficient represents a correction to Martin's idealized formula, including effects of kinetic energy carry over and compressibility. A similar approach is used by Morrison et al¹⁸.

$$\alpha_{labyrinth} = \frac{\dot{m}}{A_{cl} \phi_{Martin} \frac{P_1}{\sqrt{RT_1}}} \quad (18)$$

Total Pressure Loss

The efficiency of a particular seal design or configuration can be represented in terms of the loss of total pressure across the seal. This can be non-dimensionalized in the form:

$$\frac{P_{t(inlet)} - P_{t(exit)}}{P_{t(inlet)}} \quad (19)$$

This is useful in that it is a direct measure of the energy being dissipated by the seal internal flow losses.

DIMENSIONAL ANALYSIS

A dimensional analysis of the stepped labyrinth seal was carried out; Table 2-1 summarizes the 13 non-dimensional groupings obtained and provides a brief description of each. Table 2-1 also contains a qualitative estimate of the relative importance of these parameters based on a thorough review of the available data as reported by Tipton et al¹⁵.

Table 2-1 – Non-Dimensional Groupings

Non-Dimensional Grouping	Description	Relative Influence ¹⁵
$dP/\rho V_{cl}^2$	Euler Number	Not reported
$\rho V_{cl}^2 cl/\mu$	Reynolds Number	Moderate
V_{cl}/a	Mach Number	Not reported
K_p/cl	knife pitch/clearance	Weak
K_t/cl	knife tip thickness/clearance	Moderate
K_n	number of knives	Strong
S_w/cl	step height/clearance	Weak
DTC/cl	distance to contact/clearance	Weak to moderate
P_r/P_1	Ratio of differential pressure across seal	Strong
K_θ	Knife angle	Moderate
K_r/cl	Knife relative sharpness	Moderate
K_h	Knife height	Weak
\dot{m}	Mass flow rate	Dependant variable

Chapter 3

EXPERIMENTAL SET-UP

COMPUTER MODEL

Three mathematical models of seal leakage prediction, those of Egli, Kearton and Keh, and Miyake, were implemented in a Microsoft Visual Basic program. The purpose of this effort was to provide an interactive estimate of leakage rates which may be expected from a given seal configuration. As well, various design parameters may be changed to estimate their general influence on the leakage flow. Features of the program are visible in the screen capture of Figures 3-1 and 3-2; these features include:

- (a) simple user interface;
- (b) "slider" type controls to vary parameters;
- (c) instant plotting;
- (d) calculation of estimated seal critical pressure ratio; and
- (e) Ability to toggle between the model scale and full size.

Figure 3-1 shows the result of a calculation of the estimated mass flow through a model scale seal, while Figure 3-2 shows the same calculation made for the actual size seal. The computer model allowed rapid calculation of estimated mass flows and choking points – this information was invaluable in the design and selection of measurement apparatus. The underlying computer code is simple and easily modified to incorporate various models, or experimental data obtained during this study.

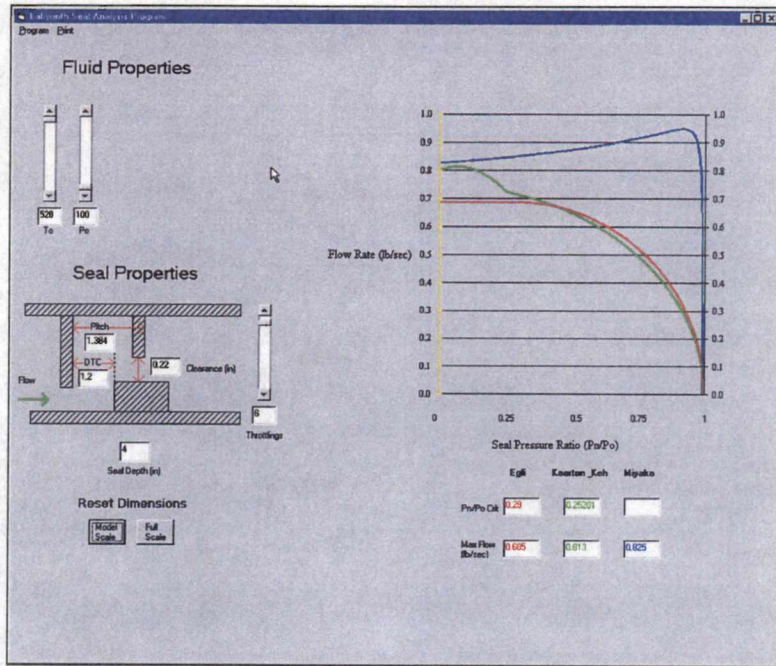


Figure 3-1 - Labyrinth Seal Computer Model (Model Scale)

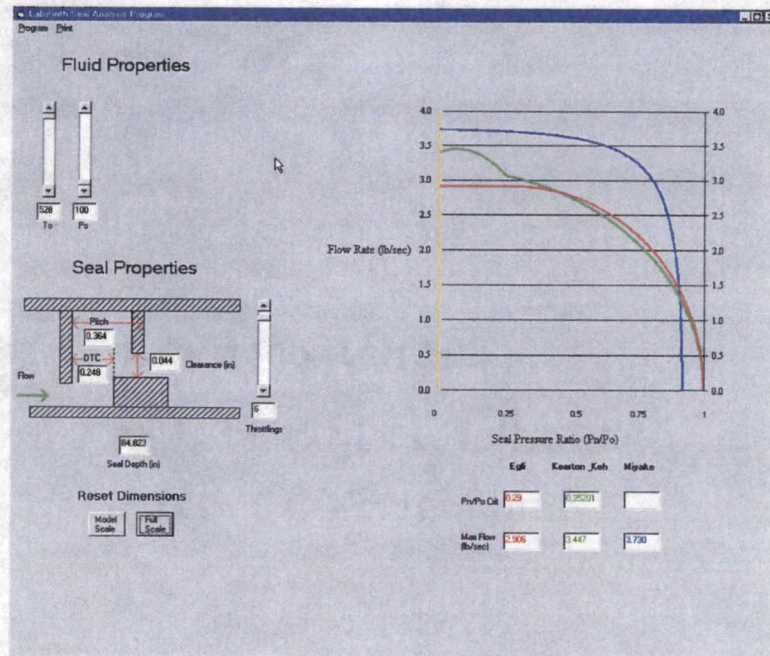


Figure 3-2 - Labyrinth Seal Computer Model (Full Scale)

2-D FLOW VISUALIZATION

In order to gain a basic understanding into the physics of labyrinth seal flow, a scaled one-dimensional flow visualization model was designed. The model, shown in Figure 3-3, was based on a labyrinth seal design provided by TVA; the geometric scale is 10 times the dimensions of the TVA seal. Design considerations for the flow visualization model included:

- a) low pressure (approximately 1.3 psi available at seal inlet);
- b) ability to vary geometric parameters of interest;
- c) optical access for lighting and visualization of flow in the model;
- d) provision for dye ports and probes throughout the model; and
- e) requirement for a secure fit in water tunnel.

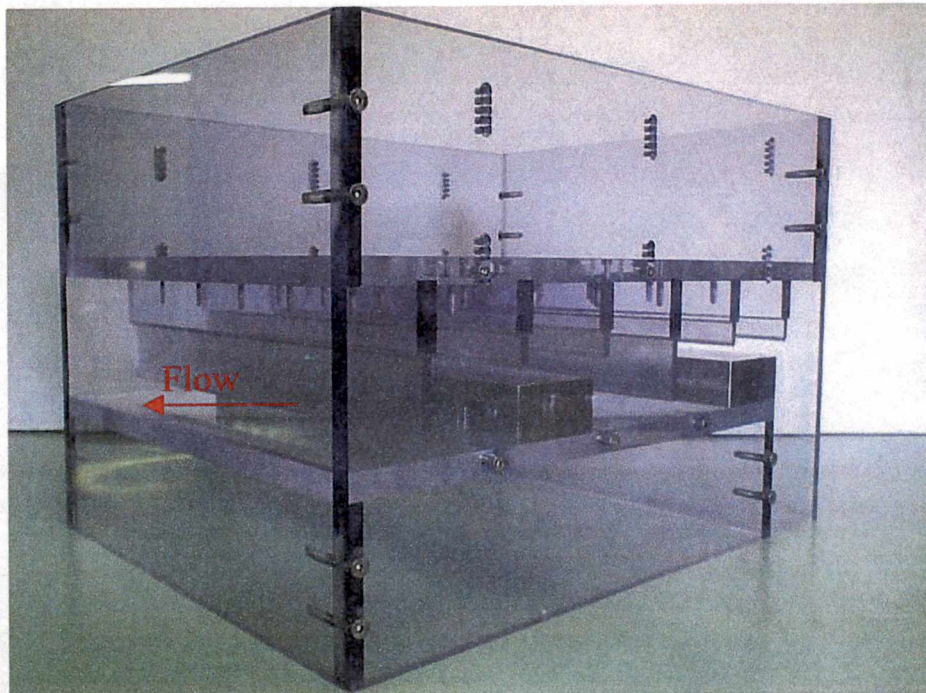


Figure 3-3 - Labyrinth Seal Flow Visualization Model

In order to achieve the goals outlined above, the model was constructed of polycarbonate and acrylic plastics in a modular construction form with all major parts attached using heli-coil type fasteners. The top plate, which has the attachment points for the seal knives, is movable in the vertical plane to enable one of the key parameters, seal clearance, to be easily varied. Other designs of knives and steps could be easily installed.

Flow visualization studies were carried out using this model installed in a water tunnel. Fluorescent dye was injected at various points in the flow field and illuminated using a laser light sheet. Details of the water tunnel installation are shown in Figure 3-4 and 3-5. Reynolds numbers for the flow through the restrictions ranged between 75 and 6000. This range of Reynolds numbers is well below that of the actual seals in operation, which are typically on the order of $10^5 < Re < 10^6$. However, because most of the losses are due to separated flow around the corners, Reynolds number does not play a large role in modeling of the global flow physics.

The velocity achievable in the water tunnel with the model installed was limited by the power of the impeller that drives the tunnel flow, and by the inability to sufficiently seal the model relative to the tunnel to allow for large pressure differentials across it. Video footage of each test was taken for further analysis, with select portions of the video later digitized as still images.

2-D FLOW MEASUREMENTS

The next phase of this study involved design of a 5 times scale 2-D airflow model. The model was used to obtain quantitative data on the leakage flow of air through a labyrinth seal of similar arrangement as the one used for flow visualization. It was foreseen that the upstream pressure would reach up to 125 psia, therefore, an analysis was carried out to ensure that suitable materials were used in the model construction that would resist deformation or failure at this pressure. The air flow facility takes high-pressure air, routes it through a calibrated orifice plate for measurement of mass flow and then directs it into a straightening chamber.

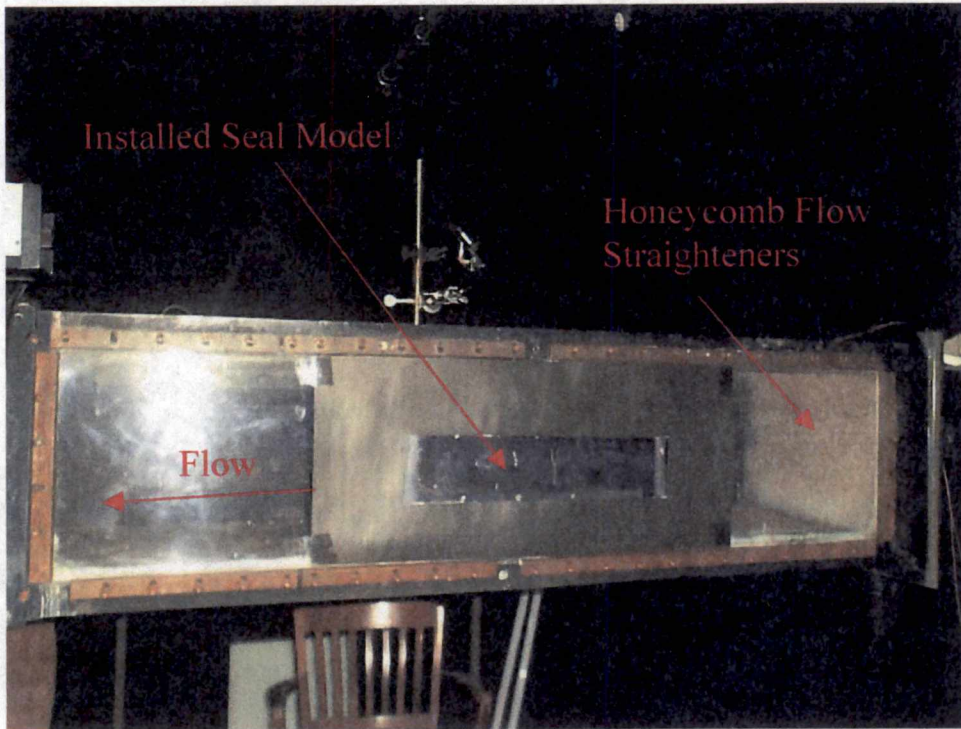


Figure 3-4 – Water Tunnel Seal Model Installation

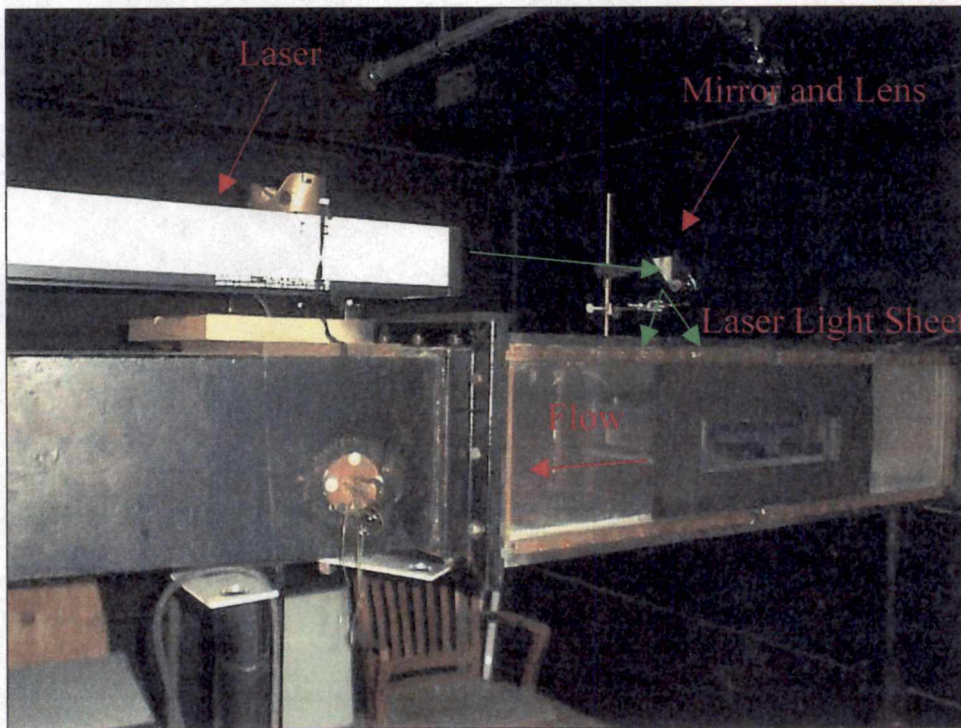


Figure 3-5 - Water Tunnel Laser Installation

After passing through a honeycombed section, the air flows into a test section holding the seal model, finally exhausting to ambient conditions. Pressure measurements were made upstream and downstream of the model, on either side of the orifice plate, as well as at various locations within the model. Figure 3-6 shows the locations of the static pressure ports while Figures 3-7 and 3-8 show the installed airflow model and the 2-D flow measurement experimental set up respectively.

Following installation of a sealing cap at the model exit, a static leak check was carried out with the model pressurized to 125 psia. The closed system volume was calculated, i.e. the internal volume of the model, straightening chamber and all associated piping, and pressure readings were taken every minute over a one-hour period. Static system leakage, i.e. leakage from around fasteners and joints, was estimated to be approximately 0.3% of the expected mass flow rate at an upstream pressure of 125 psia.

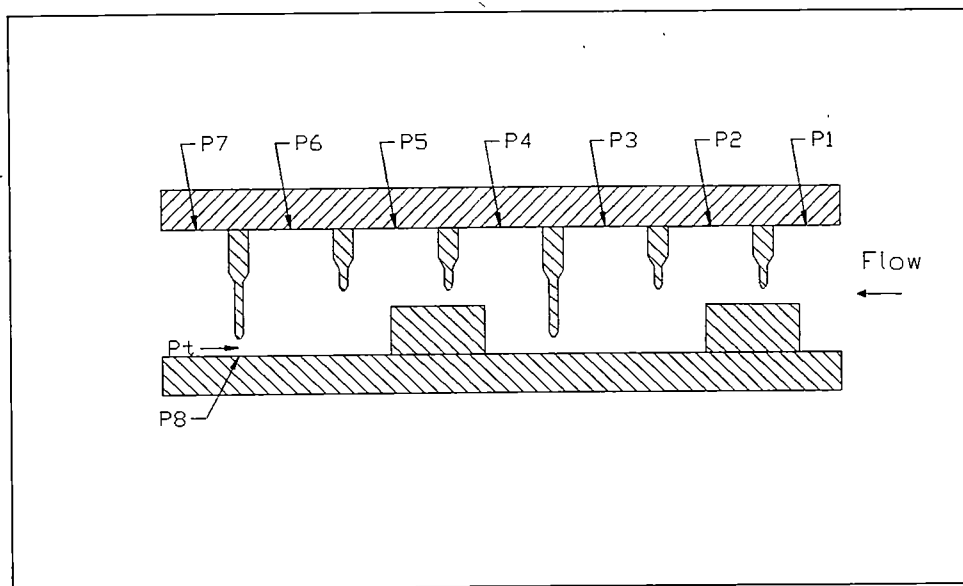


Figure 3-6 – 2D Airflow Measurement Pressure Tap Locations

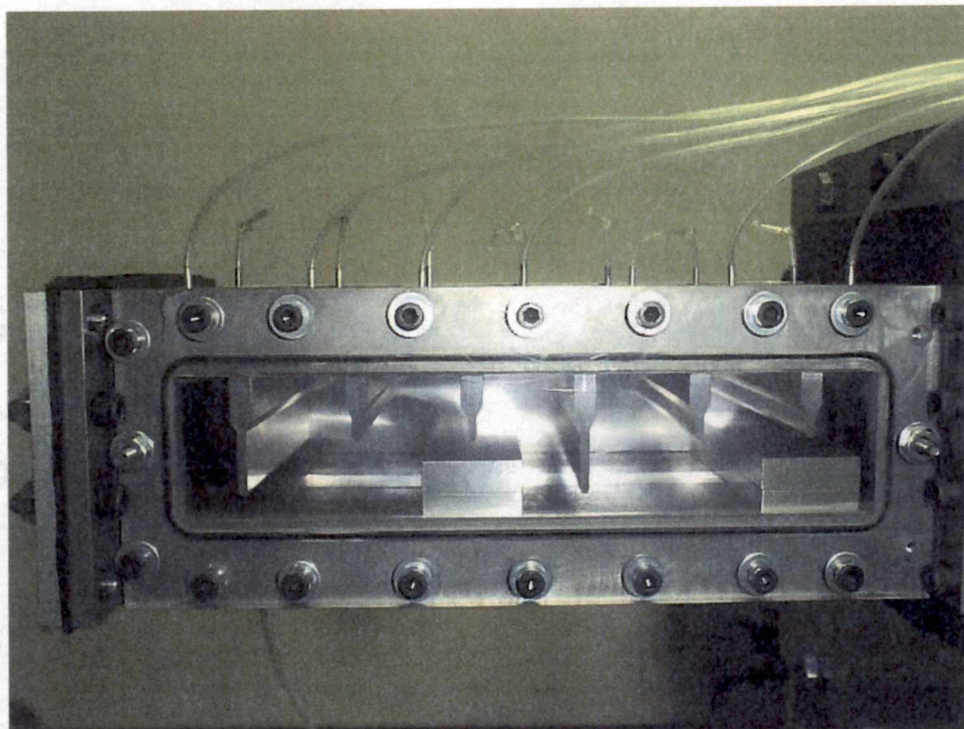


Figure 3-7 - 2D Airflow Measurement Model

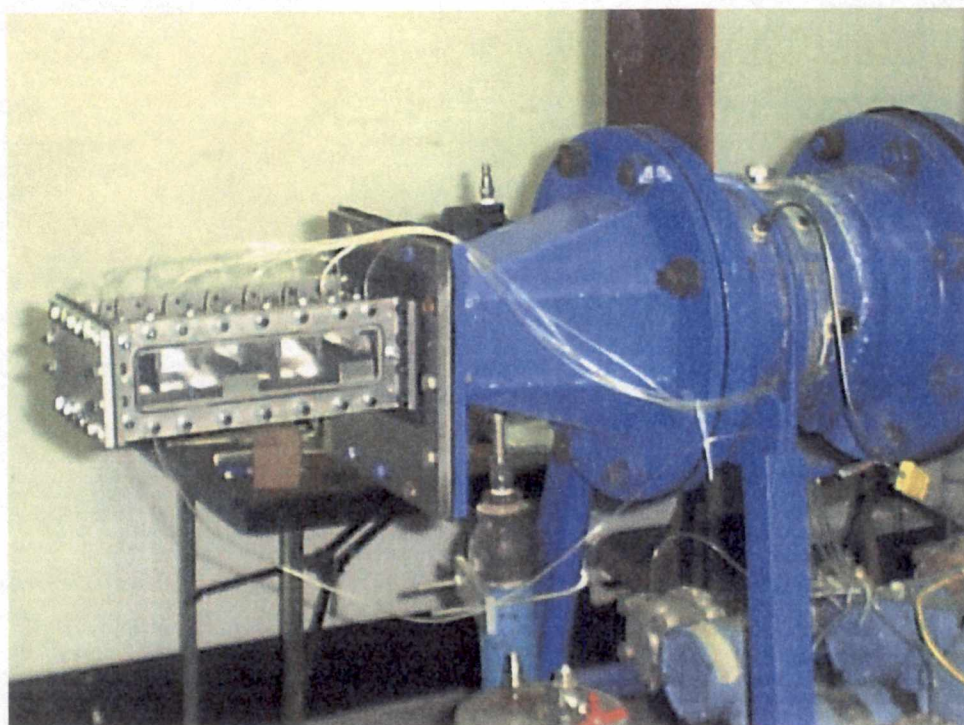


Figure 3-8 -2D Airflow Measurement Model Installation

Design considerations for the flow measurement model included:

- a) fairly high design pressure (~100 psi) requiring more care in sealing seams of model;
- b) optical access for particle image velocimetry (PIV) measurements;
- c) various pressure measurement ports;
- d) a known orifice at flow exit and a calibrated orifice plate for mass flow measurement upstream of test section; and
- e) temperature measurements upstream of orifice plate.

The various measured quantities were made using a LabView-based data acquisition system to facilitate further analysis. The screen capture of Figure 3-9 shows the data acquisition program. The system displays and archives the following information for each test run:

- (a) temperature upstream of orifice plate;
- (b) static pressures upstream and downstream of orifice plate;
- (c) total pressure upstream of seal model;
- (d) temperature upstream of seal model;
- (e) static pressures in each chamber of the seal model;
- (f) total pressure under the last knife in the seal;
- (g) static pressure under the last knife in the seal;
- (h) flow parameter, Φ ;
- (i) Mach number (at last knife);
- (j) mass flow rate; and
- (k) seal pressure distribution.

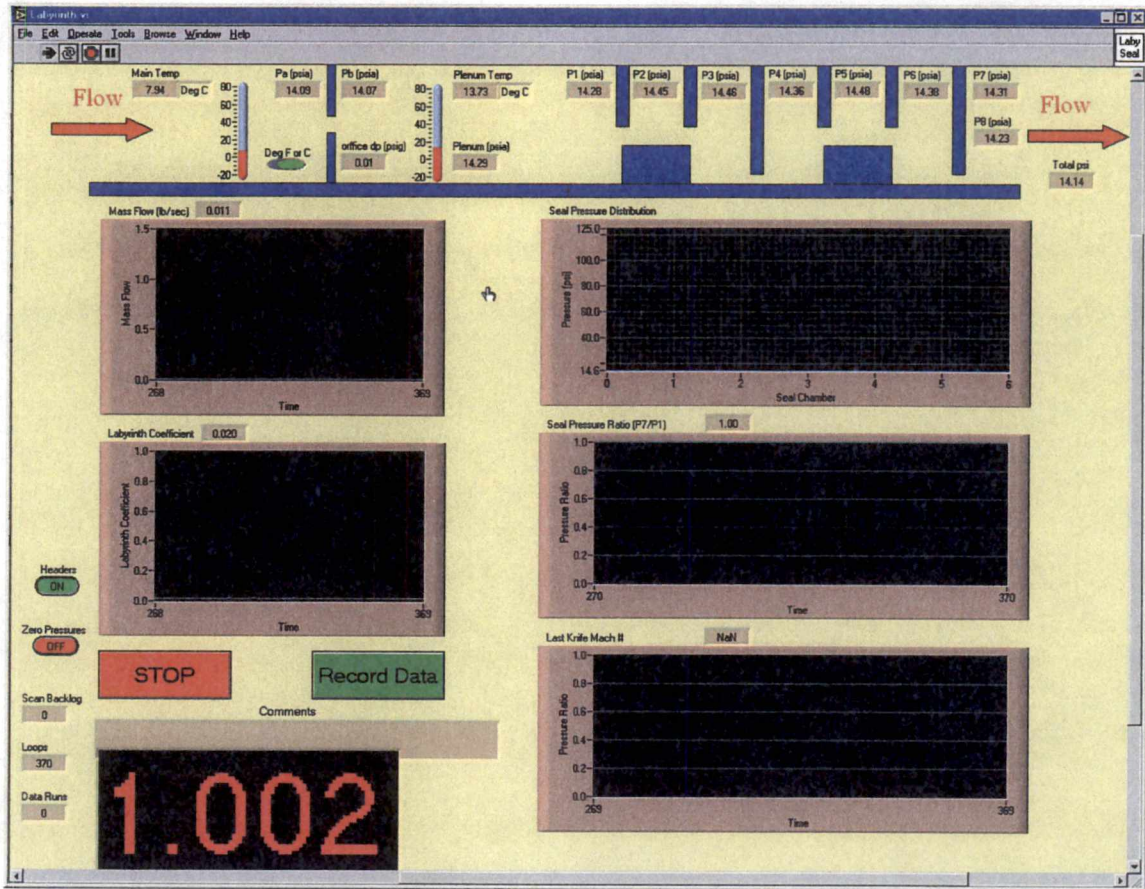


Figure 3-9 - Instrumentation Screen View

PARTICLE IMAGE VELOCIMETRY

Particle Image Velocimetry (PIV) is a non-intrusive method of measuring the velocity field of a fluid flow. In this method, a flow is seeded with tiny light reflective particles. The seed particles are carefully selected to have appropriate physical characteristics that will allow them to follow the flow. These seed particles are illuminated, typically with a laser light sheet, and their images are captured by some optical device. In current systems this is generally a charge-coupled device (CCD). If sequential images of the particles can be captured at a high rate, and the time elapsed between exposures is recorded, then the velocity of the individual particles can be calculated.

$$u = \frac{\Delta x}{\Delta t} \quad (20)$$

PIV measurements provide a method of quantifying a velocity field as opposed to the single point measurements provided by other techniques, making it an extremely valuable addition to the fluid dynamicist's "toolbox".

The PIV system currently in use at UTSI uses two continuum Nd:YAG lasers to provide the required planar light sheet. Images are captured with a TSI[®] PIVCAM and software processing is carried out using TSI[®]'s Insight[®] software installed on a Pentium 233 MHz personal computer. Post processing of the data was carried out using TecPlot[®] software. Liu²³ provides a detailed description of PIV, as well as valuable technical details of the UTSI PIV system. Meganathan²⁴ provides a specific application of the UTSI PIV system to a flow study.

The UTSI PIV system was incorporated into the same experimental setup as was used for the 2-D airflow measurement study. This allowed for precise measurement and control of seal pressure ratios. For the current study, the seed particles were tiny droplets of alcohol that were

injected into the first chamber of the seal at a pressure of approximately 20 psi above the upstream seal pressure. The alcohol was quickly atomized providing droplets of appropriate size and in a concentration that allowed for useful results to be obtained. The viewing areas selected provided a scale of $61.41\mu\text{m}/\text{pixel}$ for this study. Figures 3-10 and 3-11 show the PIV system installed with the 2-D airflow model, while Figure 3-12 shows the location of the seed particle injection point.

All internal areas of the seal model were painted matte black to minimize reflections of the laser light. The Plexiglas top window that was utilized during the 2-D airflow measurement tests was replaced with a glass window after tests showed that the Plexiglas would suffer immediate heat damage from the laser.

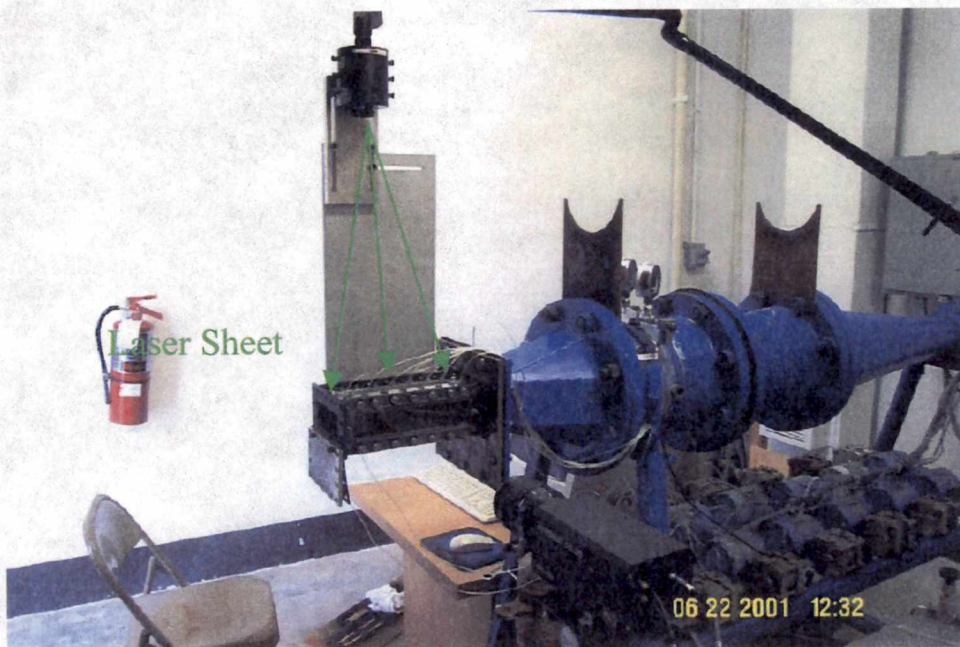


Figure 3-10 – PIV Laser Sheet Orientation

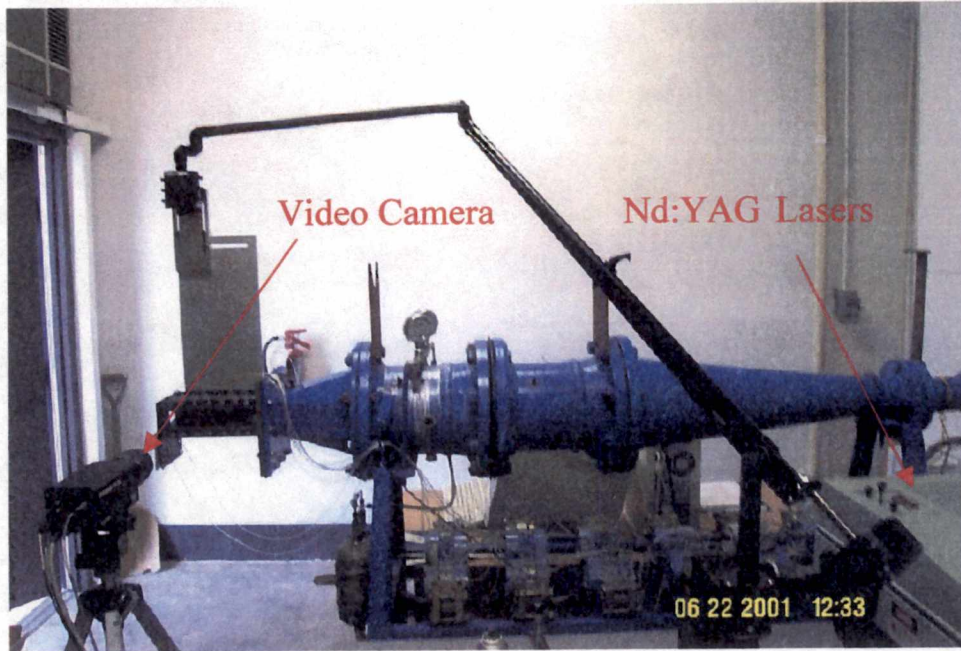


Figure 3-11 – PIV Camera and Laser Arrangement

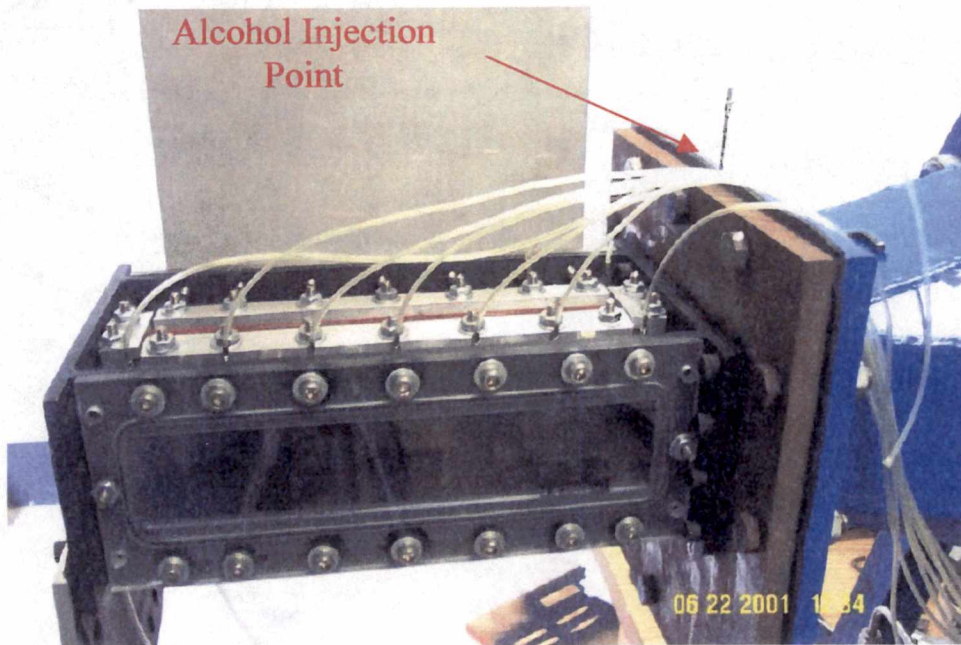


Figure 3-12 – PIV Seed Particle Injection Point

OVERALL EXPERIMENTAL STUDY

The experimental process for the labyrinth seal analysis was as follows:

- (a) 2-D water model flow visualization using colored and florescent dye/laser light to study major flow features;
- (b) 2-D air model flow pressure measurements over a range of seal pressure ratios to determine pressure distribution across seal and leakage mass flow rate;
- (c) Modification of geometric parameters in the 2-D airflow model based on both the observed flow structure in the flow visualization experiments, and information available in the literature; and
- (d) PIV measurements of select configurations in order to quantify the velocity field to gain a better understanding of the vorticity, and turbulence effects within the particular seal configuration.

EXPERIMENTAL CONFIGURATIONS

Flow Visualization

The basic seal configuration tested during the flow visualization experiments is shown in Figure 3-13. Table 3-1 shows a summary of the tested configurations and flow regimes. Only a limited number of configurations were tested in order to develop a physical understanding of the basic flow structures. For the flow visualization experiments the parameters of Reynolds number (Re) and relative axial positions of the steps were varied; all other geometric parameters remained fixed. As shown in Figure 3-13, the axial position of the steps is represented by the parameter x/L . This parameter was varied for three discrete locations by re-attaching the steps in pre-determined positions.

Table 3-1 - Flow Visualization Configurations

Test Configuration	Axial Step Position, x/L	Re
A	-0.190	75
B	-0.190	3200
C	-0.190	6000
D	.213	3200
E	.213	6000
F	.425	3200
G	.425	6000

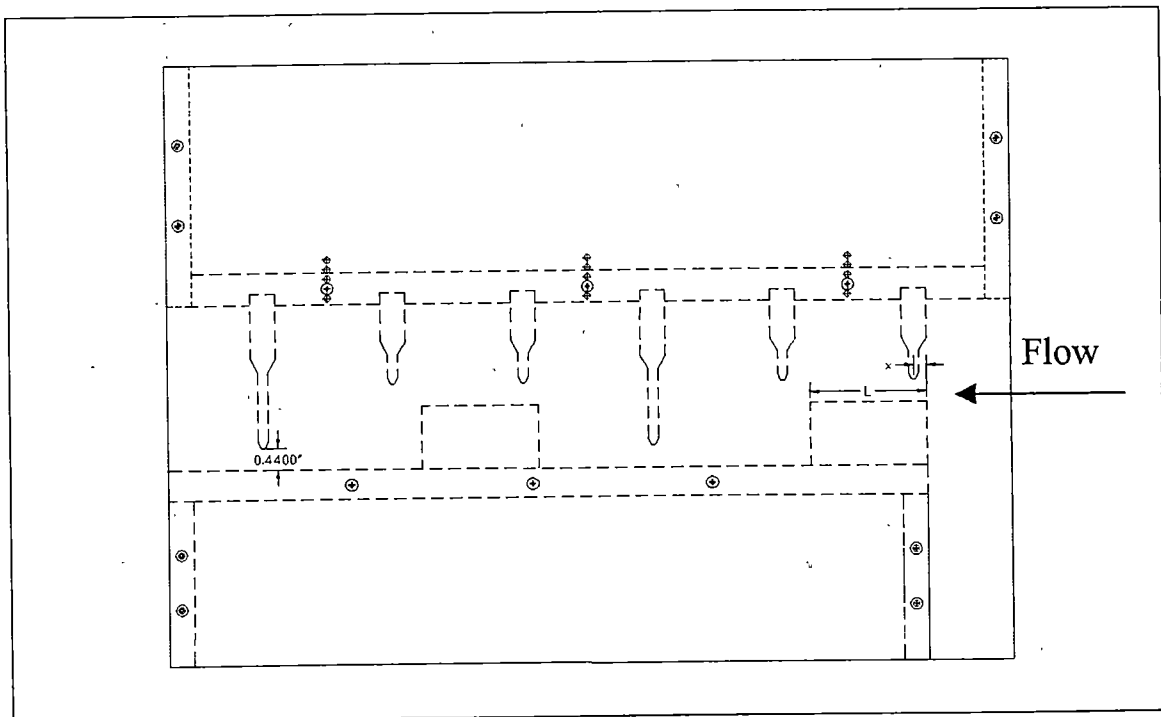


Figure 3-13 - Flow Visualization Model Configuration

2-D Flow Measurements

In the 2-D airflow measurement experiments, a more extensive range of configurations were tested in order to evaluate if improvements in the seal leakage rate could be achieved with relatively minor geometric changes. The tested configurations are summarized in Table 3-2 and each configuration is shown at a generic step axial position in Figures 3-14 to 3-20. The varied parameters included axial travel (x/L), Step Height (Sh), and knife angle ($K\theta$). The clearance area was fixed; although reducing the clearance would obviously reduce leakage, reduction of this parameter is limited in practice by a need to reduce likelihood of contact between the knife tips and the steps and land of the seal. The rationale for altering step height and knife angle was based on results available in the literature^{14,22}, and by our flow visualization study results for the baseline configuration. The ratio of downstream pressure to upstream pressure across the seal was varied between 0.1 and 1 in increments 0.05 for each seal configuration.

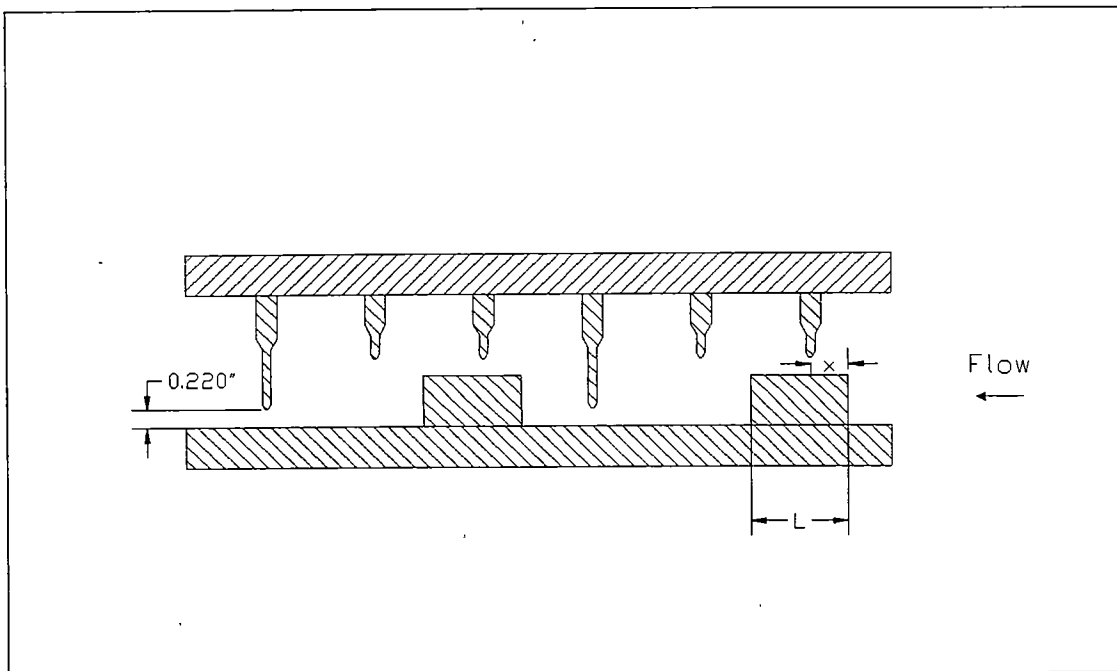


Figure 3-14 – Configuration “A” (Baseline)

Table 3-2 – 2D Flow Measurement Model Configurations

Test Configuration	Step Height, Sh	Axial Step Position, x/L	Knife Angle, Kθ
A	0.628"	0.043 0.128 0.383 0.511	90°
B	0.878"	0.043 0.128 0.383 0.511	90°
C	0.628"	0.34 0.213 0.128 0.043 -0.128	75°
D	0.628"	0.128 0.043 -0.181 -0.268	60°
E	0.628"	0.128 0.043 -0.181 -0.268	90° long knives 75° short knives
F	0.878"	0.043 0.128 0.383 0.511	90° short knives 75° long knives
G	0.878"	0.043 0.128 0.383 0.511	90° short knives 60° long knives

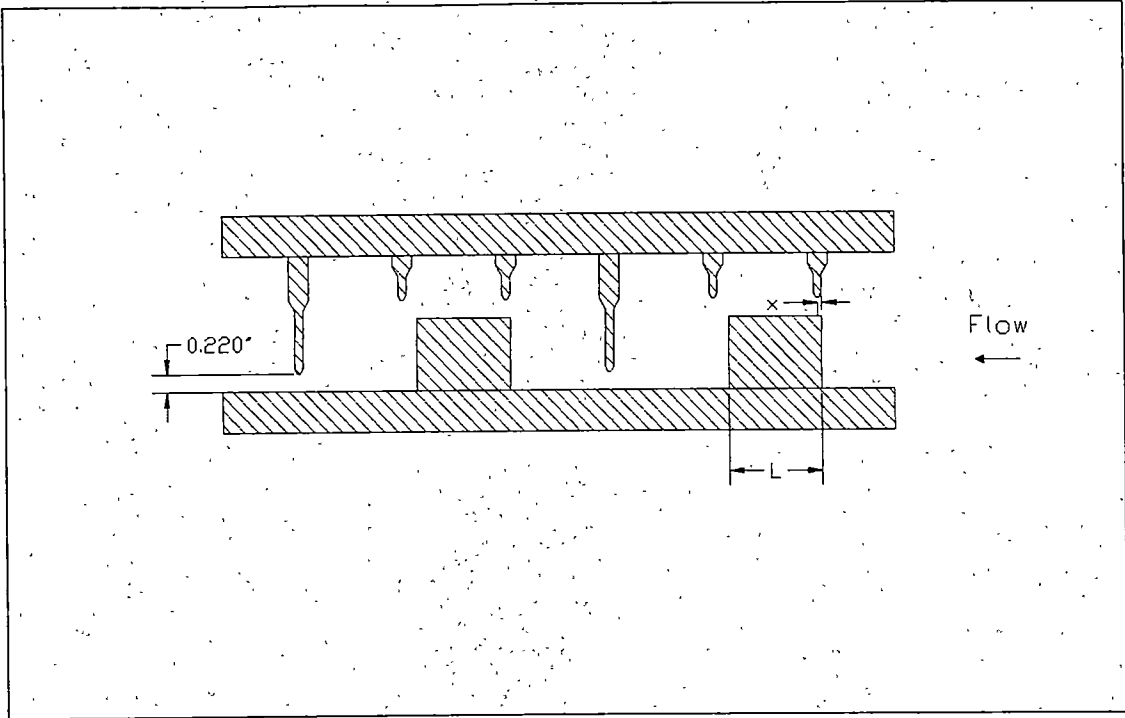


Figure 3-15 – Configuration "B" (High Step)

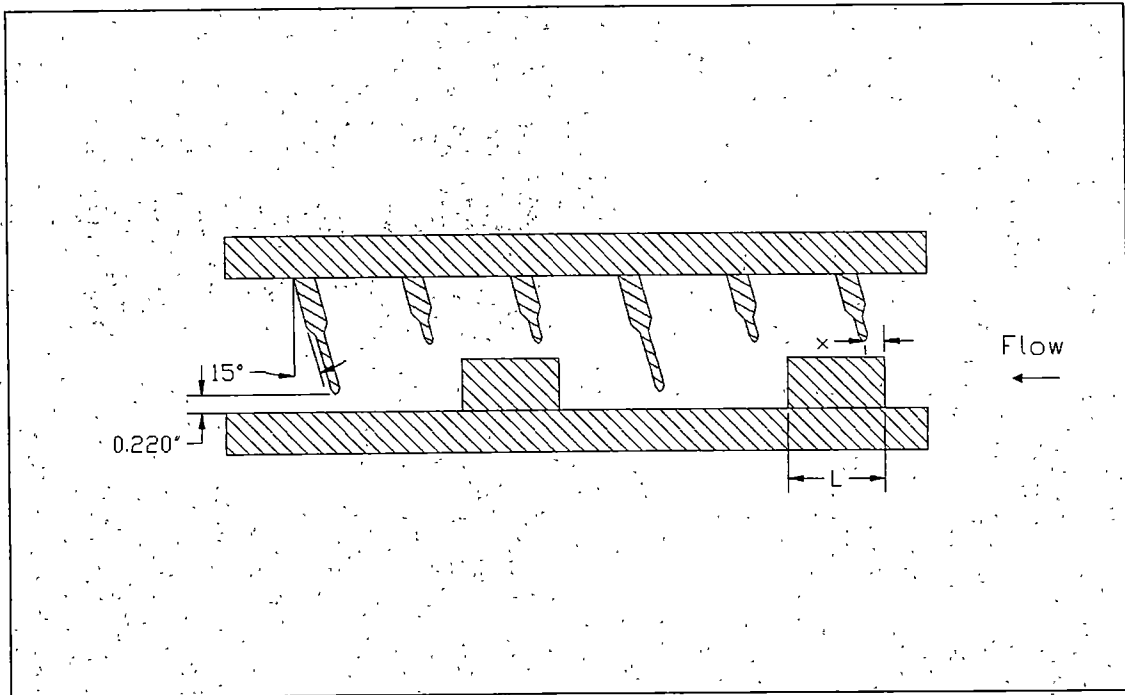


Figure 3-16 – Configuration "C" (15 degree Slant Knife)

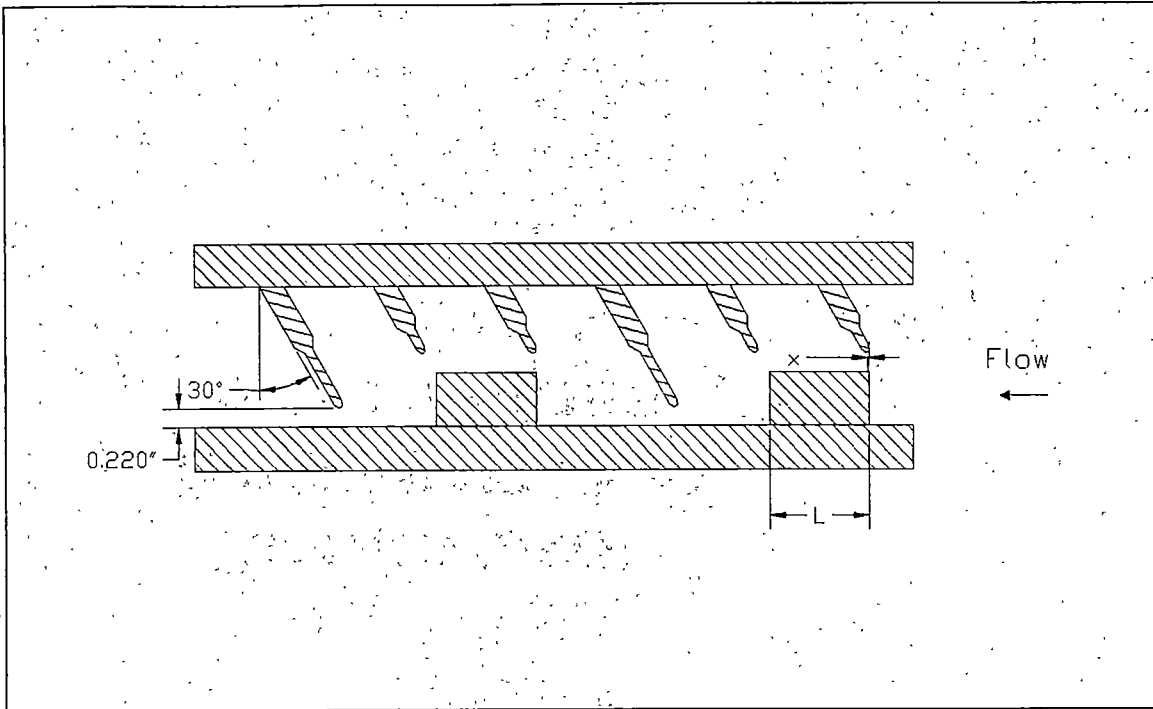


Figure 3-17 - Configuration "D" (30° Slant Knife)

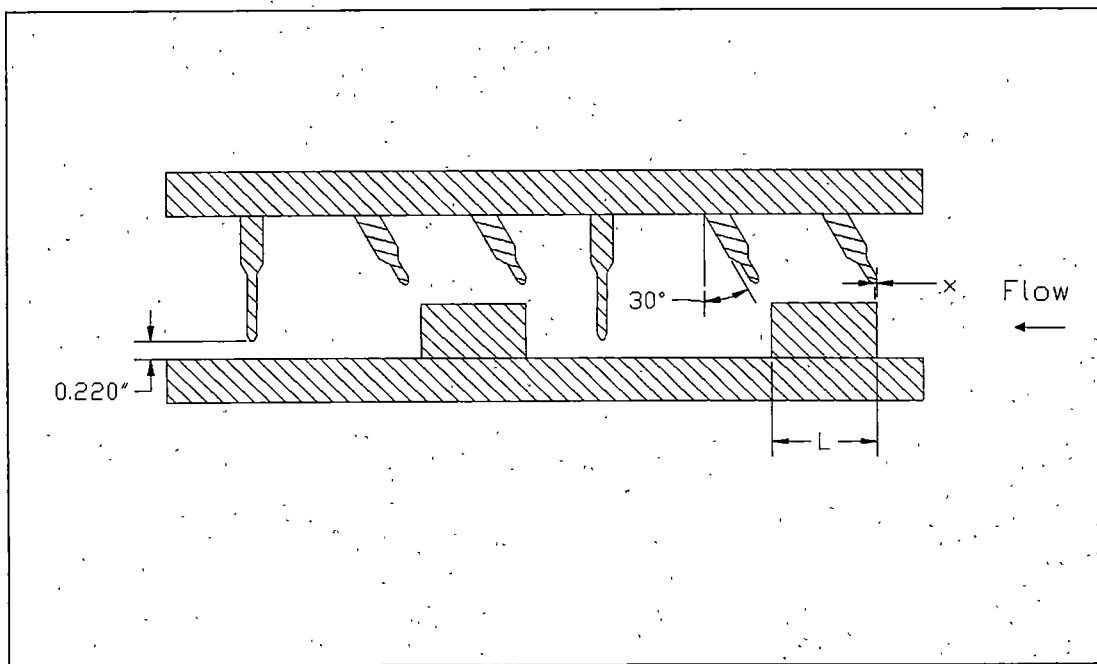


Figure 3-18 - Configuration "E" (30° Short Knives/Straight Long Knives)

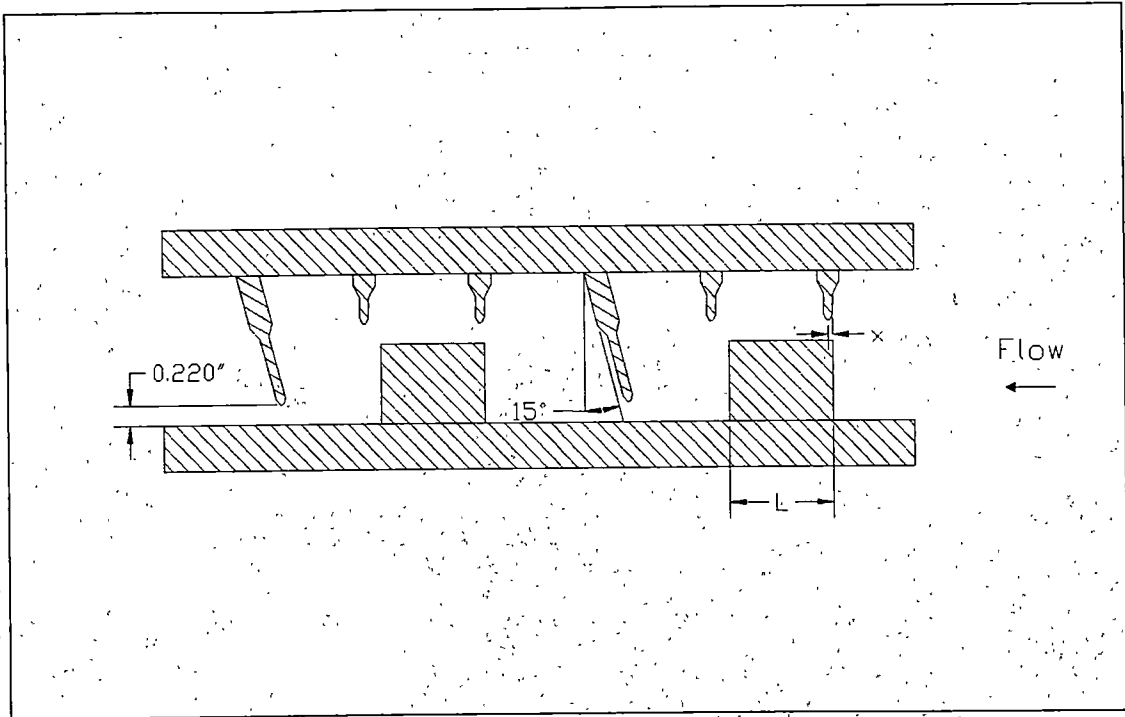


Figure 3-19 - Configuration "F" (15 ° Long Knives/High Step)

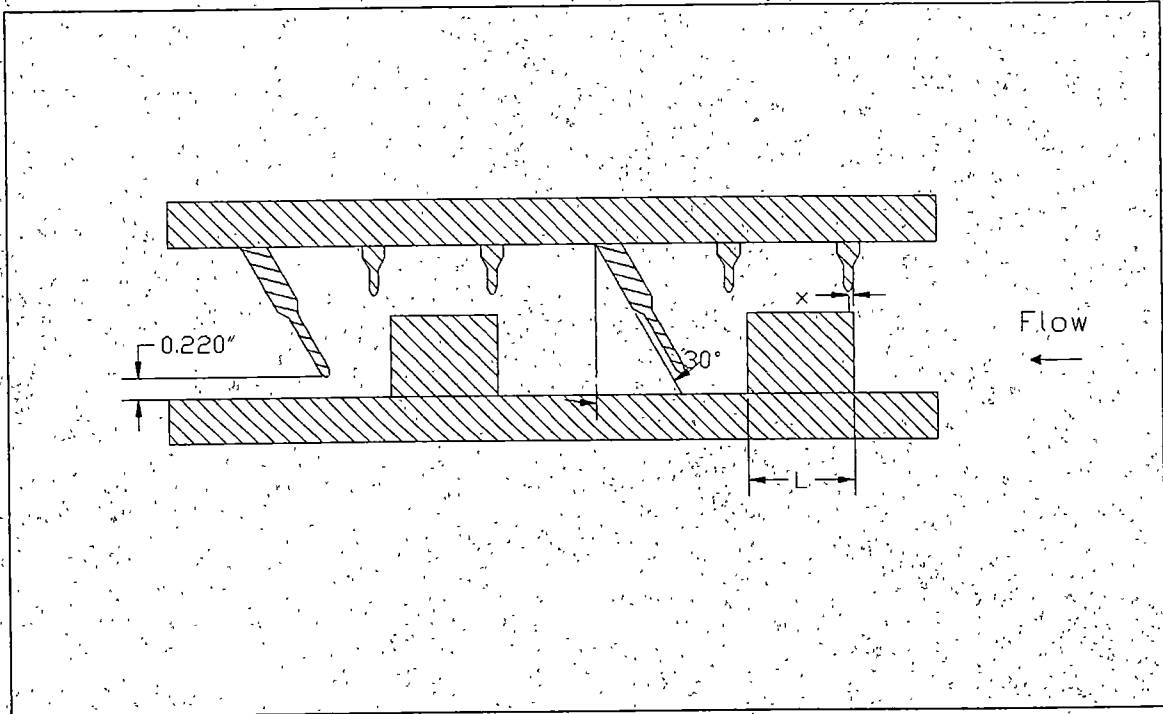


Figure 3-20 - Configuration "G" (Hybrid 15 ° Long Knives/High Step)

Particle Image Velocimetry

The PIV technique was carried out on the Configuration "A" seal, previously shown in Figure 3-14, and the Configuration "G" seal shown in Figure 3-20. This was done in order to investigate the physical mechanism for the significant leakage reduction that was obtained during the flow measurement experiments using the Configuration "G" seal. Both of these configurations were tested at a seal pressure ratio (P_1/P_7) of approximately 7.6 and a step axial location of $x/L = 0.043$, which allowed for direct comparison between the two designs.

EXPERIMENTAL RESULTS AND DISCUSSION

FLOW VISUALIZATION

The images shown in this section are representative of observations made during the flow visualization experiments. These still images were digitally obtained from VHS video footage taken over the course of the experiments. The direction of the flow in various zones of re-circulation is somewhat difficult to discern from these still pictures. The arrows indicate flow direction in these figures. In all tests, the injected dye appeared to remain laminar and coherent as it entered the first chamber. However, the rapid acceleration that occurred as the dye streaks traveled through the throttlings quickly caused large amounts of turbulence and mixing with the system water, making the flow patterns more difficult to ascertain as the flow moved through the seal. Best results were obtained using two colors of fluorescent dye injected at different points in the model. In Figure 4-1 ($x/L = -0.190$), the dye is injected upstream of and below the first step near the seal entrance. As the fluid jets through the throttlings, viscosity causes vortices to be formed in the chambers of the seal. As discussed previously, the energy required to dissipate the jet turbulence and drive this vortex action represents a major loss mechanism in each chamber of the seal. In Figure 4-2, dye is being injected upstream of the seal, at a vertical height level with the first step at the seal entrance. In both Figures 4-1 and 4-2, it can be seen that a re-circulation "bubble" forms over the step. Within this area the fluid was observed to be re-circulating relatively slowly. The large amount of turbulence generated as the fluid jets through the throttling is apparent in Figures 4-1 to 4-3. The flow jetting past the restriction at the step "bends" towards the throttling imposed by the long knife next in the flow path. This is shown as area "1" on Figure 4-1. At the long knife, a portion of the jet impinges on the knife surface and is redirected into the chamber above the jet causing unsteady re-circulation there. This is shown as

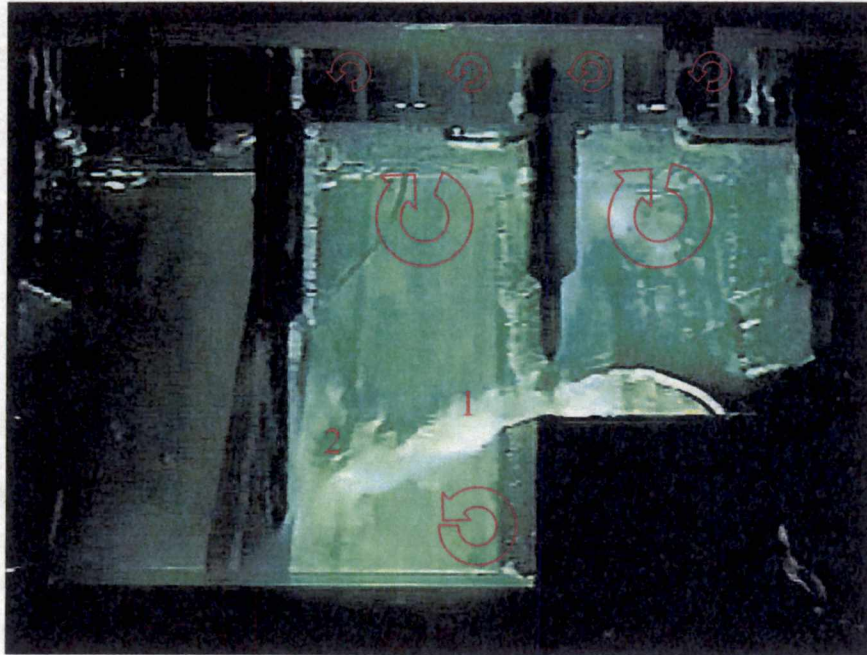


Figure 4-1 - Flow Visualization, $x/L = -0.190$, $Re = 6000$, View 1

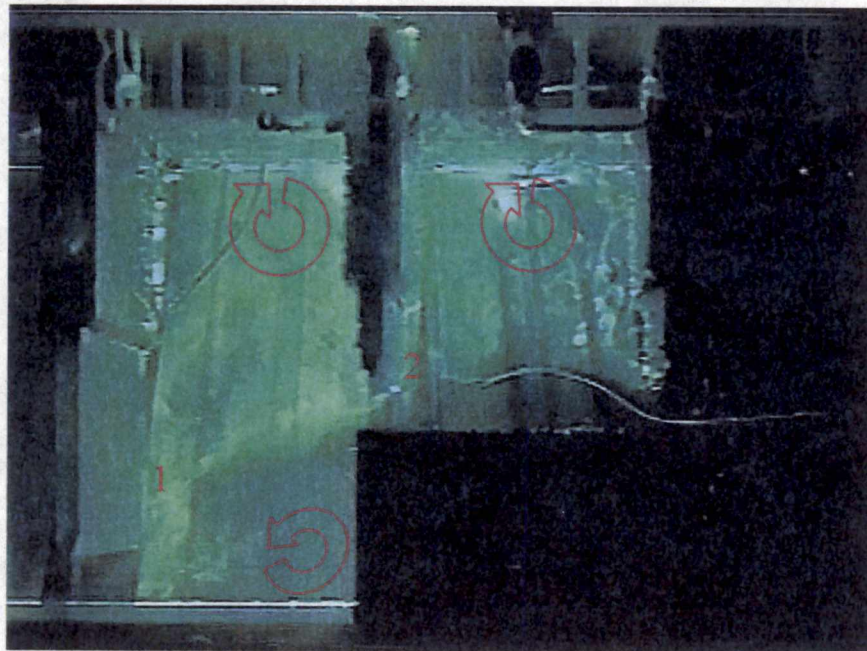


Figure 4-2 - Flow Visualization, $x/L = -0.190$, $Re = 6000$, View 2

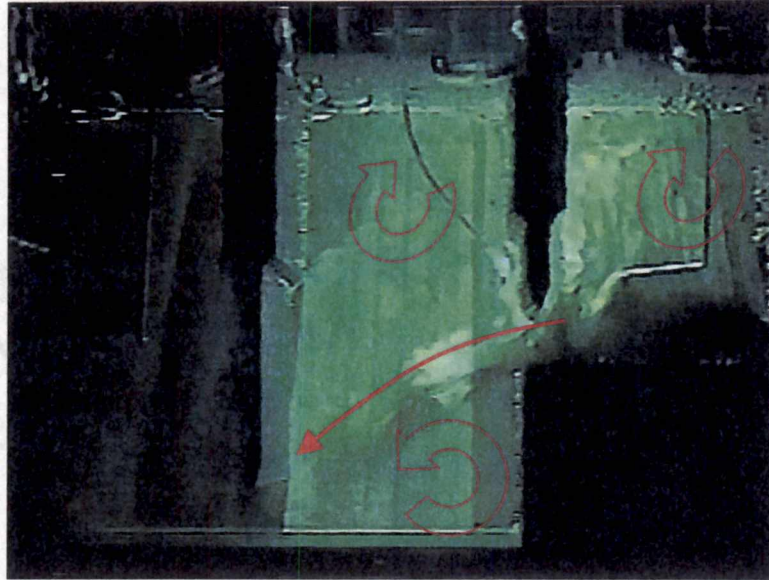


Figure 4-3 - Flow Visualization, $x/L = -0.190$, $Re = 6000$, View 3

area "2" on Figure 4-1. At the knife surface, an area of stagnated flow was visible. This stagnation area was observed to move slightly up and down in an irregular fashion. This was caused by the unsteadiness of the shear layer formed as the fluid jets through the throttling. A portion of the jet fluid carries over through the long knife restriction and into the next chamber, and some flow is re-directed below the jet to re-circulate there. The chamber re-circulation is driven by the viscous effects and shear layers formed between the jet and the slow moving chamber fluid. In Figure 4-2, it can be seen that the stagnation area has moved slightly demonstrating the unsteadiness of the flow. This area is designated as area "1" in Figure 4-2. There is also an area of stagnated flow near the tip of the short knife shown as area "2" in Figure 4-2. Although the corner vortices at the knife roots are not indicated with arrows in succeeding images, they were present in every test, although they were generally weak, poorly defined and not considered to be a major contributor to losses within the seal.

Figure 4-3 shows dye being injected over the second step in the seal. It can be seen that although the flow is much more turbulent than at the seal entrance, the loss mechanisms at this second step in the seal are qualitatively similar to those at the first step. The stagnation area on the face of the 2nd long knife appeared to be larger than that observed on the first long knife (Figure 4-1).

Figure 4-4 shows the chamber re-circulation over the second step. The flow was much more turbulent here than was the case over the first step (Figure 4-1) and therefore the re-circulation “bubble” was not as easily observed.

The flow along the bottom of the seal leading up to the second step is shown in Figure 4-5. Since the solid surfaces of the step and bottom of the seal force the velocity of the fluid to be zero at these walls, the fluid path must “bend” upward. In the corner area, there is an area of weak re-circulation.

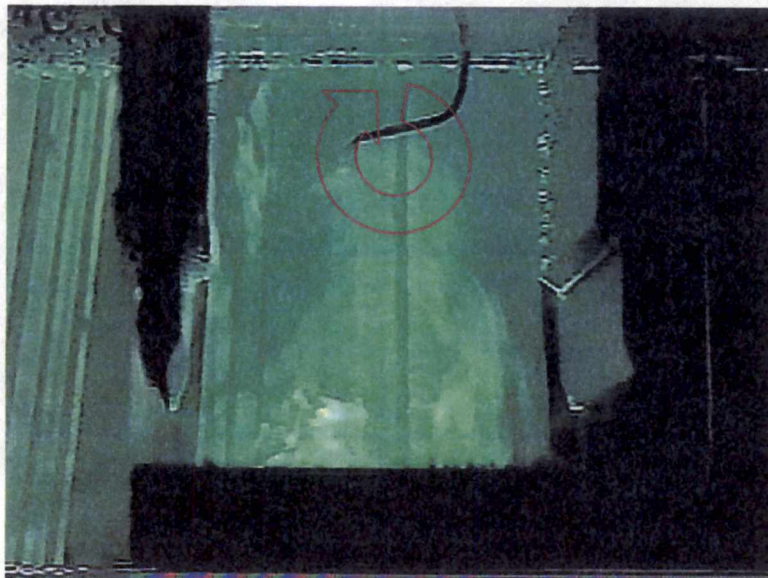


Figure 4-4 - Flow Visualization, $x/L = -0.190$, $Re = 6000$, View 4

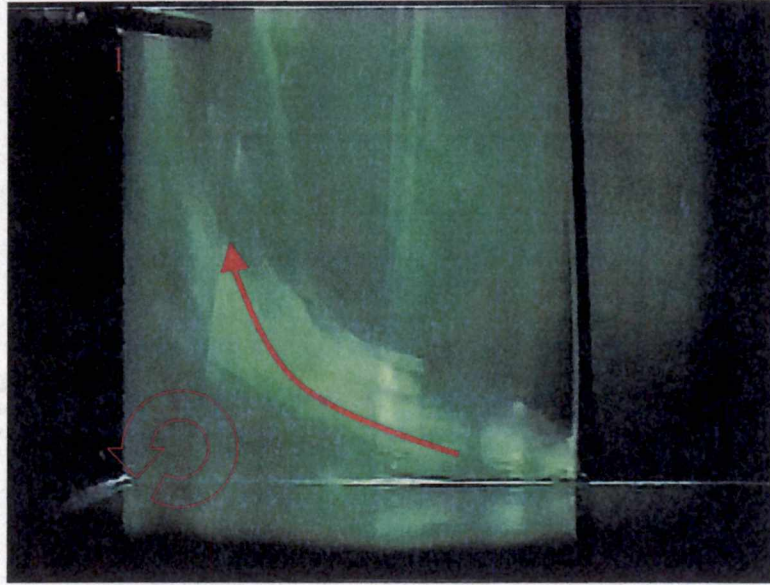


Figure 4-5 - Flow Visualization, $x/L = 0$, $Re = 6000$

In Figures 4-6 and 4-7, each of the steps has been shifted so as to place a knife further downstream of the leading edge of the step, i.e. at $x/L = 0.213$. By direct comparison to Figures 4-1 to 4-5 it can be seen that the bubble that formed over the step has been greatly reduced in size. The presence of the knife after the leading edge of the step forces the streamlines to bend downward rather than allowing the fluid to jet upward into the chamber. Only a small recirculation zone can be seen as the dye traverses the leading edge area of the step. It is worth noting that the flow in this area, as indicated by the arrow in Figure 4-5 is forced to turn rapidly to climb the face of the step. At the top leading corner of the step (area "1" in Figure 4-5) the flow is forced to turn rapidly again to continue over the step. These rapid changes of direction and the resulting areas of stagnated flow cause energy losses that increase the sealing ability of the seal. Figure 4-7 shows the flow visualization in the area around the second seal step. At the short knife immediately following the step the fluid has an effectively larger area to pass through as compared to the case depicted in Figures 4-1 to 4-5.



Figure 4-6 – Flow Visualization, $x/L = 0.213$, $Re = 6000$, View 1



Figure 4-7 - Flow Visualization, $x/L = 0.213$, $Re = 6000$, View 2

As energy losses are directly related to throttling size this section of the seal is likely made less effective by the axial change in step location. Although changing the axial location of the knives over the steps has modified the flow to some extent, it can be seen that the overall location and sense of the chamber re-circulation areas remain constant. The effect of increasing the x/L parameter on the flow beyond the step is shown in Figure 4-7. The fluid jet leaving the long knife (area "1" in Figure 4-7) has a relatively large kinetic energy; since the next step ("2" in Figure 4-7) is now closer to the throttling point, the jet retains a higher amount of kinetic energy as it is forced to rapidly turn at the step face, thus increasing losses.

Finally, in Figures 4-8 and 4-9, the steps have been positioned such that the knives are located even further downstream of the leading edge of the steps, at $x/L = 0.425$. The features observed in the $x/L = 0.213$ case are even more pronounced. Because the steps have been shifted in the downstream direction, the turbulent jet leaving the throttling over the first step (area "1" in Figure 4-9) has a longer distance to travel before reaching the first long knife, designated as "2" in Figure 4-9.

Over this greater distance, turbulence in the jet has more time to dissipate energy through viscous effects. Also the jet widens to form a larger stagnation area, shown as "3" in Figure 4-9. Leaving the throttling at the long knife, the jet must make two rapid turns to continue over the step. These changes combine to increase losses from the initial case of $x/L = 0$.

Figure 4-10 shows a generic sketch of the main flow structures visible in the flow visualization. The major loss mechanisms observed in the flow visualization study are shown:

- (a) viscous dissipation losses in the turbulent jets at the throttlings;
- (b) viscous losses as the chamber vortices are driven by the shear flow;
- (c) losses at stagnation areas as the flow is stagnated in a non reversible process; and
- (d) losses incurred as the fluid makes sudden sharp changes in direction.



Figure 4-8 - Flow Visualization, $x/L = 0.425$, $Re = 6000$, View 1

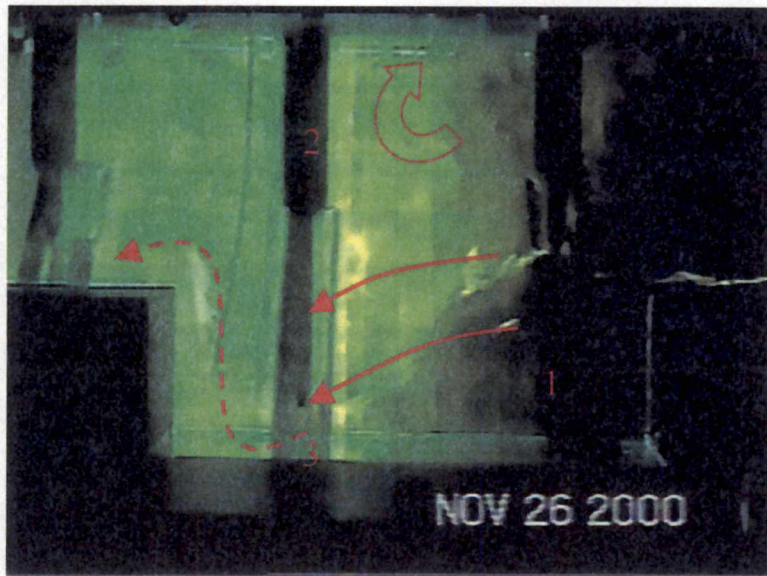


Figure 4-9 - Flow Visualization, $x/L = 0.425$, $Re = 6000$, View 2

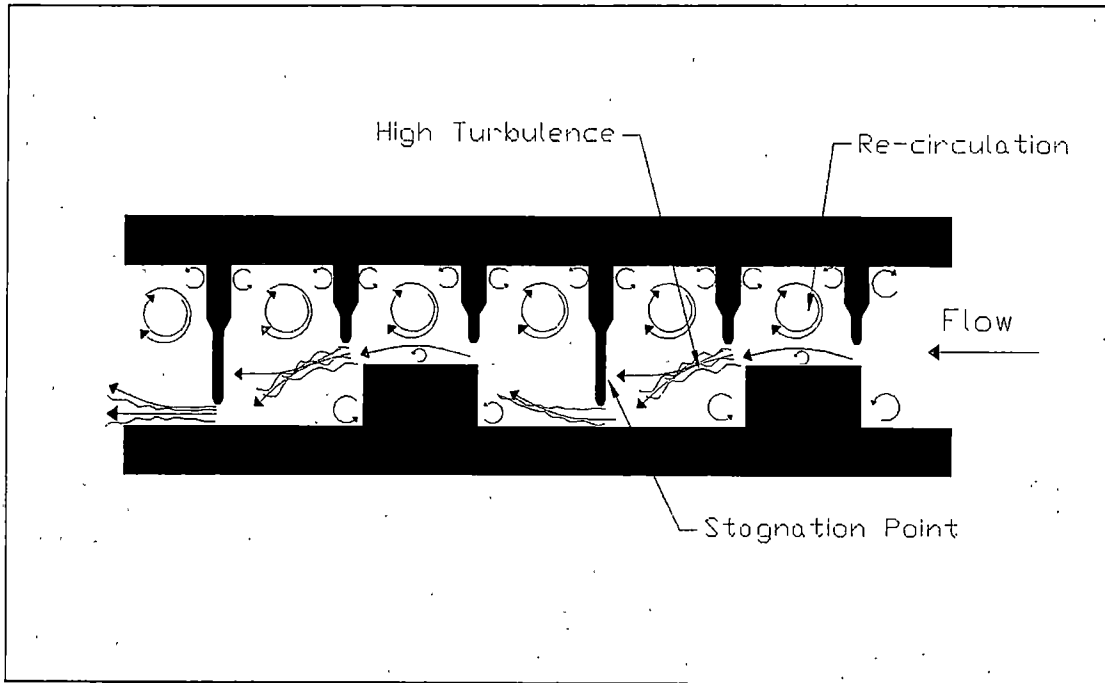


Figure 4-10 – Sketch of Main Labyrinth Flow Features

Based on results of the flow visualization study, it appears that desirable modifications to the baseline seal should focus on increased flow stagnation, greater turbulence generation, and more dramatic turning of the flow streamlines.

FLOW MEASUREMENTS IN THE 2-D AIR MODEL

Configuration A – Baseline

Figures 4-11 to 4-15 show results obtained during 2-D airflow tests of the baseline configuration. The leakage of the seal, expressed by the flow parameter and the seal discharge coefficient (Figures 4-11 and 4-12 respectively), generally decreases as the knife over each step travels towards the center of the step. This observation corresponds with results published in the literature, Miyake and Duh¹⁹. Figures 4-11 and 4-12 show that leakage at $x/L = 0.383$ is slightly less than at $x/L = 0.511$.

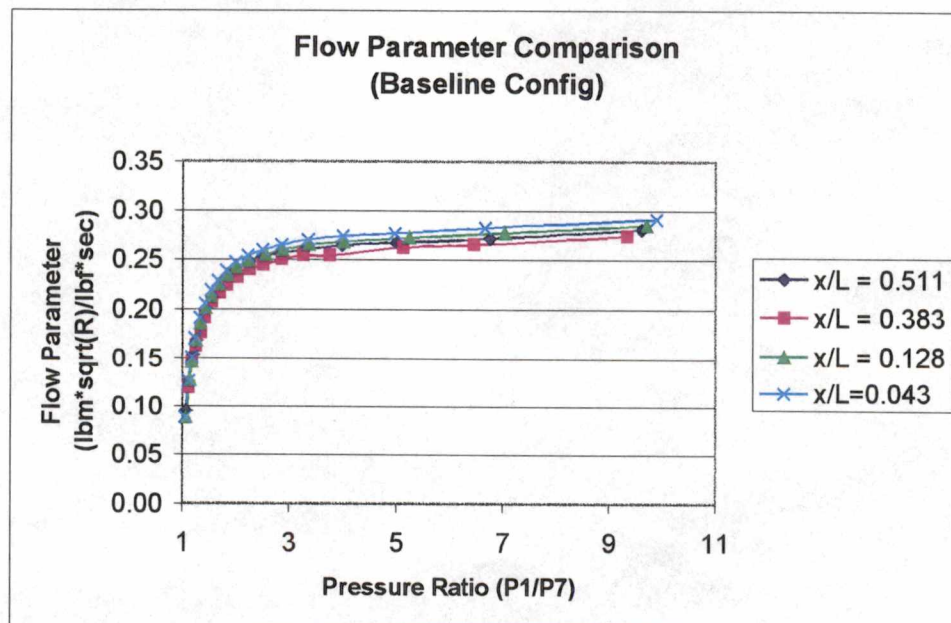


Figure 4-11 - Flow Parameter (Configuration "A")

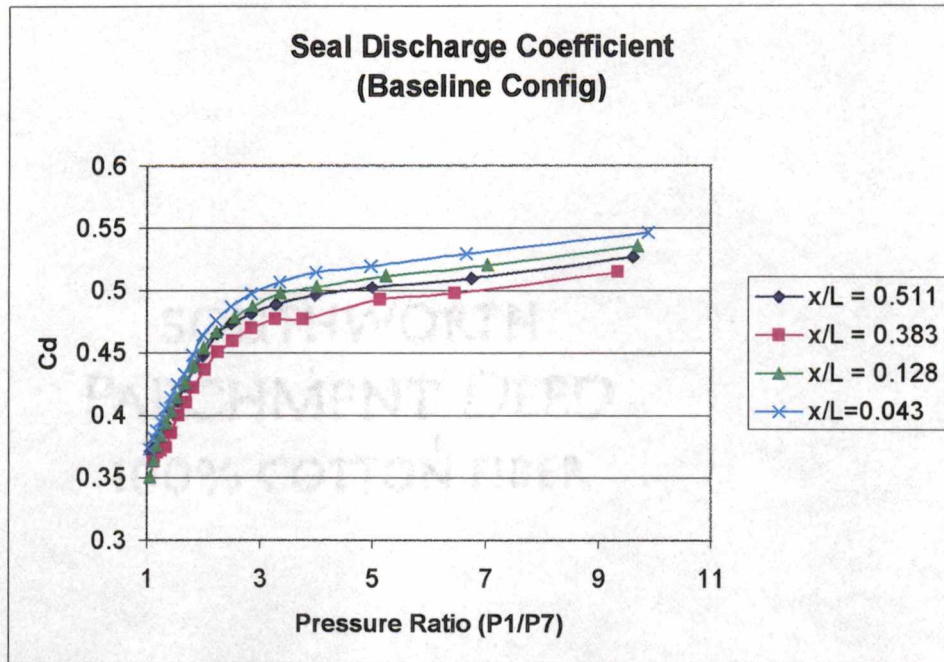


Figure 4-12 – Seal Discharge Coefficient (Configuration “A”)

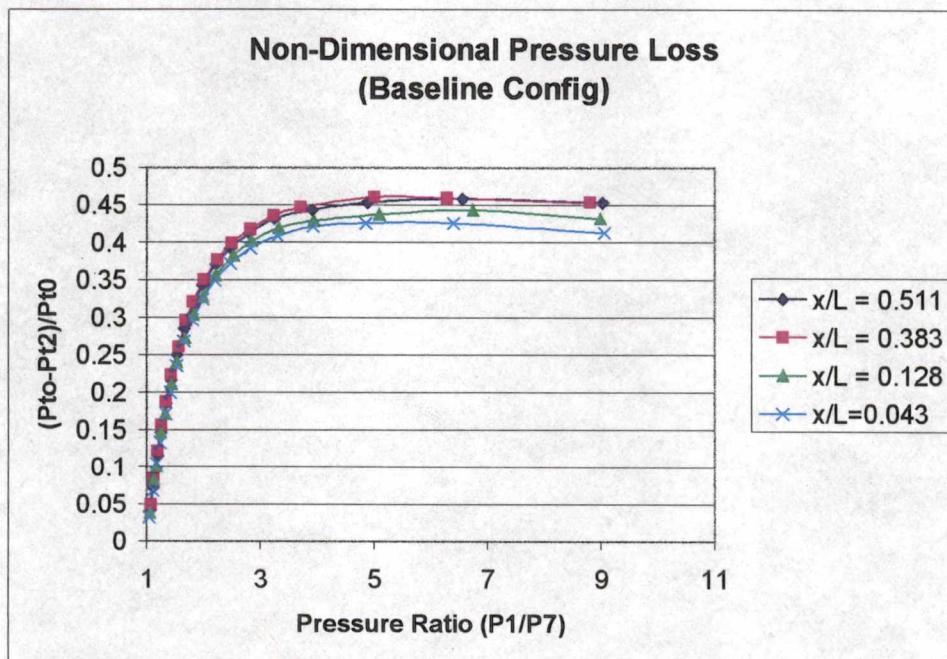


Figure 4-13 – Measured Non-Dimensional Pressure Loss (Configuration “A”)

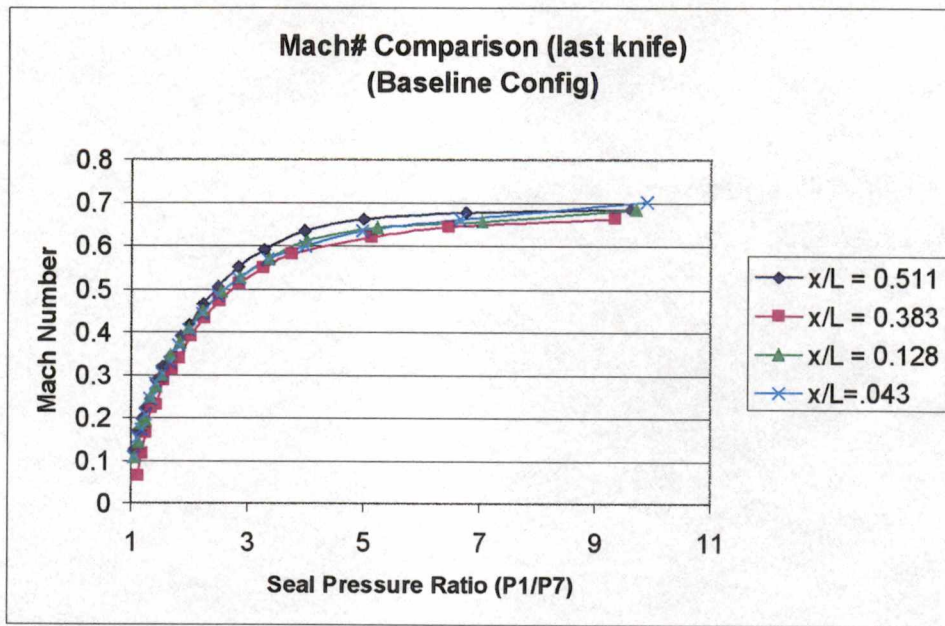


Figure 4-14 – Calculated Exit Mach Number (Configuration “A”)

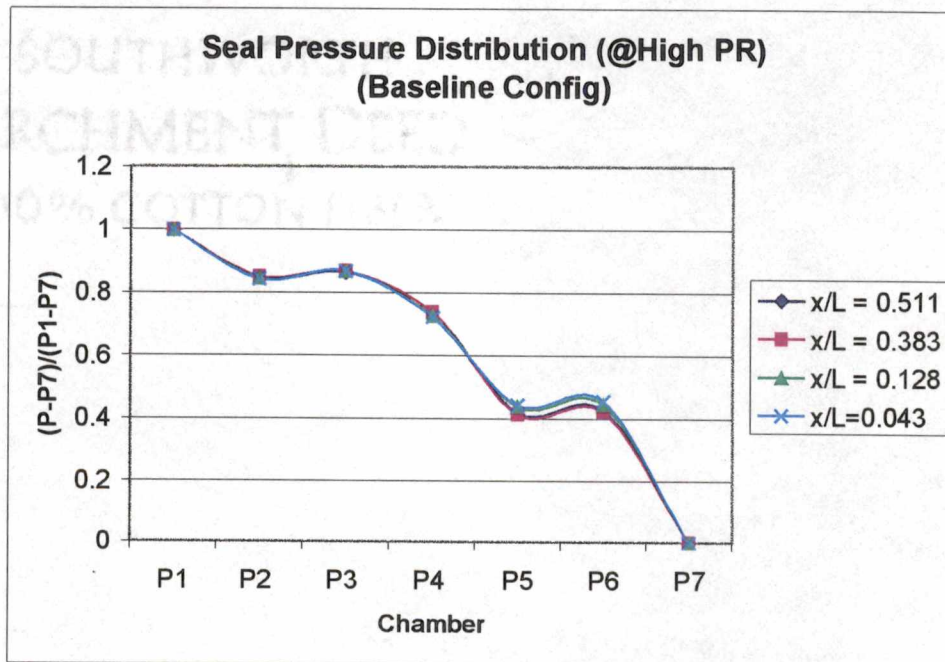


Figure 4-15 – Seal Static Pressure Distribution (Configuration “A”)

It is likely that between these two knife locations, the improvement gained by having the upstream knife approach a centered position on the step is offset by the increased opening between the step and the knife downstream.

In Figure 4-15, the non-dimensionalized static pressure distribution through the seal is plotted. The overall trend shows that the static pressure decreases through the seal, but there is a small static pressure recovery from P_2 to P_3 and for the geometrically analogous (as shown in Figure 3-6) P_5 to P_6 . This can be explained by considering that the air leaving chamber 2 of the seal is expanding into a much larger chamber where the velocity will decrease; also, the flow impinges against the large knife in its path creating a small region of stagnation flow which leads to a corresponding rise in static pressure.

Overall, the results obtained from the baseline configuration were in agreement with the physical understanding of the seal flow as depicted by flow visualization. Appendix A provides more complete results of these tests including comparisons with the models of Egli, Kearton & Keh and Miyake & Duh. However, Figure 4-16 is included here for illustrative purposes. It can be seen that the plot of flow parameter vs. seal pressure ratio obtained during this study follows a trend similar to the Egli, and Kearton & Keh models. The Miyake empirical equation is only valid for a limited Reynolds number range as shown in Figure 4-16. The under-prediction of the mass flow by the Egli and Kearton & Keh methods is likely due to the underlying assumption of no kinetic energy carry-over through the seal that is the basis of their respective analyses. The experimental flow parameter tends to increase beyond the seal choking point as predicted by Kearton and Keh's work.

Configuration B – High Step

Figures 4-17 to 4-21 show the results of increasing the model step height by 0.250" while maintaining a constant throttle clearance.

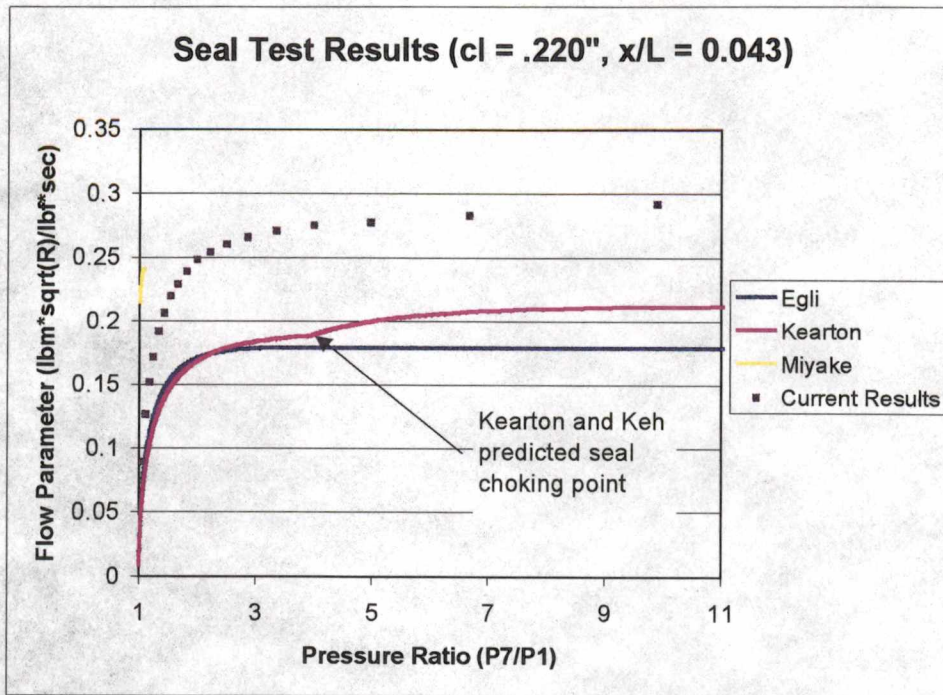


Figure 4-16 – Comparison with Models (Configuration "A")

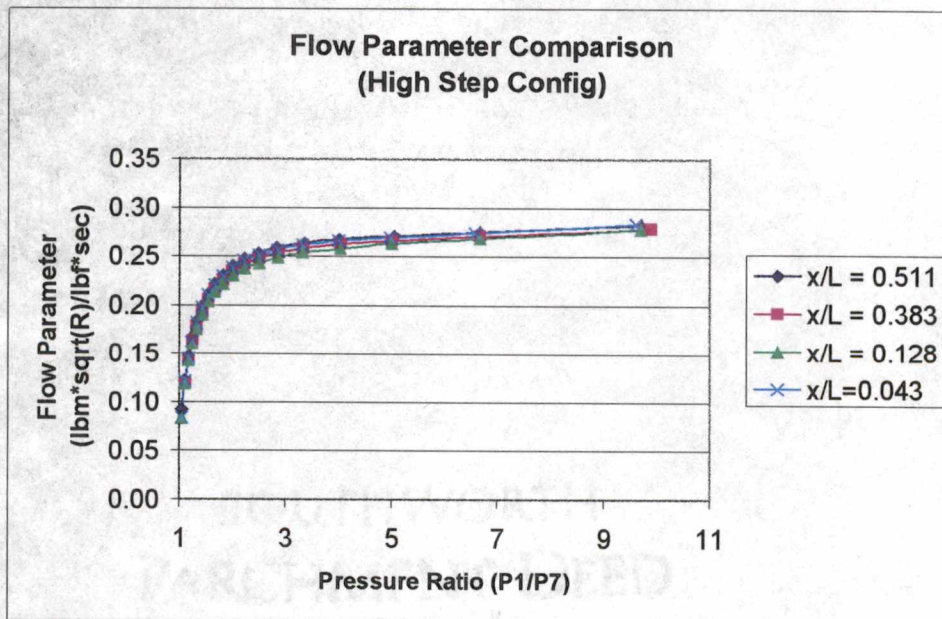


Figure 4-17 - Flow Parameter (Configuration "B")

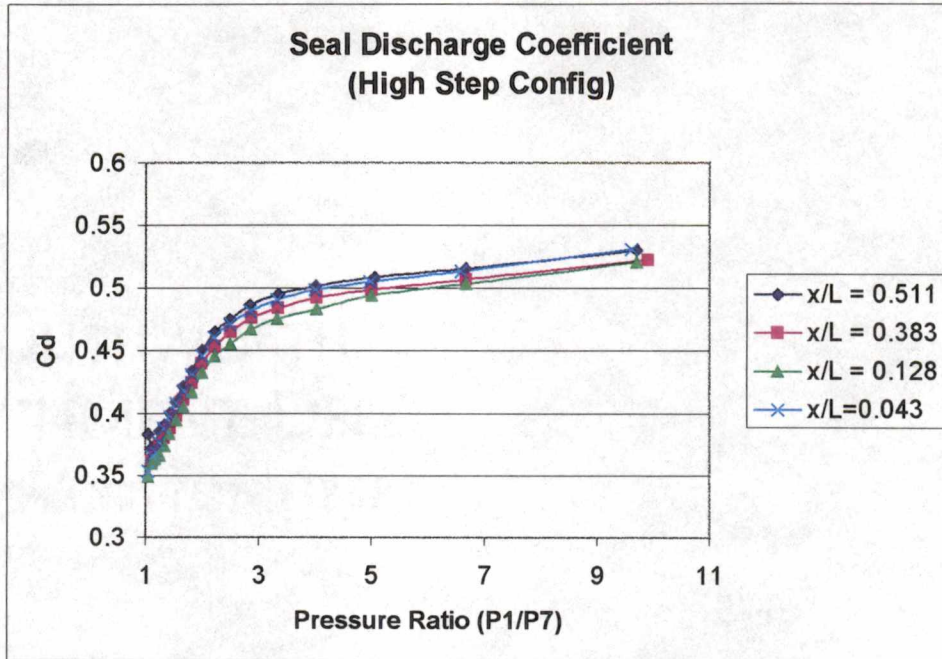


Figure 4-18 - Seal Discharge Coefficient (Configuration "B")

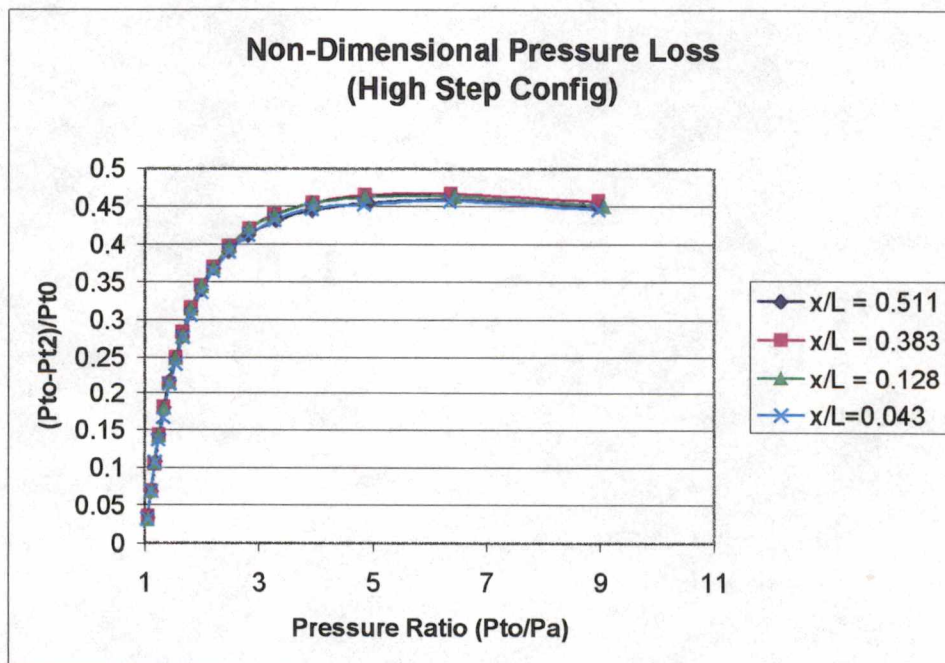


Figure 4-19 - Measured Non-Dimensional Pressure Loss (Configuration "B")

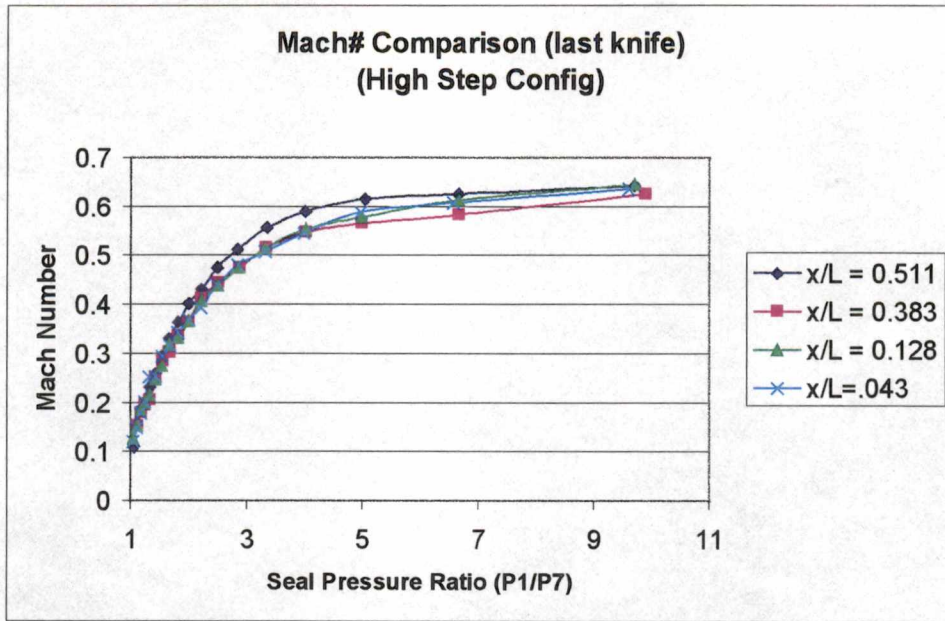


Figure 4-20 – Calculated Exit Mach Number (Configuration “B”)

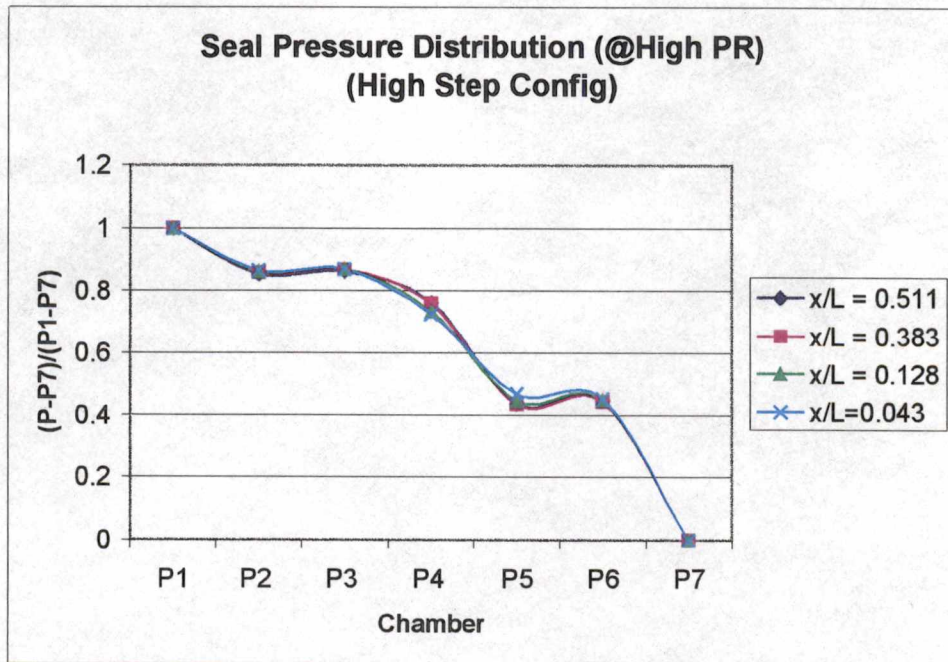


Figure 4-21 - Seal Static Pressure Distribution (Configuration “B”)

As compared to the baseline configuration, there is a slight reduction in leakage flow at given pressure ratios, averaging 2.4%. In this configuration, the seal demonstrated a different trend with respect to leakage as a function of step axial location. Maximum leakage was generally obtained with the upstream knife near the step midpoint. In addition, comparison between the high step and baseline configurations shows that there are minimal changes in leakage flow with axial changes in step location. This is of special interest for practical application, since labyrinth seals in use operate in various axial positions due to loading and thermal effects. A seal that demonstrates consistent leakage regardless of axial location would be of benefit. Addition of the higher step forces the flow streamlines to bend to a greater degree over a set distance than the baseline design as they travel over the step.

Configuration C – 15 Degree Slant Knives

Inclining the knives 15 degrees into the flow while maintaining throttling clearance also reduced leakage from that obtained with the baseline configuration. Figures 4-22 to 4-26 show the measurement results obtained with this design. Overall, this modification resulted in an average leakage reduction of approximately 5.4% from the baseline. Model limitations prevented testing for all of the step axial locations as for the baseline. The x/L ratio of 0.511 could not be obtained. This modification likely increased flow stagnation as the flow impinged to a greater degree on the long knives in the seal. Additionally, a portion of the flow is forced to turn around the tip of the knives rather than jetting past it. A portion of the flow generates an increased amount of re-circulation as it is directed by the knife inclination into the upper chambers of the seal. These changes to the flow structures result in increased losses compared to the baseline geometry, thereby decreasing flow through the seal at a given pressure ratio. In Figure 4-25, it can be seen that the seal exit Mach number has reached supersonic values at the higher seal pressure ratios. As detailed previously, the final total pressure and static pressure of the seal were measured at a fixed point under the last straight knife in the baseline configuration.

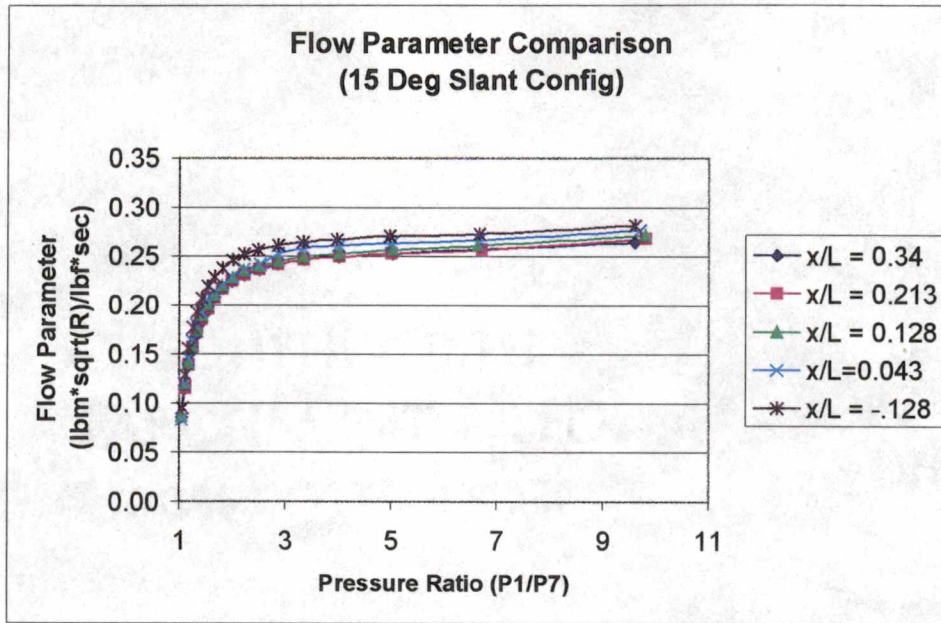


Figure 4-22 – Flow Parameter – (Configuration “C”)

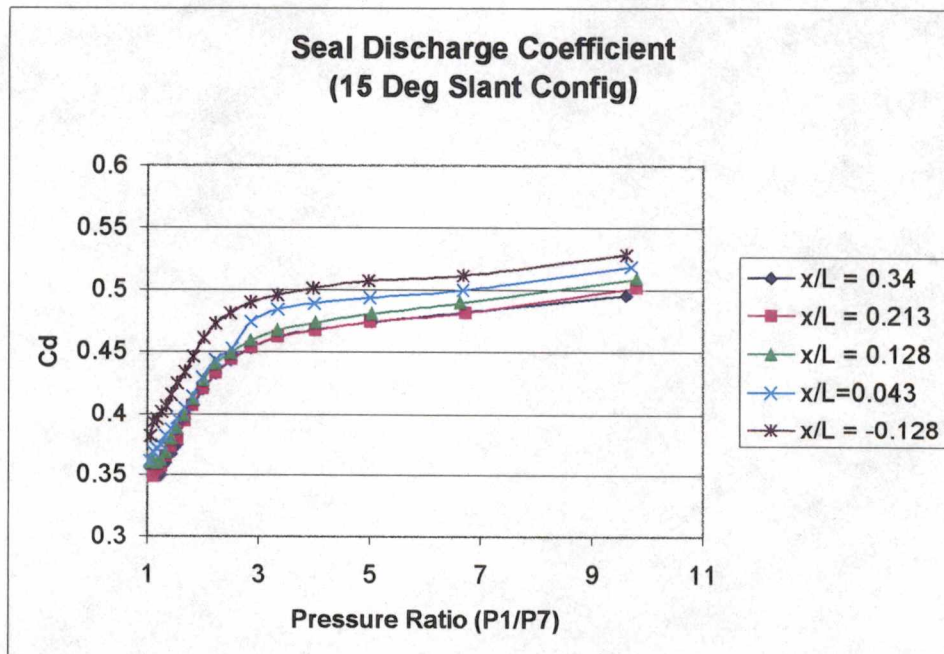


Figure 4-23 - Seal Discharge Coefficient (Configuration “C”)

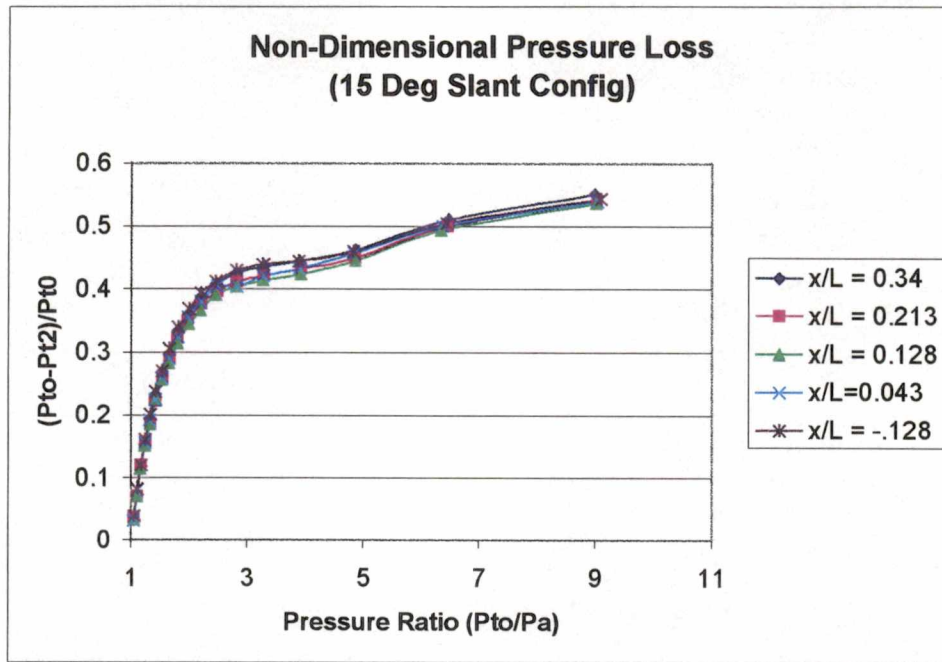


Figure 4-24 – Measured Non-Dimensional Pressure Loss (Configuration “C”)

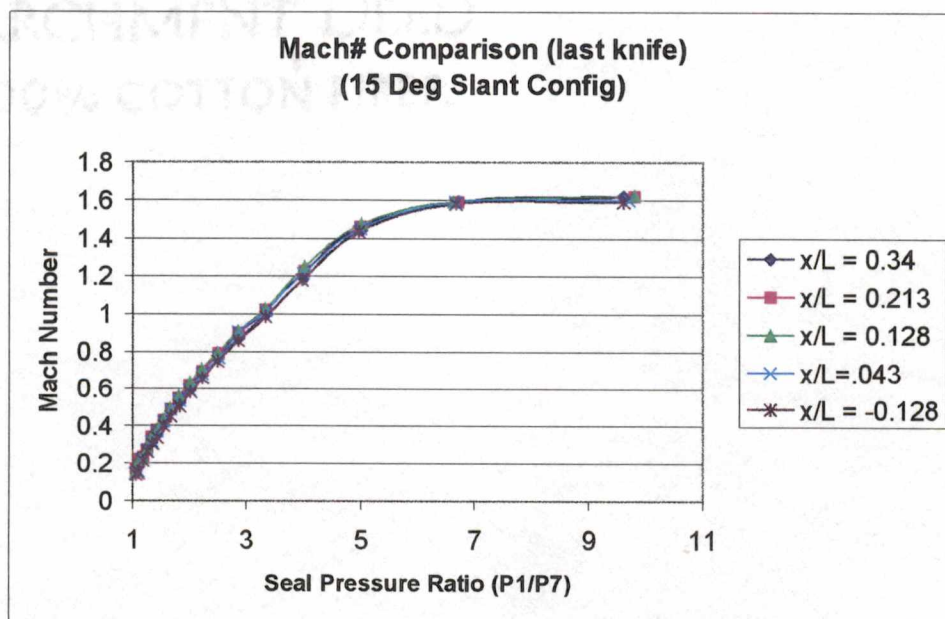


Figure 4-25 – Calculated Exit Mach Number (Configuration “C”)

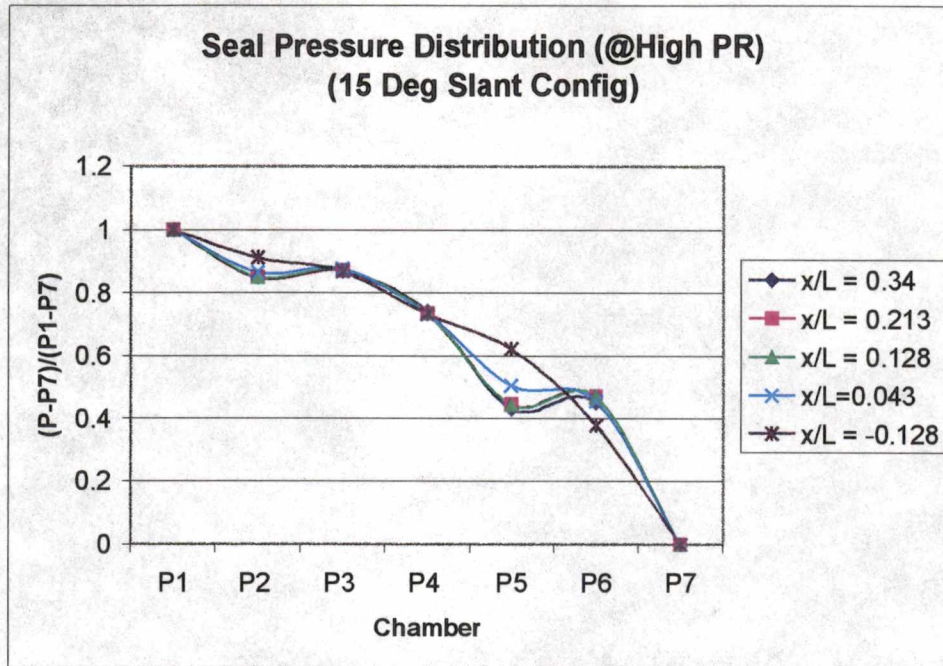


Figure 4-26 - Seal Static Pressure Distribution (Configuration "C")

Inclining the knives effectively moved this measurement point downstream of the minimum area point of the flow through the last slanted throttling station. Flow through this throttling, physically similar to a convergent-divergent nozzle, reaches locally supersonic speeds downstream of this minimum area point.

In Figure 4-26, the seal pressure distribution for the case of $x/L = -0.128$ is of some interest. This axial location provided the maximum obtained leakage in the 15-degree slant knife configuration. In this position, the steps were located between knives, immediately up and downstream of the step – this effectively increased the throttle size at each location, reducing turbulence and thus decreasing seal effectiveness. Figure 4-26 shows that in the $x/L = -0.128$ case, the local static pressure in the chambers does not follow the same pattern as the other axial step locations in that it does not rapidly decrease and then rise again.

Configuration D – 30 Degree Slant Knives

In a similar manner as the preceding case, all knives were inclined into the flow at the angle of 30 degrees from the vertical. Again, because of model limitations, not all x/L locations achievable with the baseline configuration could be tested with all knives inclined at 30 degrees; only two step axial locations common with the baseline could be tested. Figures 4-27 to 4-31 show the test results for this configuration. Overall, this configuration performed similarly although slightly worse in terms of leakage for, a given seal pressure ratio and step axial location, to configuration “C” (15 degree slant knives). There is an apparent inconsistency in the calculated exit Mach number for this configuration that is apparent in Figure 4-30. At this test point, a sudden rise in static pressure at the P8 measurement point caused a corresponding drop in the calculated Mach number at a seal pressure ratio of 5. A possible explanation is that, since at that pressure ratio the seal is just beginning to operate in a choked condition, the minimum area point and therefore the point where a Mach wave would occur caused a high static pressure to occur at the location of the static port.

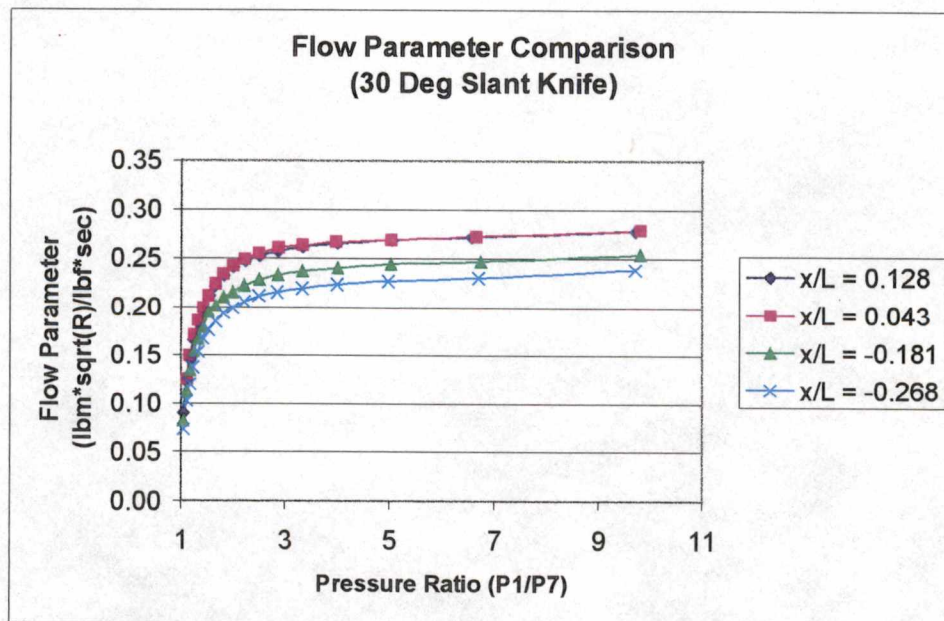


Figure 4-27 – Flow Parameter (Configuration “D”)

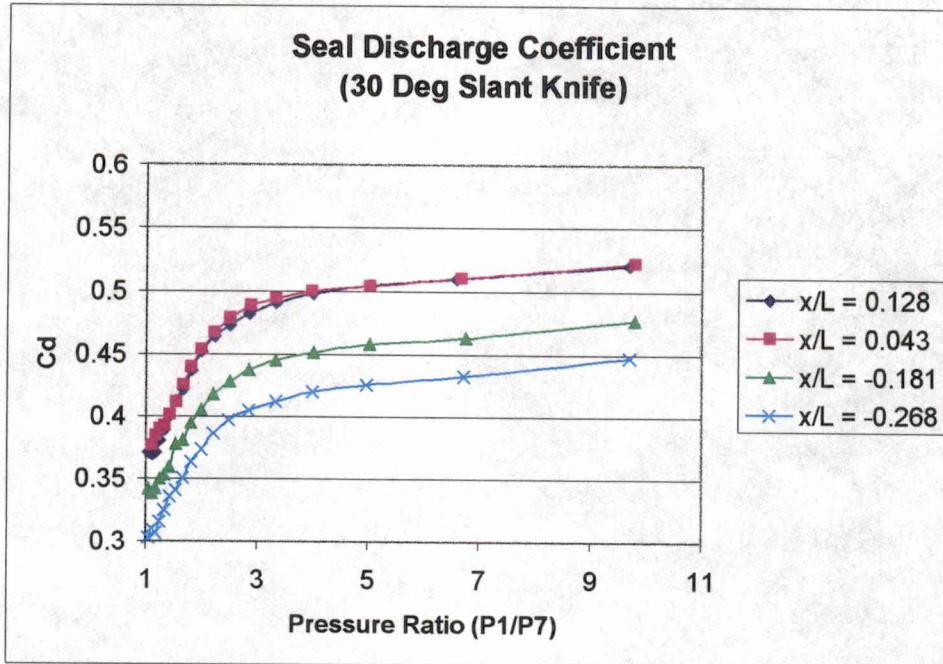


Figure 4-28 - Seal Discharge Coefficient (Configuration "D")

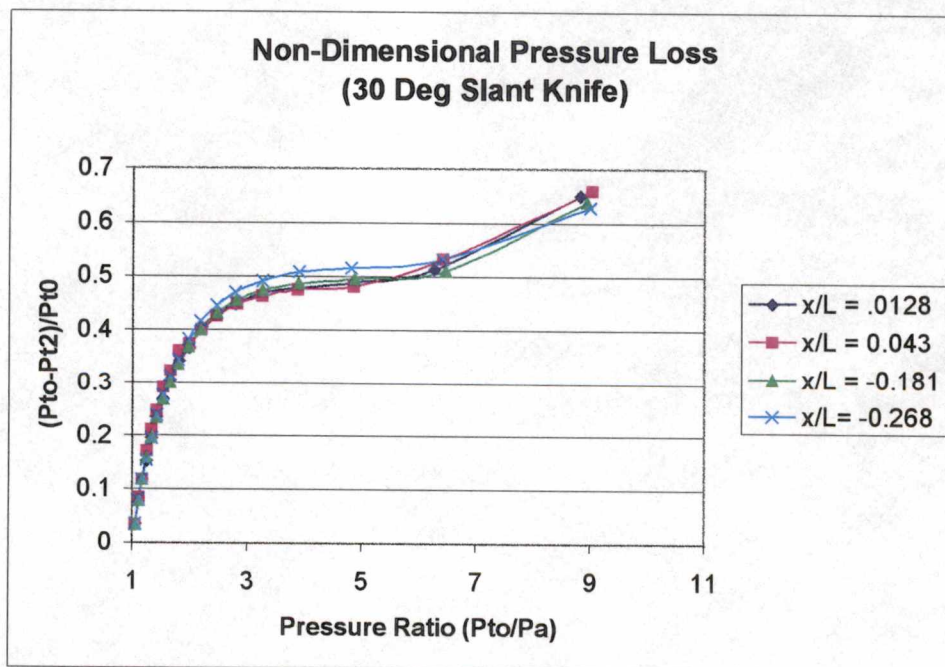


Figure 4-29 – Measured Non-Dimensional Pressure Loss (Configuration "D")

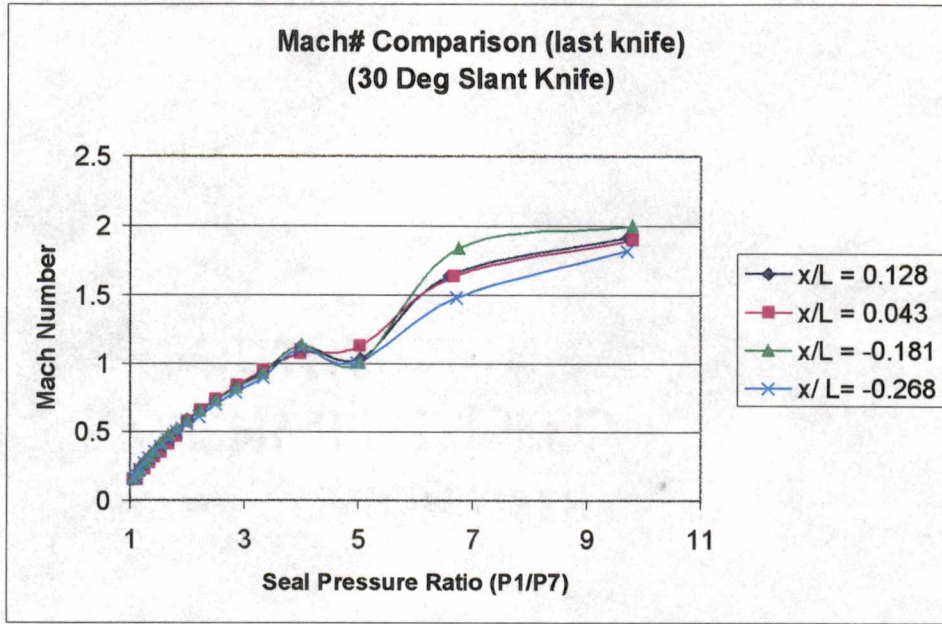


Figure 4-30 – Calculated Exit Mach Number (Configuration “D”)

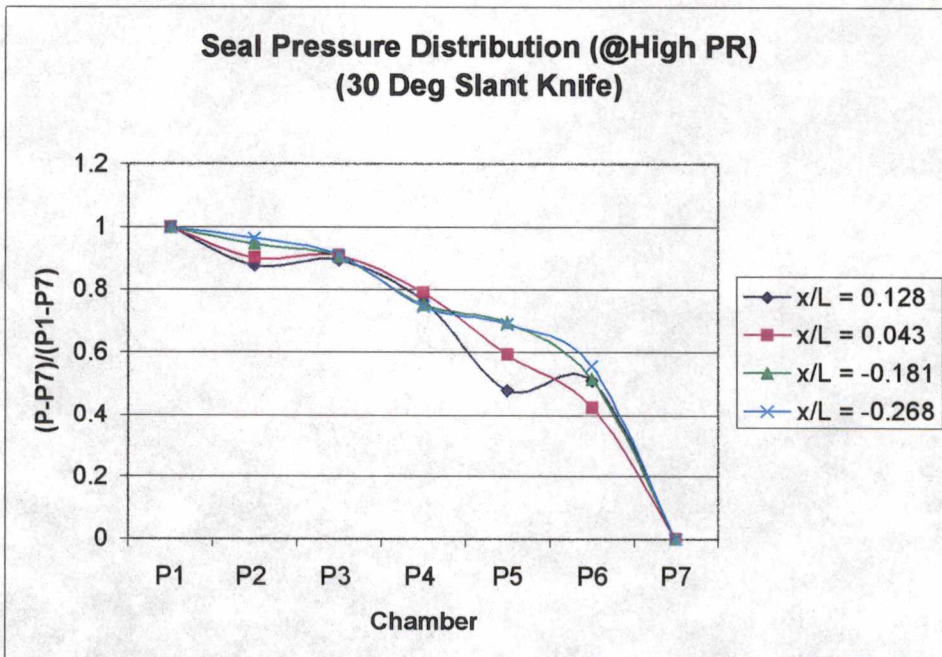


Figure 4-31 - Seal Static Pressure Distribution (Configuration “D”)

Configuration E – Hybrid, 30 Degree Slant Short Knives and Straight Long Knives

In order to investigate the relative effects of slanting only the short knives vs. the long knives, a hybrid configuration was created with two straight long knives, and all short knives inclined 30 degrees into the flow. This configuration showed a slight degradation in leakage performance as compared to the baseline case. It is likely that inclining the short knives makes little difference because the effective blockage presented to the flow is not changed. Because of the apparent inutility of inclining the short knives alone, further variations of this configuration were not explored.

Figures 4-32 to 4-36 show the results obtained testing Configuration “E”. The most improved leakage in this case was obtained at $x/L = -0.268$. This is likely due to the fact that at this axial location, the knife following the reference knife is now located over the step creating another throttling point.

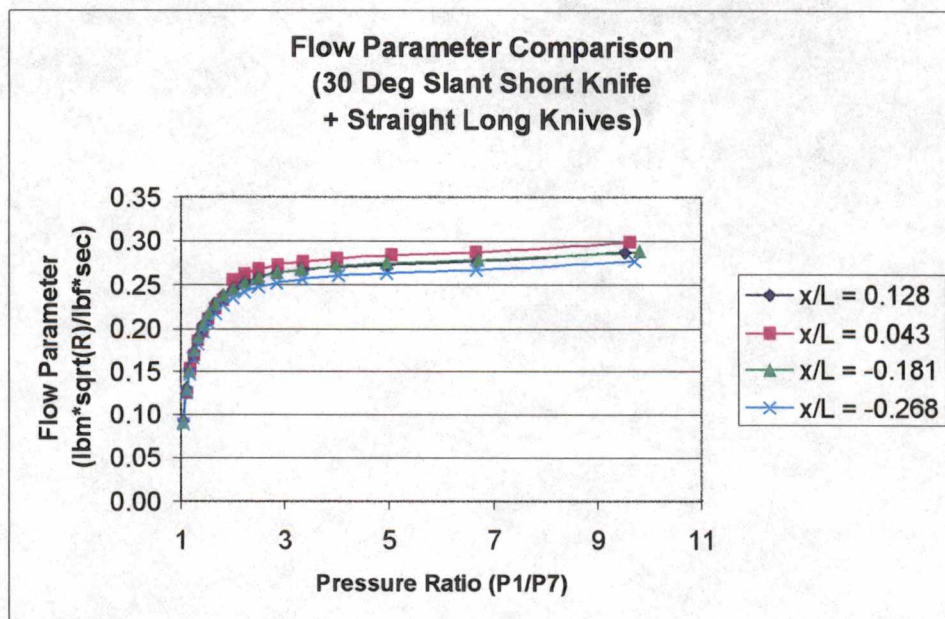


Figure 4-32 – Flow Parameter – (Configuration “E”)

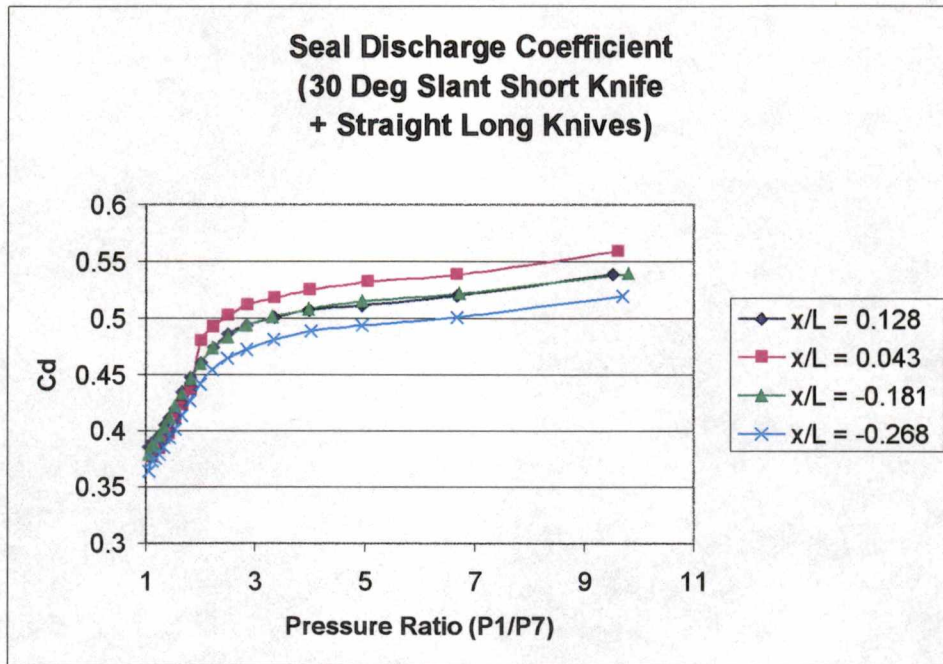


Figure 4-33 - Seal Discharge Coefficient (Configuration "E")

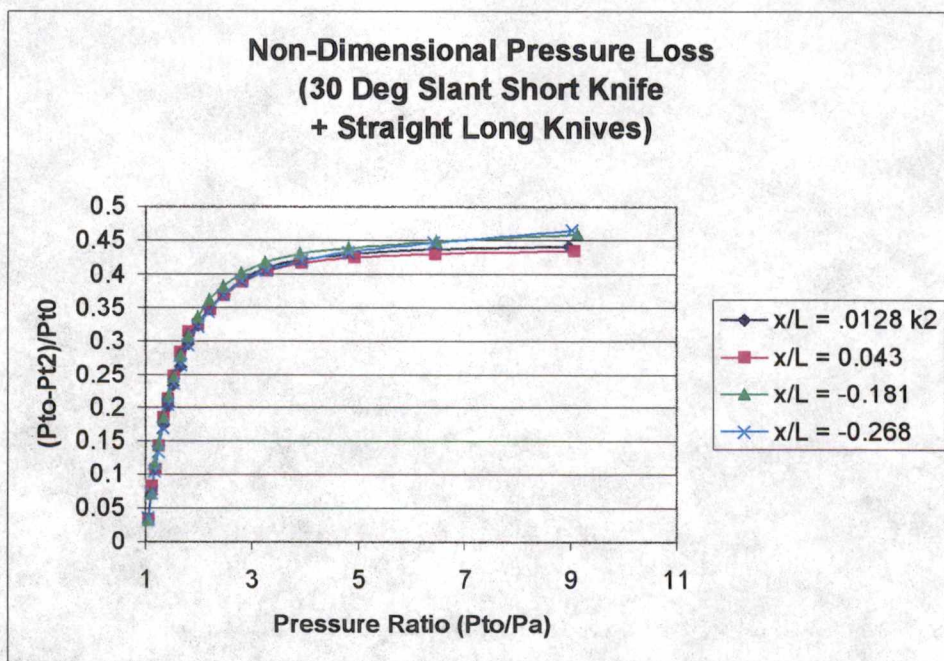


Figure 4-34 – Measured Non-Dimensional Pressure Loss (Configuration "E")

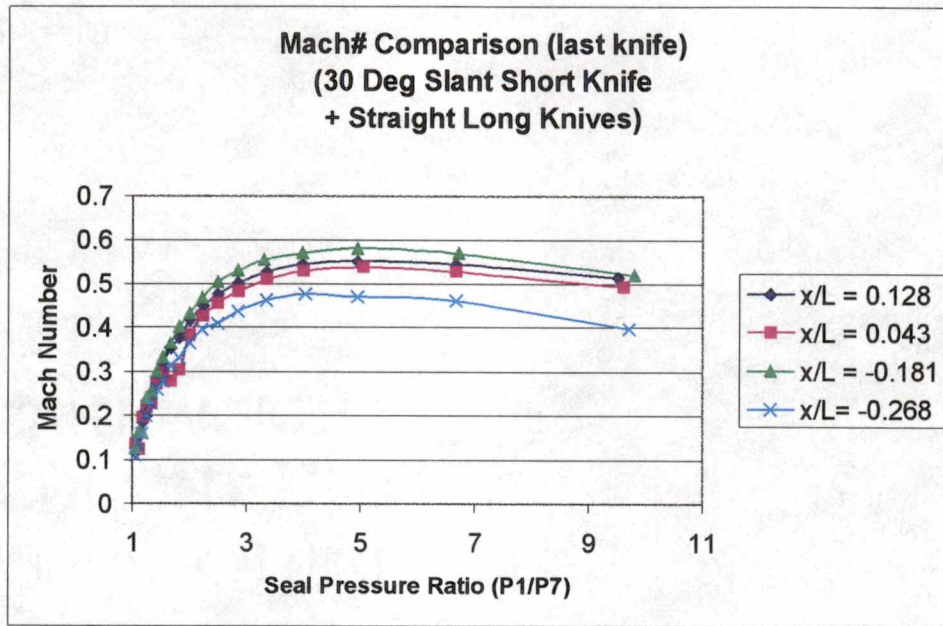


Figure 4-35 – Calculated Exit Mach Number (Configuration “E”)

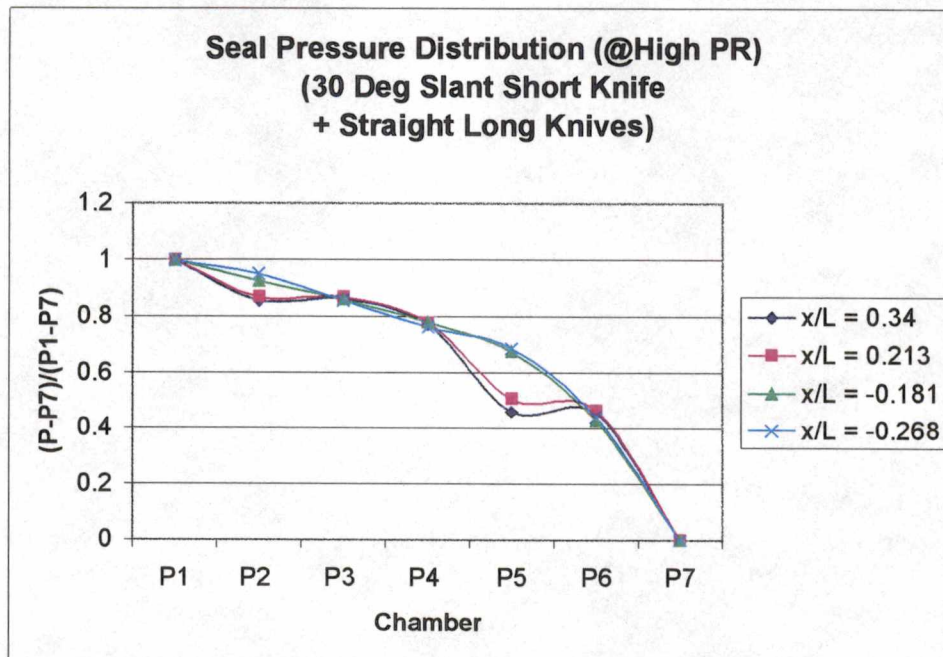


Figure 4-36 - Seal Static Pressure Distribution (Configuration “E”)

Configuration F – Hybrid, High Steps and 15 Degree Slant Long Knives

Based on the results obtained in previous tests, it was surmised that the limited blockage presented to the flow by the short knives made inclining them of limited benefit in reducing leakage. Therefore, the next test involved fixing the short knives and inclining the long knives 15 degrees into the free stream. In addition, the high step configuration was used to capture the benefits obtained from the high step configuration. A significant reduction in leakage as compared to the baseline was realized from the changes. Comparing only equivalent x/L tests, the hybrid Configuration F with high step and 15 degree slant long knives provided an average reduction in leakage of 9.7 %. As was observed in the high step configuration test, the high step made the seal leakage more consistent as the step axial position was varied. Figures 4-37 to 4-41 show the results obtained testing Configuration “F”.

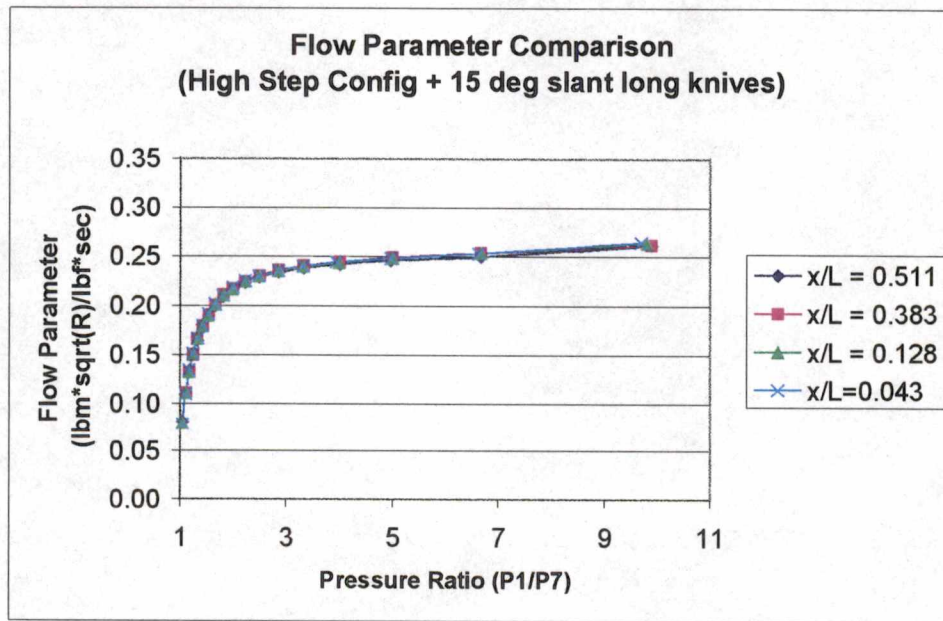


Figure 4-37 - Flow Parameter (Configuration “F”)

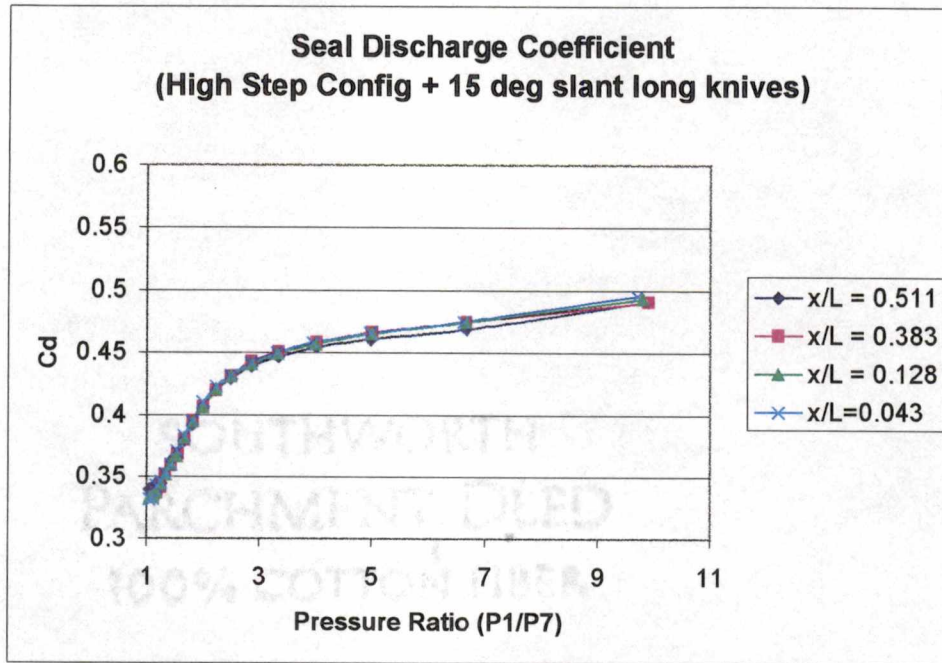


Figure 4-38 – Seal Discharge Coefficient (Configuration “F”)

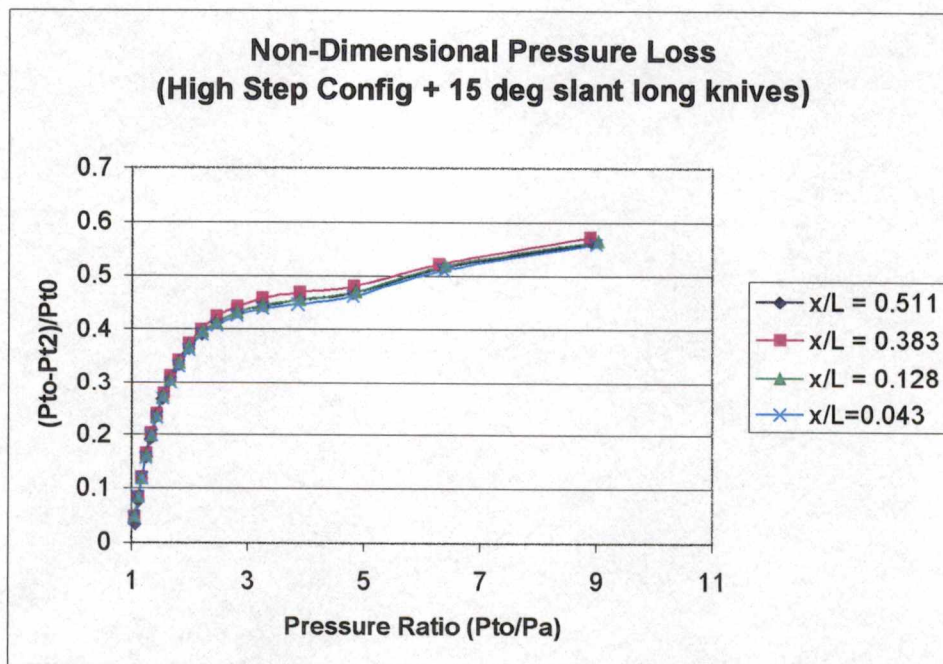


Figure 4-39 – Measured Non-Dimensional Pressure Loss (Configuration “F”)

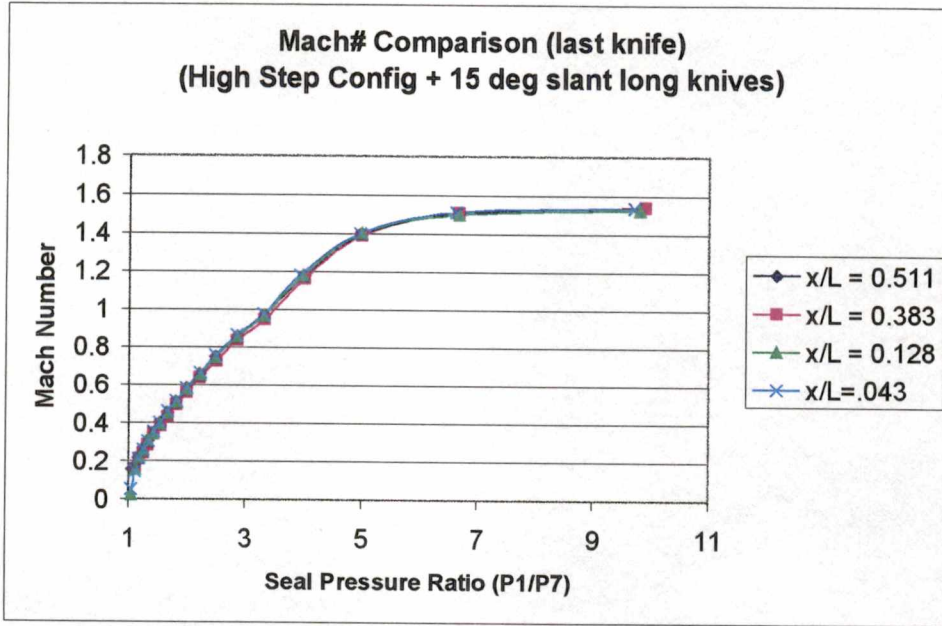


Figure 4-40 – Calculated Exit Mach Number (Configuration “F”)

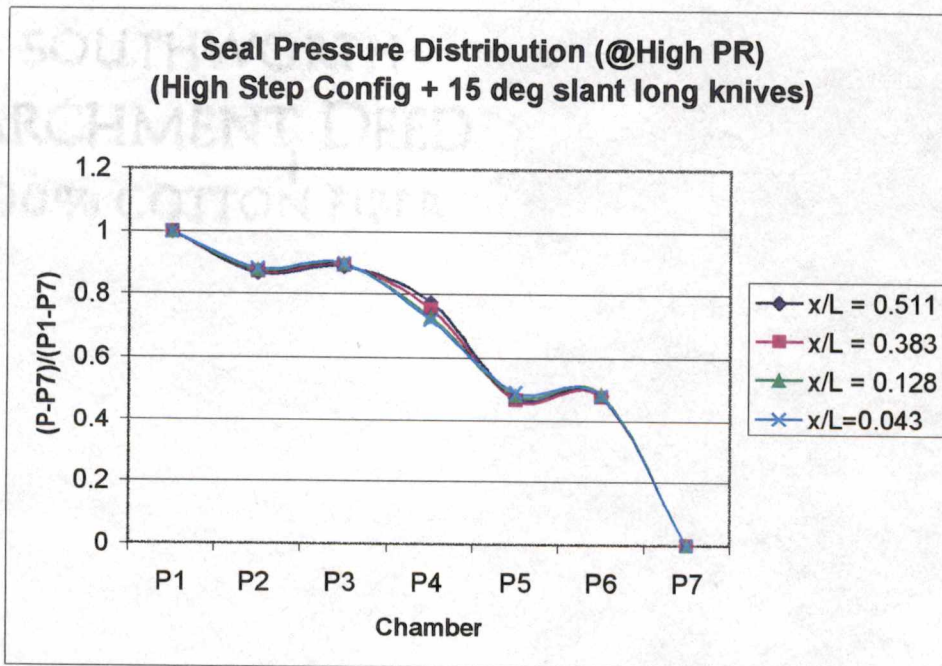


Figure 4-41 - Seal Static Pressure Distribution (Configuration “F”)

Configuration G – Hybrid, High Steps and 30 Degree Slant Long Knives

Following the approximately 10% improvement in leakage performance that was obtained with the high step and 15 degree inclined long knife configuration, the 15 degree long knives were removed and 30 degree long knives were installed. Leakage performance improved considerably over the baseline case (13.8 % on average) with a best performance at $x/L = 0.43$ (17.3 %).

Figures 4-42 to 4-46 show the results obtained from tests carried out on Configuration “G”. Of all seal designs tested, Configuration “G” proved the most effective.

Results show that the best axial step position in this case is $x/L = 0.383$. Of all the configurations tested, this represents the most effective geometry for generating turbulence and flow stagnation. Further optimization of the step height and knife inclination could be accomplished with further testing.

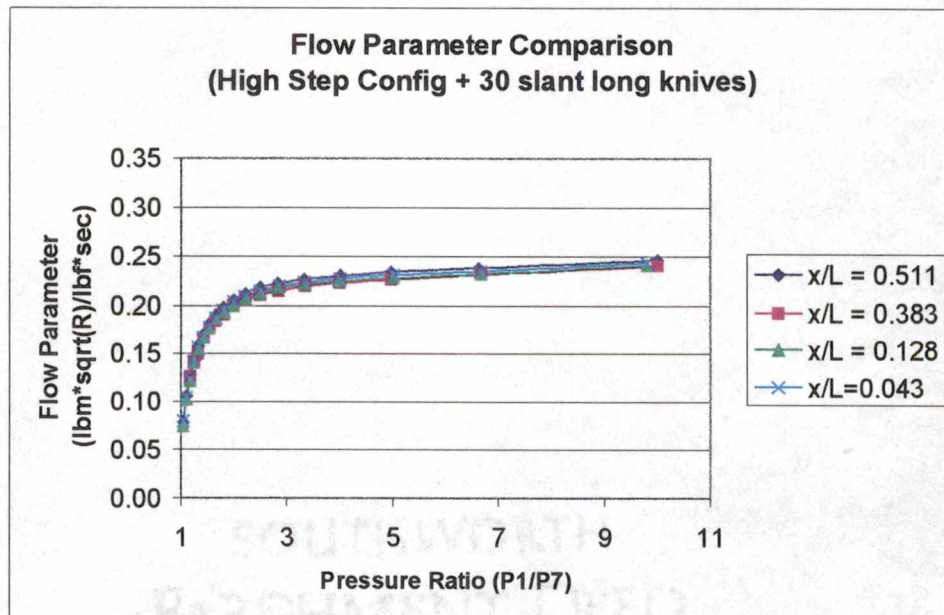


Figure 4-42 - Flow Parameter (Configuration “G”)

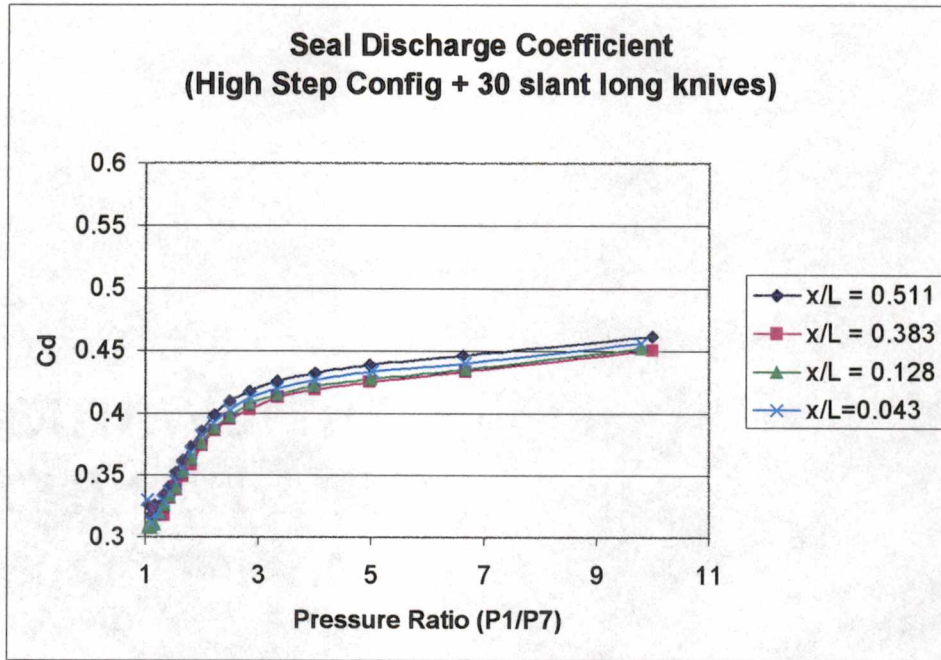


Figure 4-43 - Seal Discharge Coefficient (Configuration "G")

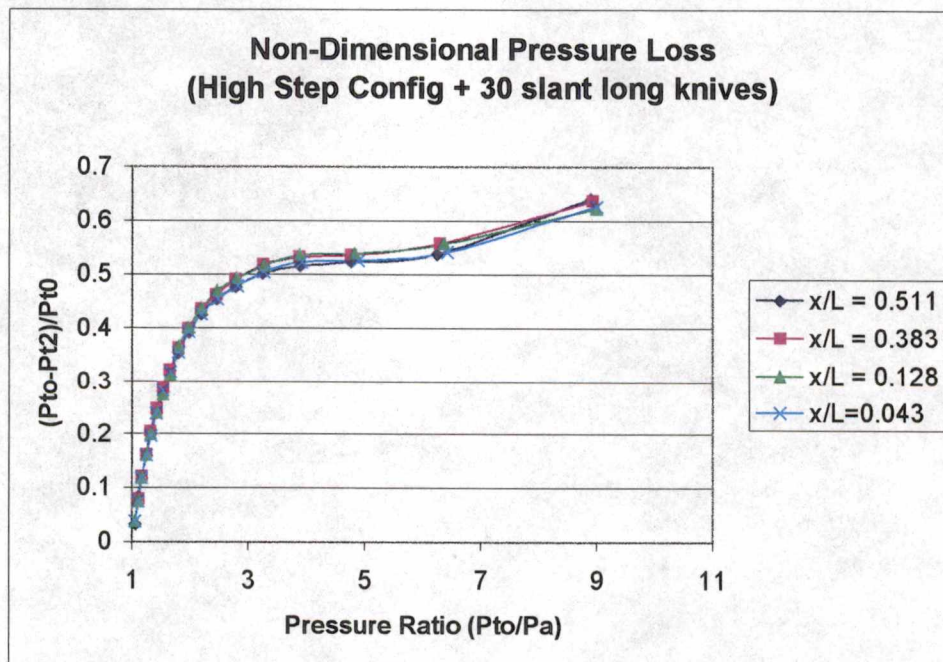


Figure 4-44 – Measured Non-Dimensional Pressure Loss (Configuration "G")

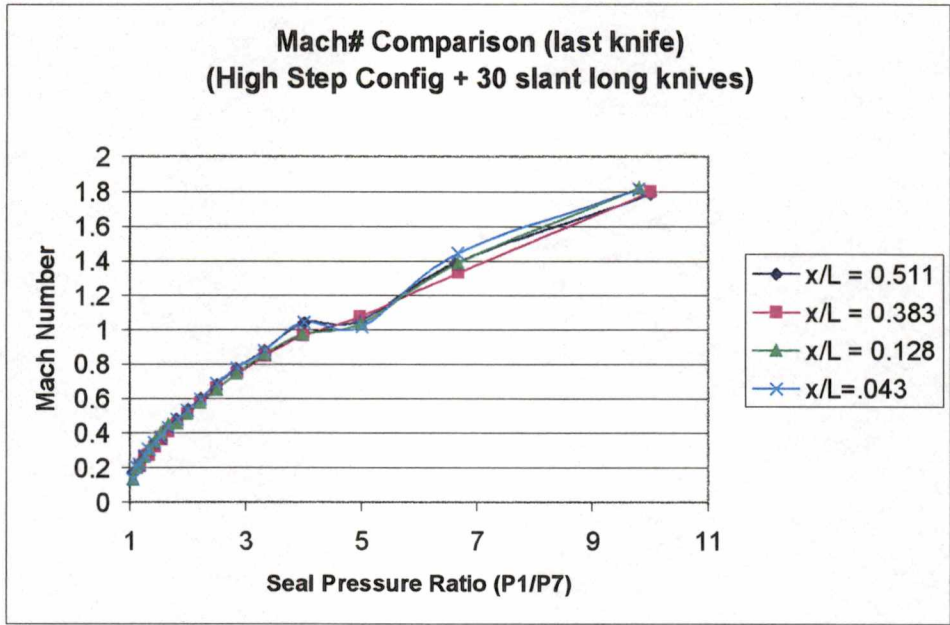


Figure 4-45 – Calculated Exit Mach Number (Configuration “G”)

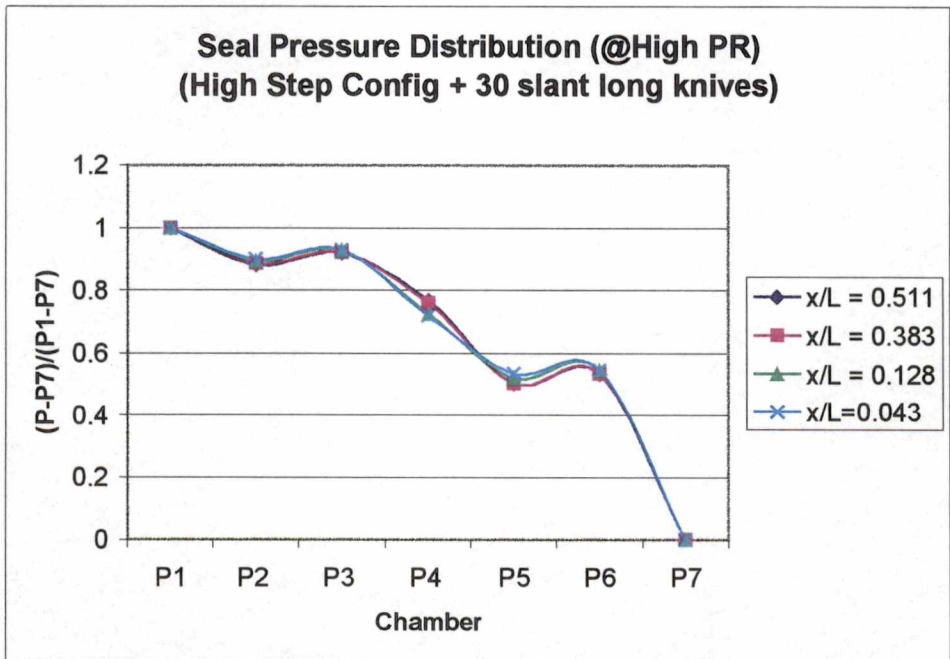


Figure 4-46 - Seal Static Pressure Distribution (Configuration “G”)

Configuration Comparison

Figures 4-47 to 4-54 compare and summarize the leakage performance of the tested configurations at common step axial locations. The best performance was obtained using a combination of the high step configuration with 30 degree slanted long knives. The improvement can be attributed to:

- (a) increased inclination of the slanted knives causing increased circulation in these seal chambers, increased flow stagnation areas at the knives, and greater bending of the flow streamlines around the knife tips;
- (b) the more tortuous path provided by the high step sections causing increased turbulence viscous losses as the fluid is forced to turn a greater amount by the high step arrangement.
- (c) a slightly sharper edge being presented to the flow at the throttlings defined by the slanted knives, thus decreasing the effective area and therefore the flow coefficient for individual knives;

PARTICLE IMAGE VELOCIMETRY

Particle image velocimetry was carried out at selected regions of the models on the Configuration "A" and Configuration "G" designs. Configuration "A" represents the baseline design while Configuration "G" provided the least leakage during testing. Uniform seeding of the flow proved to be a challenging proposition, with alcohol being selected as the seed fluid after some trial and error. Two regions in the seal models were selected for PIV measurements and further study. All tests were conducted at a pressure ratio (P_1/P_7) of approximately 7.6. Slight variation of this set-point pressure ratio is due to difficulty in precisely setting the system pressure controls.

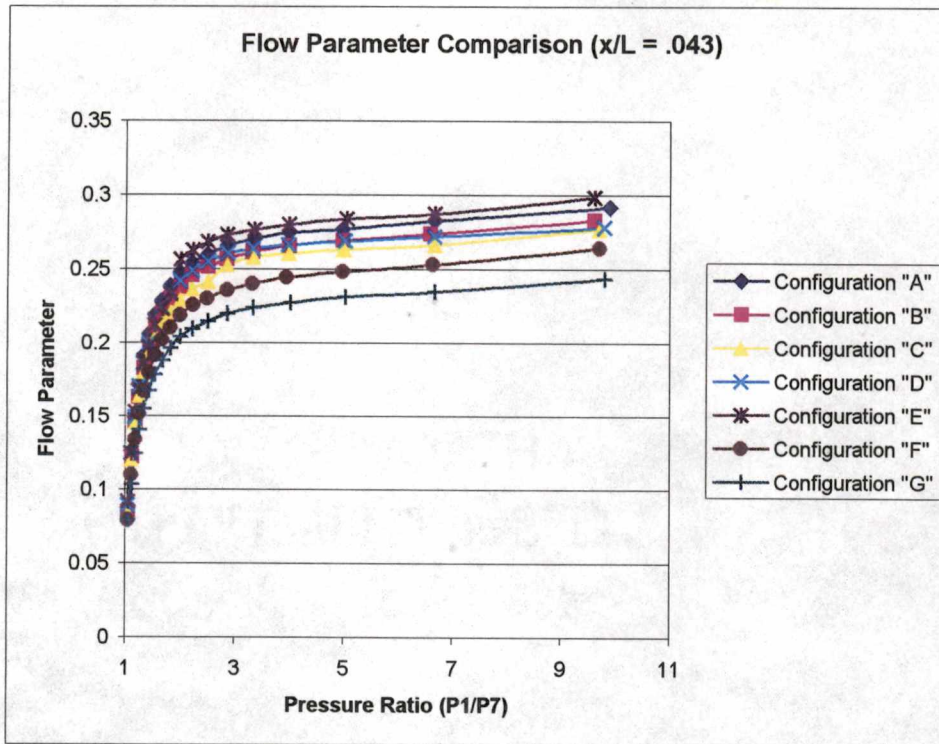


Figure 4-47 - Flow Parameter Comparison ($x/L = 0.043$)

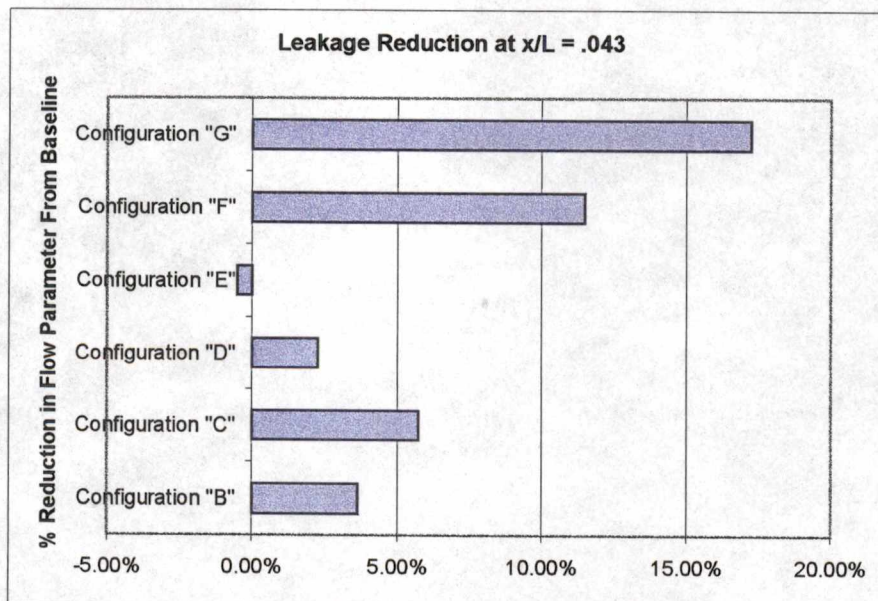


Figure 4-48 - Average Leakage Reduction ($x/L = 0.043$)

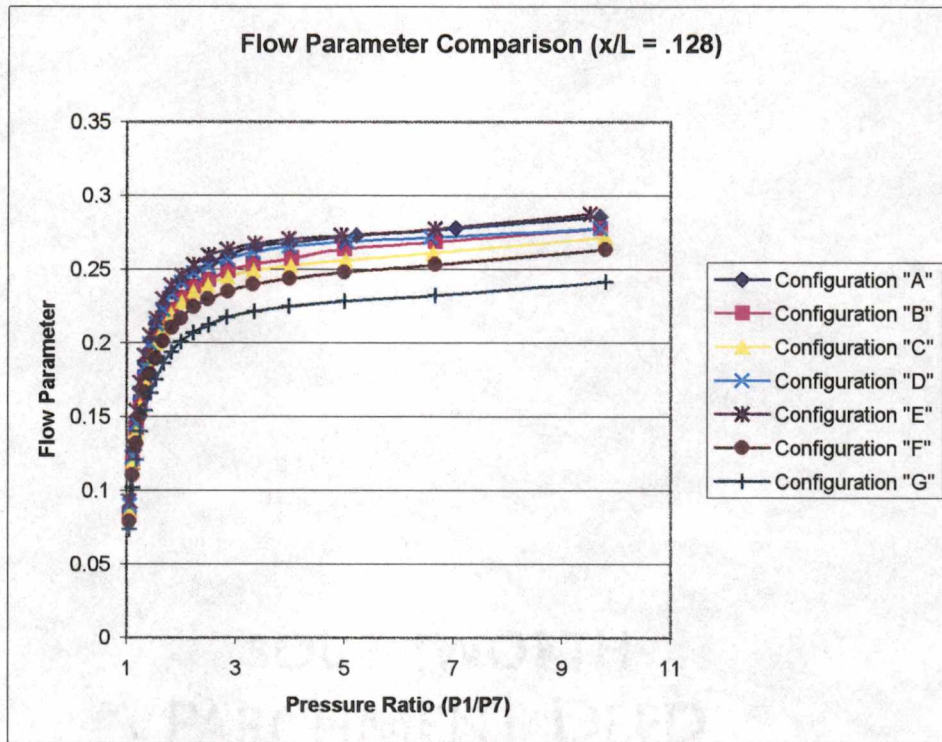


Figure 4-49 - Flow Parameter Comparison ($x/L = 0.128$)

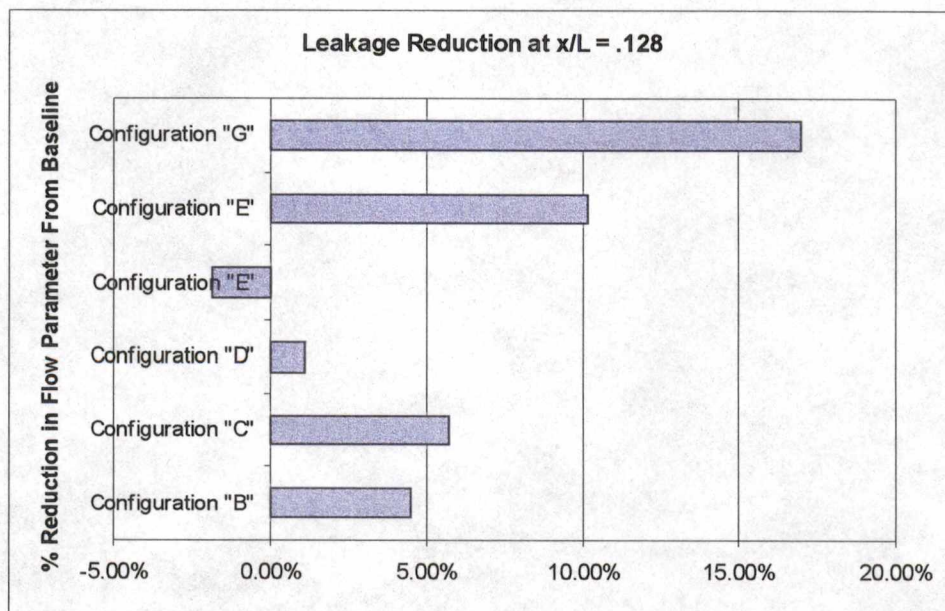


Figure 4-50 - Average Leakage Reduction ($x/L = 0.128$)

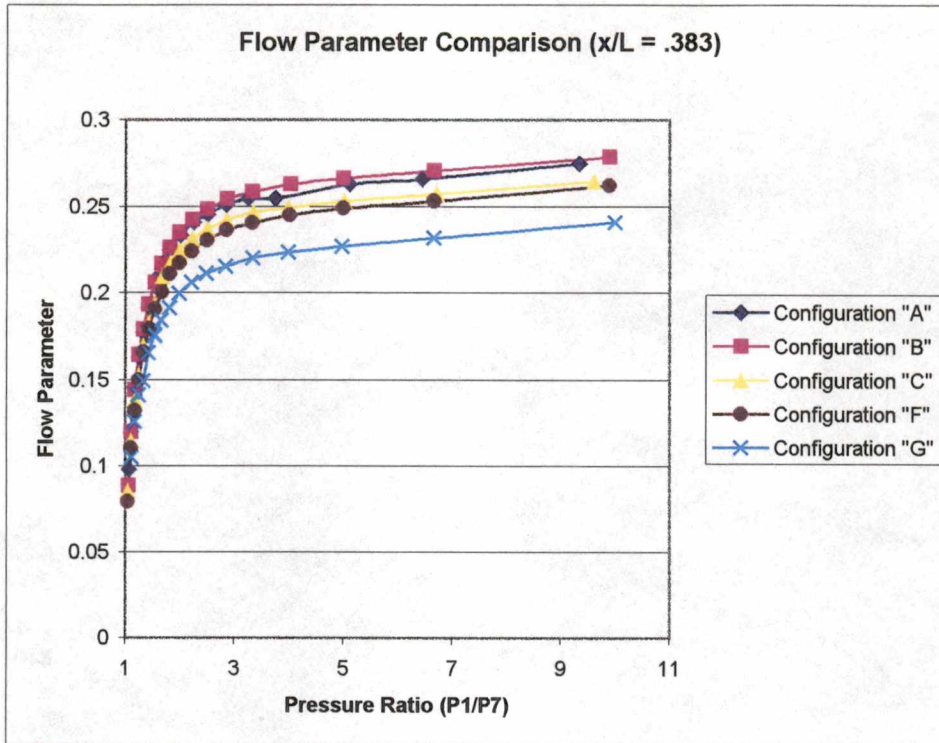


Figure 4-51 - Flow Parameter Comparison (x/L = 0.383)

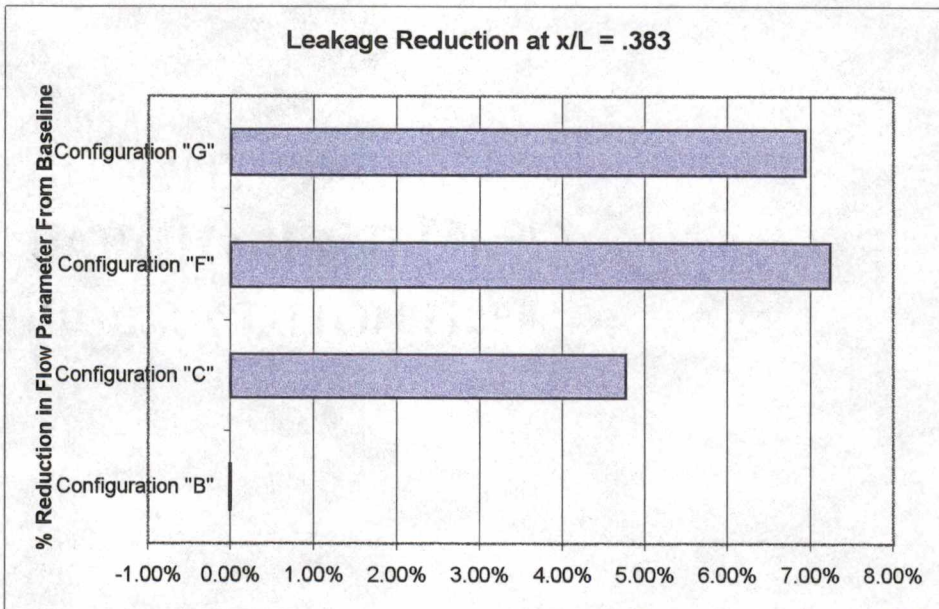


Figure 4-52 - Average Leakage Reduction (x/L = 0.383)

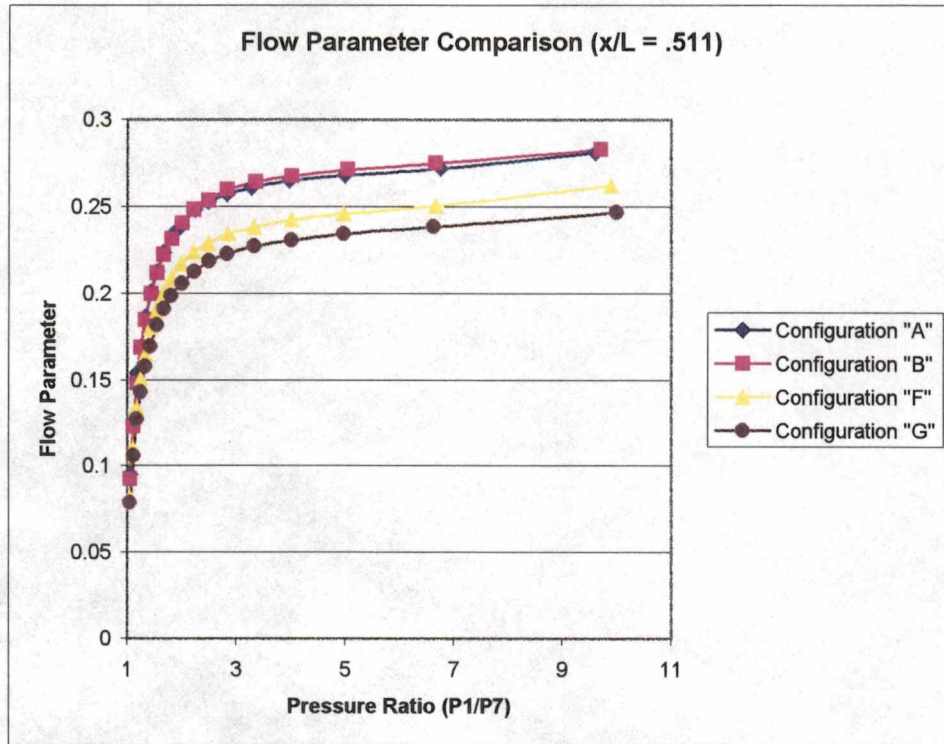


Figure 4-53 - Flow Parameter Comparison ($x/L = 0.511$)

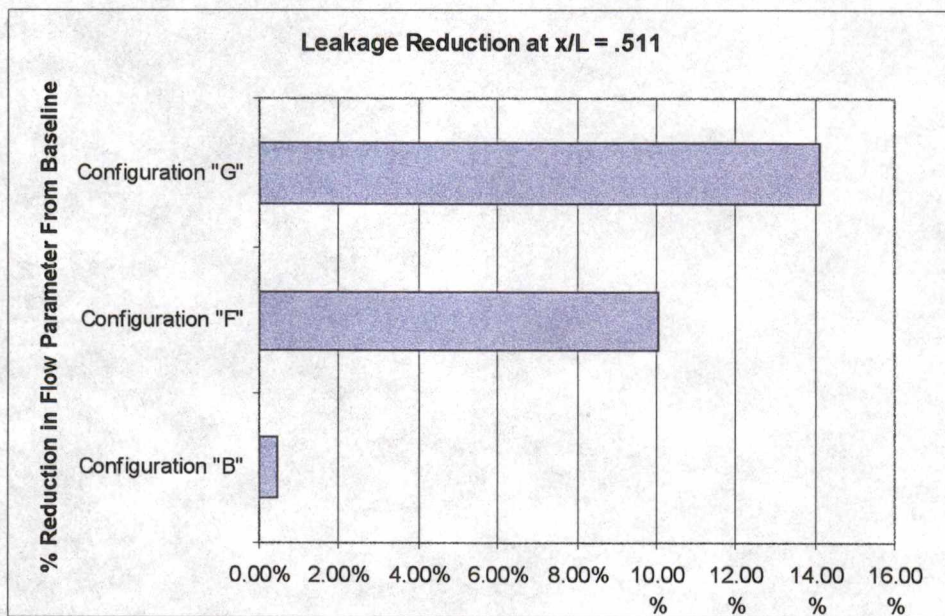


Figure 4-54 - Average Leakage Reduction ($x/L = 0.511$)

The schematics of Configurations "A" and "G" are shown in Figures 4-55 and 4-56 respectively. For the PIV measurements, the seal configurations were tested at nearly the same pressure ratio in order to establish a reasonable basis of comparison for the study. It is useful to note that 60 PIV images taken of the flow were averaged to generate all PIV results. Figure 4-57 shows the velocity vectors obtained during a test of the Configuration "A" seal; the plot is shaded by speed intensity. Figure 4-58 is a similar plot, shaded by vorticity intensity. The high flow speed and large amounts of vorticity generated in the jet of fluid passing through the throttling is apparent. Also visible in these Figures as well as Figure 4-59 are the areas of chamber recirculation. There is one large vortex in the chamber above the fluid jet as well as another smaller one in the area immediately downstream of the step. In the individual images, a small amount of flow unsteadiness was apparent, as the center of these vortices tends to shift slightly in successive images. This unsteadiness was qualitatively observed to increase in the PIV images of the improved Configuration "G", reflecting the increased turbulence generated by this geometry.

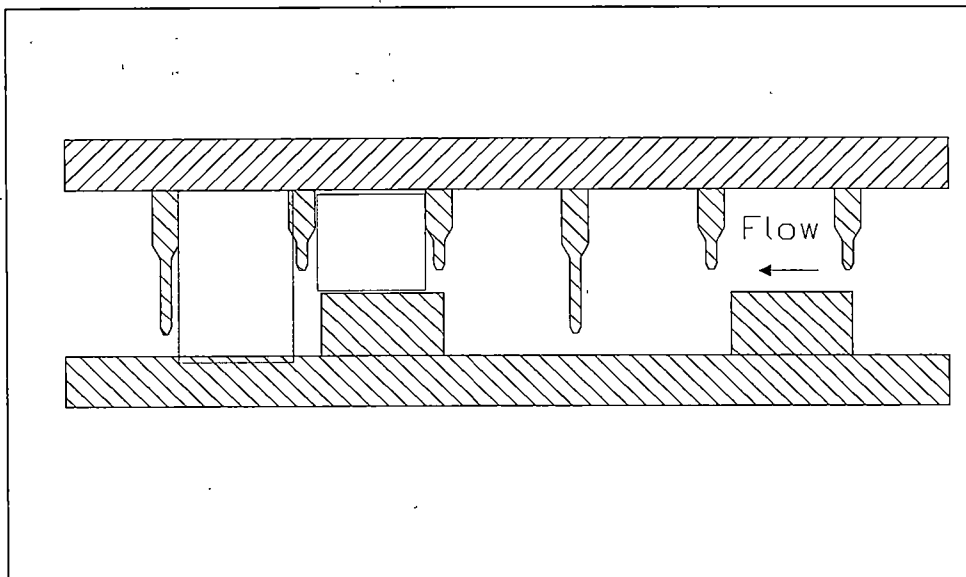


Figure 4-55 – PIV Test Area (Configuration "A")

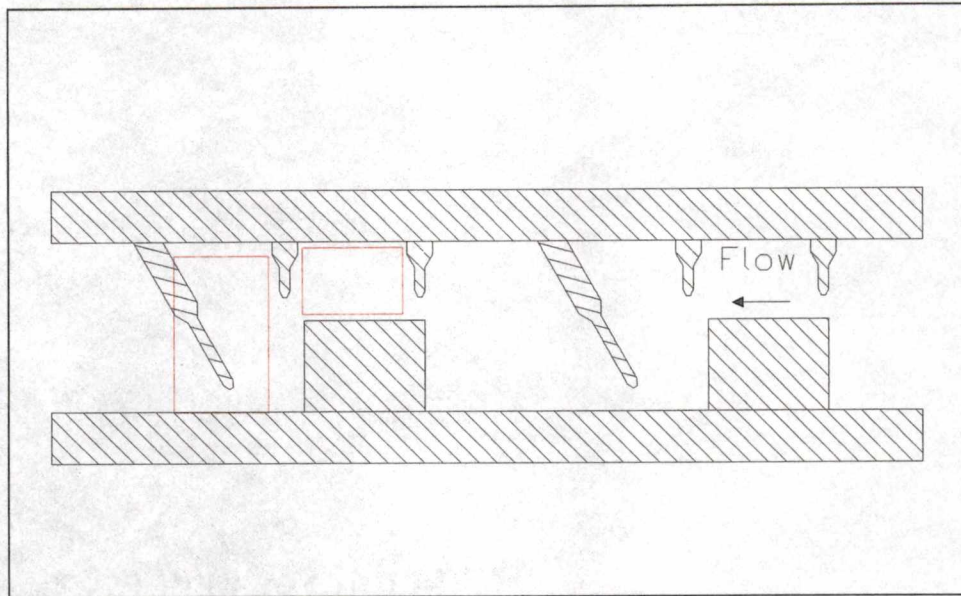


Figure 4-56 - PIV Test Area (Configuration "G")

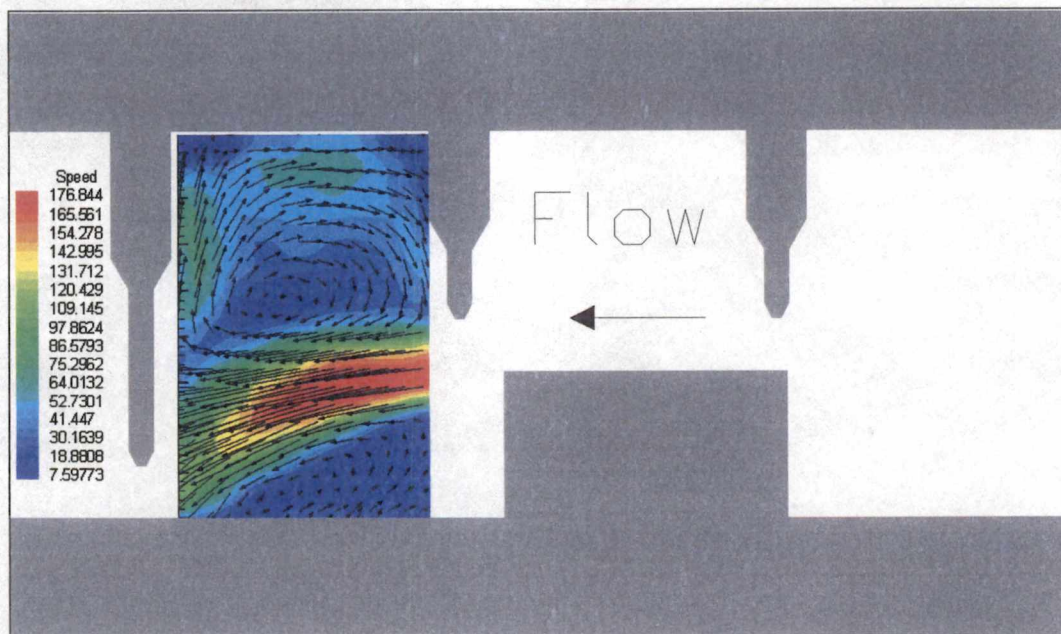


Figure 4-57 - Configuration "A" Speed Contour ($P_1/P_7 = 7.58$)

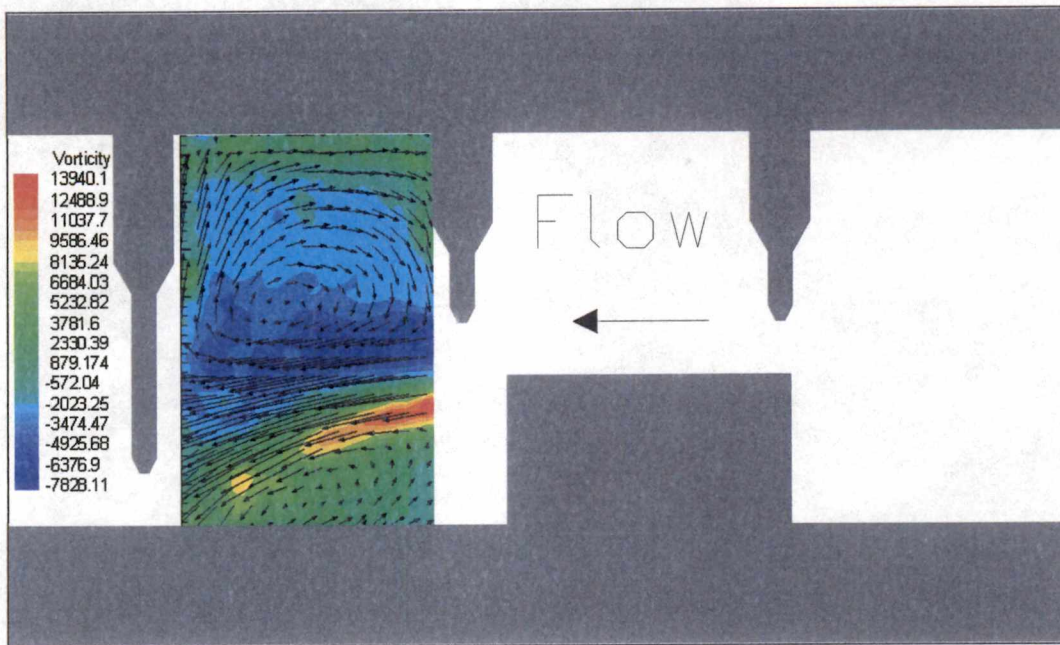


Figure 4-58 - Configuration "A" Vorticity Contour ($P_1/P_7 = 7.58$)

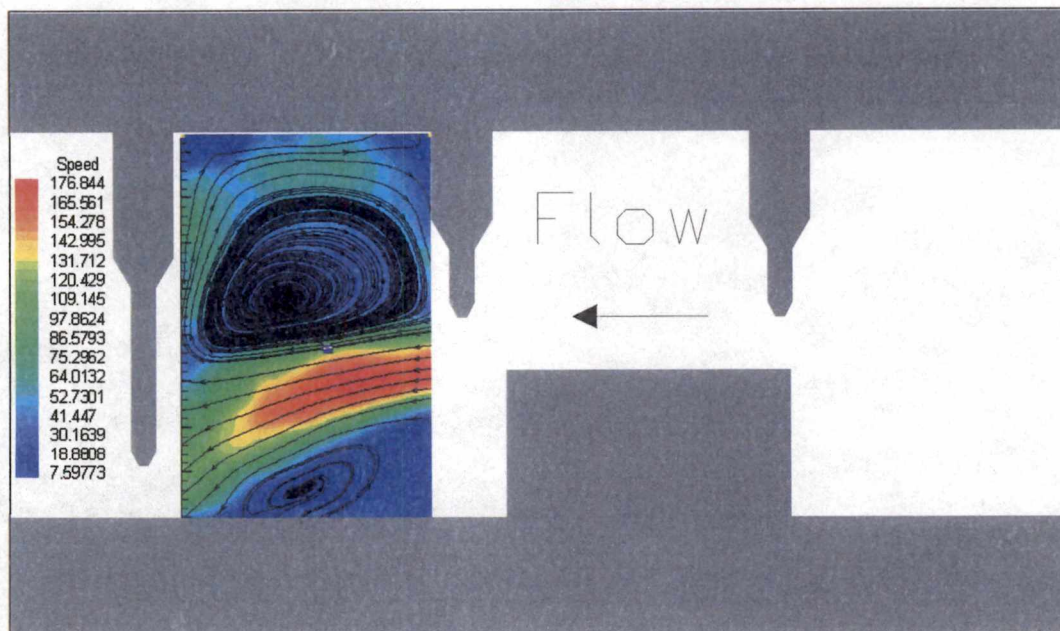


Figure 4-59 - Configuration "A" Streamlines ($P_1/P_7 = 7.58$)

Although the surface of the long knife is not visible in the PIV viewing area of Figures 4-57 and 4-58, it can be seen that some portion of the flow jetting over the step will impinge directly on the knife, causing a stagnation area. In this region, static pressure will increase substantially, but total pressure will be lost due to the non-isentropic nature of this stagnation process.

Figures 4-60 to 4-62 show the speed contours, vorticity contours and streamlines, respectively, for the flow over the 2nd downstream step in the seal. The flow over the step generally parallels the step, generating re-circulation within the chamber above the step. The increased speed and vorticity generated by the throttling at the leading edge of the step can be seen. The results shown in Figures 4-60 to 4-62 look qualitatively similar to those depicted at Figure 4-6, a flow visualization test with $x/L = 0.213$.

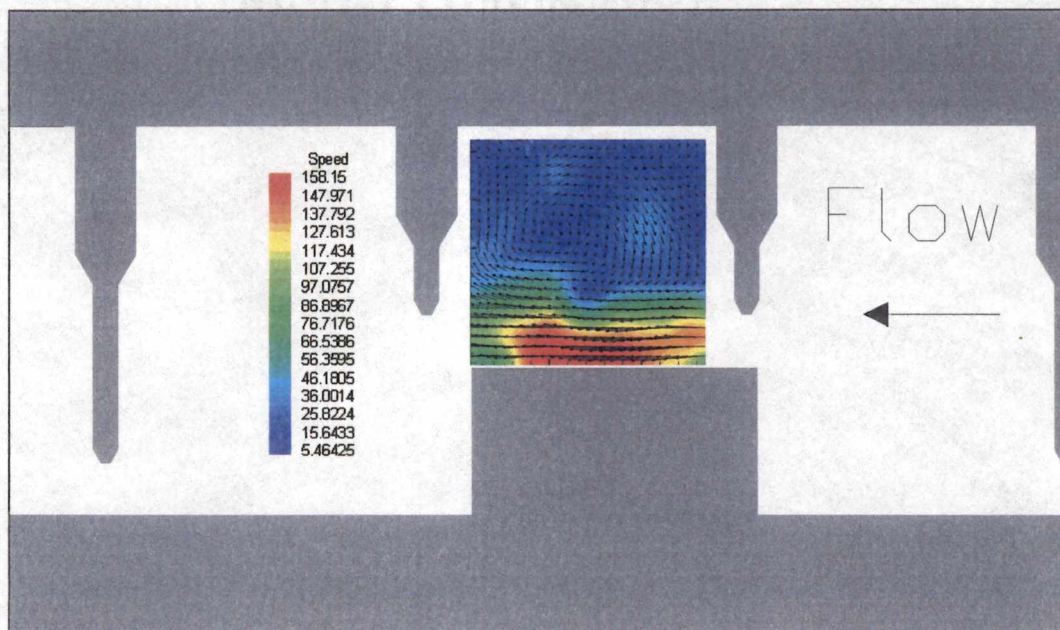


Figure 4-60 - Configuration "A" Speed Contour ($P_1/P_7 = 7.87$)

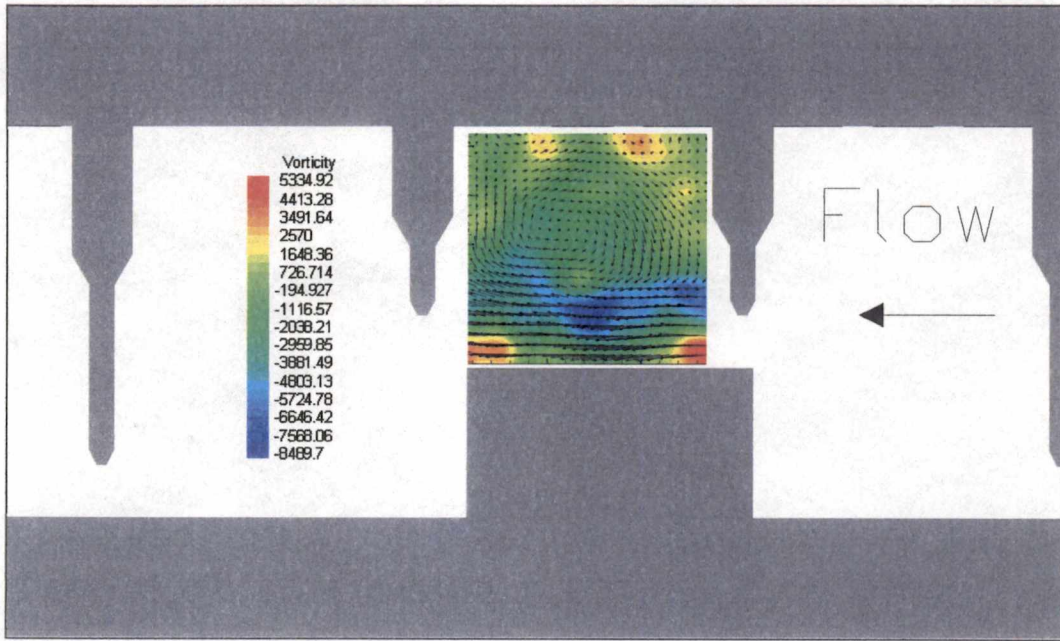


Figure 4-61 - Configuration "A" Vorticity Contour ($P_1/P_7 = 7.87$)

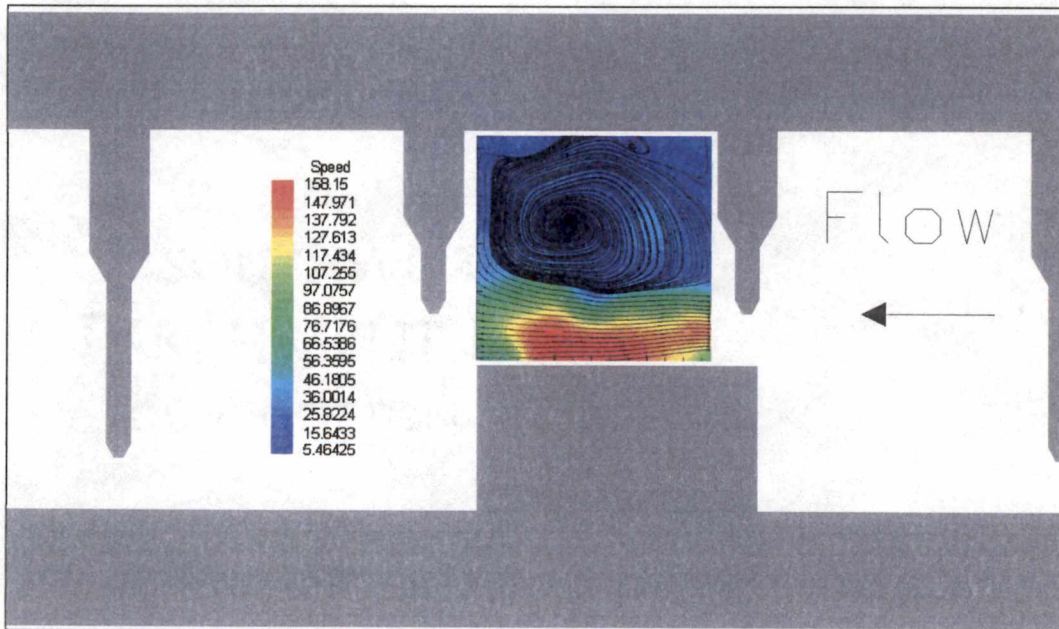


Figure 4-62 - Configuration "A" Streamlines ($P_1/P_7 = 7.87$)

In Figures 4-63 to 4-65, PIV results for the flow immediately upstream of the 2nd long knife are shown. The increased area of stagnation created as the flow impinges on the long slanted knife is clearly visible as are the sharp turns in the flow created as the flow turns down to, and then around the tip of the long knife. These changes to the flow structures cause increased losses of total pressure in the flow that result in reduced leakage. Direct comparison of the speed magnitude shown for the baseline arrangement (Figure 4-57) and the improved configuration (Figure 4-63) reflects the approximately 16.5% reduction in leakage that was measured at this pressure ratio during the 2-D flow measurement study. Figure 4-65 shows the chamber recirculation downstream of the inclined long knife; it is clearly not as well defined as that of Figure 4-59. Examination of successive PIV images for the inclined knife case showed a great deal more flow unsteadiness in this region.

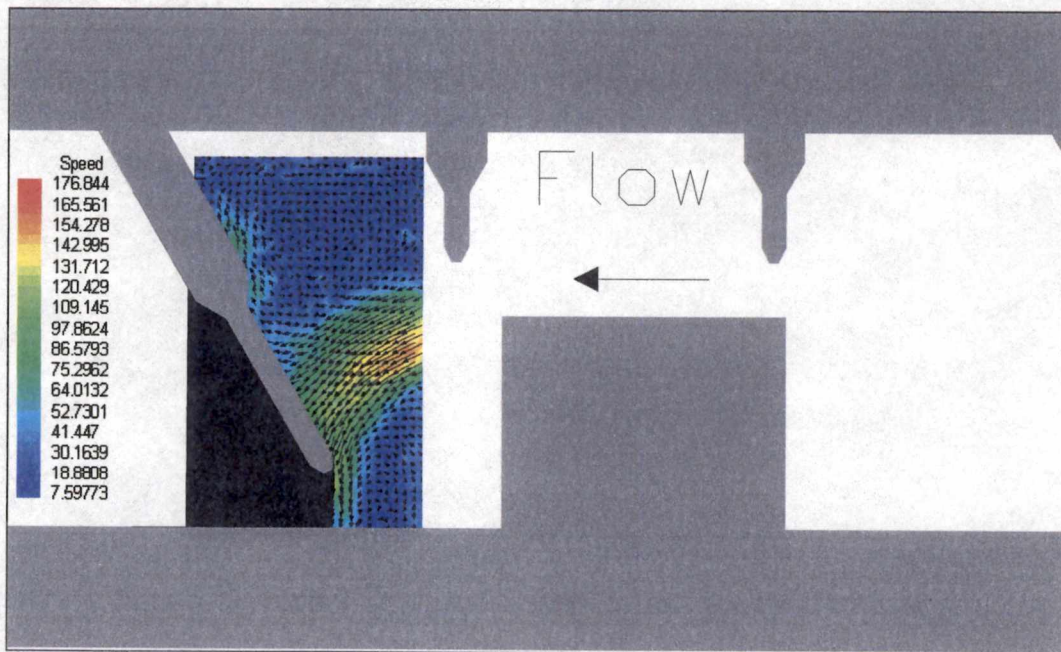


Figure 4-63 - Configuration "G" Speed Contour ($P_1/P_7 = 7.87$)

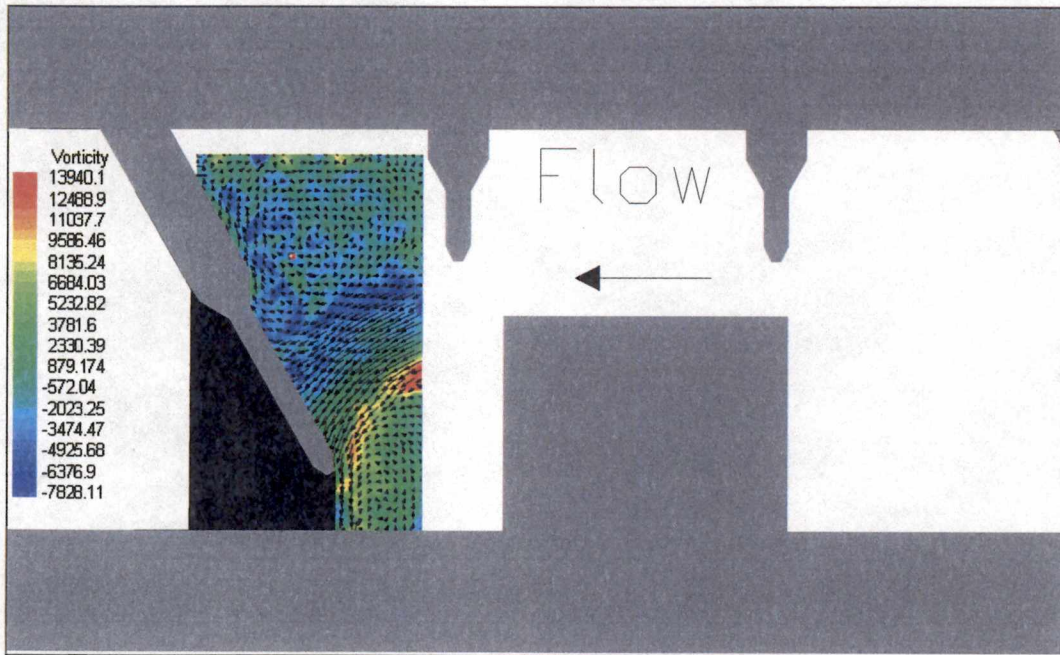


Figure 4-64 - Configuration "G" Vorticity Contour ($P_1/P_7 = 7.87$)

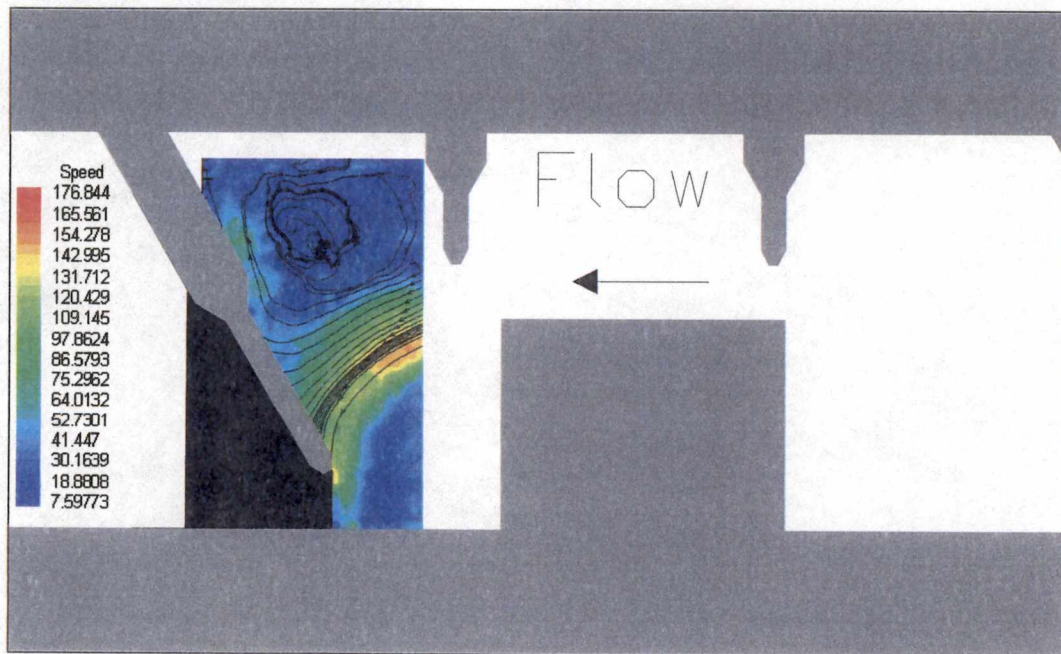


Figure 4-65 - Configuration "G" Streamlines ($P_1/P_7 = 7.87$)

In Figures 4-66 to 4-68, flow over the high step on Configuration “G” is displayed. Comparison with Figures 4-60 to 4-62 shows that with the high step modification, the size of the vortex circulating in the chamber over the step has been reduced in size. However, it appears that the area of turbulent flow over the step has increased in size. Speed over the step is reduced from the baseline case due to a reduction in mass flow through the seal that is the result of the design improvements.

The limited PIV study carried out provides a greater physical understanding of the physical mechanisms that reduce leakage in a labyrinth seal and provided some explanation of the improved sealing characteristics demonstrated by Configuration “G”. Increased understanding would be gained by carrying out the PIV technique on other areas within the seal, and by repeating the tests at various other seal pressure ratios.

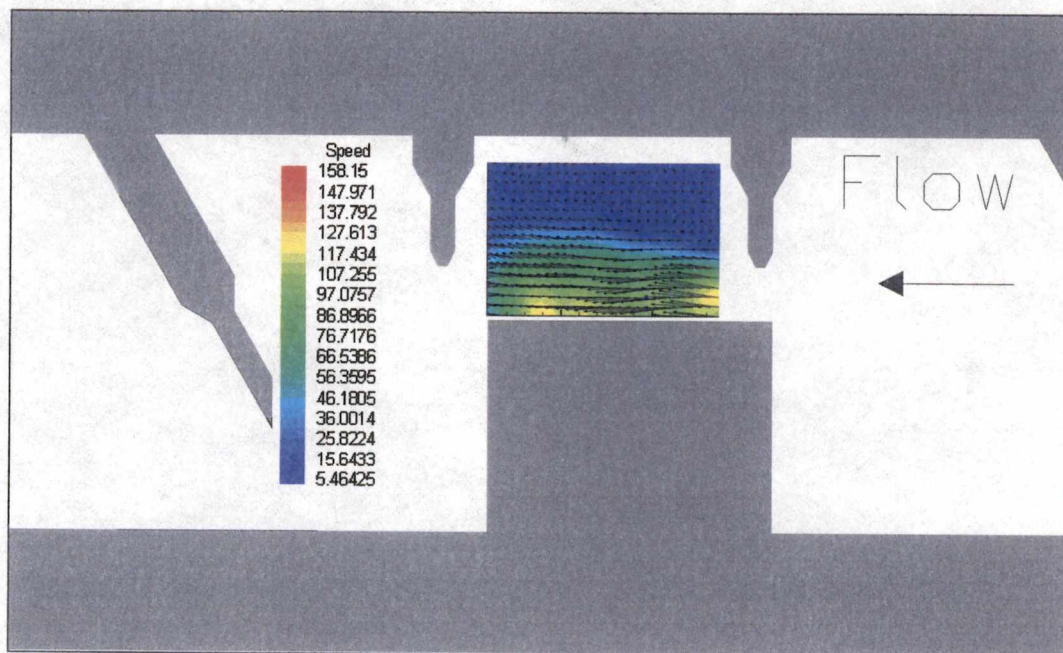


Figure 4-66 - Configuration “G” Speed Contour ($P_1/P_7 = 7.69$)

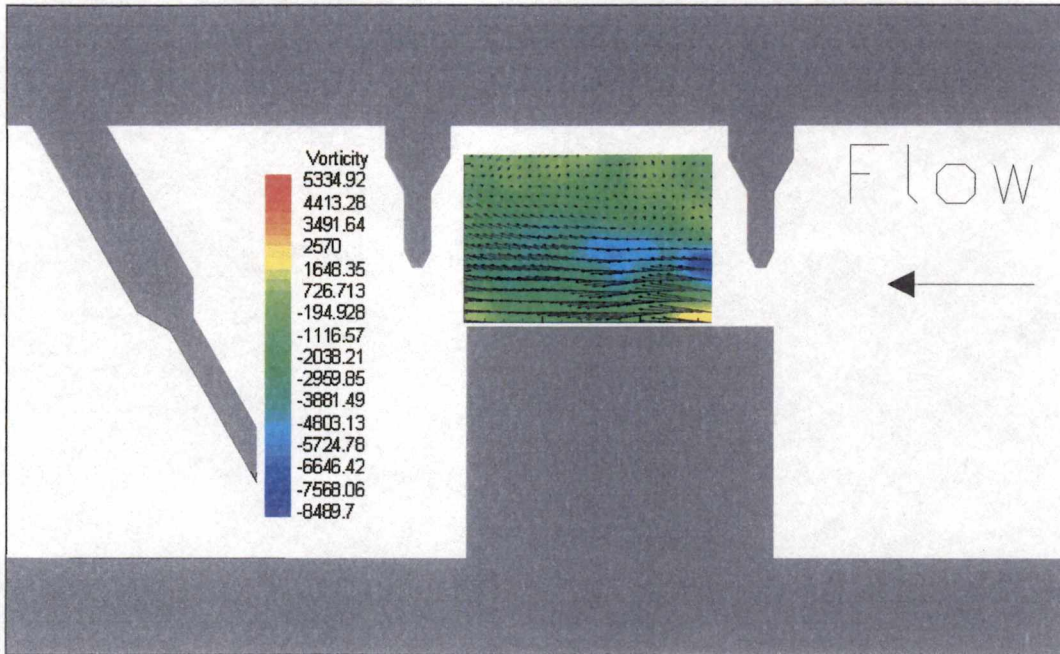


Figure 4-67 - Configuration "G" Vorticity Contour ($P_1/P_7 = 7.69$)

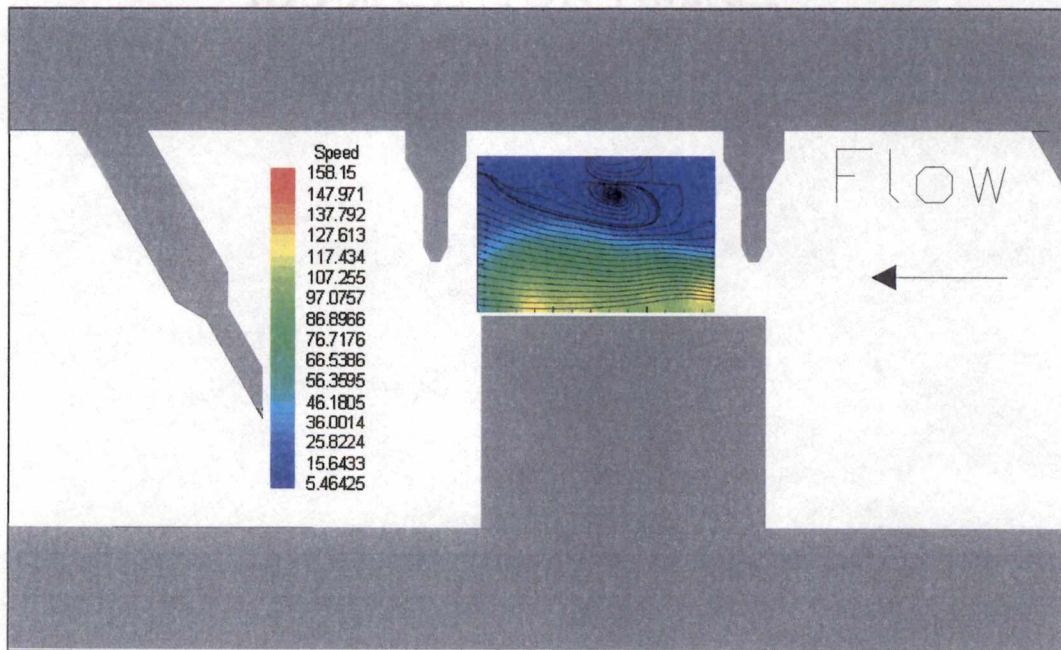


Figure 4-68 - Configuration "G" Streamlines ($P_1/P_7 = 7.69$)

CONCLUSIONS AND RECOMENDATIONS

CONCLUSIONS

Leakage through a stationary stepped labyrinth seal was investigated by means of flow visualization, discrete measurements of the flow, and particle image velocimetry.

Flow visualization demonstrates the basic mechanisms of energy loss within the seal: the fluid jetting through the successive orifices of the labyrinth becomes extremely turbulent and viscous losses incurred reduce the energy available to propel fluid through the seal. Also, the flow of the viscous fluid, forced to negotiate a rapidly changing path within the seal, generates a number of local stagnation regions and eddies within the chambers. Local flow stagnations are visible in several areas of the seal and are a major loss mechanism.

The measurement of mass flow rate parameters over a range of seal pressure ratios conforms to similar results available in the literature. As the pressure ratio across the seal increases, leakage mass flow increases to a point where the seal is choked. Following this, the mass flow increases slowly with increasing pressure ratio as the effective area at the last knife in the flow continues to change.

The axial position of the knives relative to the steps is shown to have a significant effect on the leakage through the seal at a given pressure ratio. This effect can be mitigated with minor changes in geometry.

Measurements with modified seal geometry showed that seal leakage could be readily reduced up to 17% from the baseline configuration and that uniform sealing at any axial position was improved. Particle image velocimetry of the baseline and most-improved configurations showed that the improved design, Configuration "G", increased flow stagnation significantly. The irreversibility of the sudden compression of the fluid as it stagnates provides a means to dissipate

energy thus increasing energy loss and reducing leakage through the seal. Both the high step and inclined knives of Configuration "G" tend to force the flow streamlines to turn more sharply, which also increases seal effectiveness.

The improved design showed a greater tolerance for changes in the axial location of the step relative to the knives in the seal; at a given pressure ratio, leakage remained essentially constant with changes in axial location of the steps.

RECOMMENDATIONS

The following recommendations are provided based on the results of this study:

- (a) Further flow measurement and PIV testing should be carried out on a wider range of seal configurations in order to optimize the knife angle/step height design;
- (b) Three dimensional test models should be designed and built in order to investigate the effects of seal rotation on leakage rate;
- (c) The possibility of incorporating 3-dimensional elements (i.e. a helical knife pitch) to the optimized stationary seal configuration should be investigated by CFD and experiment.

REFERENCES

REFERENCES

1. Egli, A., "Leakage of Steam Through Labyrinth Seals", ASME Transactions V57, 1935.
2. Stocker, H.L., "Determining and Improving Labyrinth Seal Performance in Current and Advanced High Performance Gas Turbines", AGARD Conference Proceedings No 237, "Seal Technology in Gas Turbine Engines, April, 1978.
3. Morrison, G.L. and Chi, D., "Incompressible Flow in Stepped Labyrinth Seals", ASME Paper 85-FE-4, Presented at the Joint ASME/ACSE Applied Mechanics, Bioengineering and Fluids Engineering Conference, Albuquerque, NM, June 24-26, 1985.
4. Wyler, J.S., "Design and Testing of a New Double Labyrinth Seal", ASME Paper 81-Lub-58, Presented at the ASME Winter Annual Meeting, Washington D.C, November 15-20, 1981.
5. Stocker, H.L., "Advanced Labyrinth Seal Design Performance for High Pressure Ratio Gas Turbines", ASME Paper 75-WA/GT-22, Presented at the ASME Winter Annual Meeting, Houston, Texas, November 3 - December 4, 1975.
6. Heidrich, F.L., "Water Flooded Single Screw Process Compressor Technology", Dresser-Rand E-Tech, New York.
7. Hendricks, R.C., Griffin, T.A., Kline, T.R., Csavina, K.R., Pancholi, A., and Sood, D., "Relative Performance Comparison Between Baseline Labyrinth and Dual-Brush Compressor Discharge Seals in a T-700 Engine Test", NASA Technical Memorandum 106360, Prepared for the 39th International Gas Turbine and Aeroengine Congress and Exposition sponsored by ASME, The Hague, Netherlands, June 13-16, 1994.
8. <http://www.eia.doe.gov/pub/energy.overview/aer1999/txt/aer0511.txt>
9. Martin, H.M., "Labyrinth Packings", Engineering, V85, January 10, 1908.

10. Shames, I.H., "Mechanics of Fluids", McGraw-Hill, New York, 1992
11. Rouse, H, "Elementary Mechanics of Fluids", Dover Publications, New York, 1946.
12. Shapiro, A.H., "The Dynamics and Thermodynamics of Compressible Fluid Flow", The Ronald Press Company, New York, 1953.
13. Kearton, W.J, Keh, T.H., "Leakage of Air Through Labyrinth Glands of Staggered Type", IME Proceedings, Vol 166, No 2, 1952.
14. Meyer, C.A. and Lowrie, J.A., "The Leakage Thru Straight and Slant Labyrinths and Honeycomb Seals", ASME Paper 74-WA/PTC-2.
15. Tipton, D.L., Scott, T.E. and Vogel, R.E., "Analytical and Experimental Development of a Design Model for Labyrinth Seals", Air Force Wright Aeronautical Laboratories Report TR-85-2103 V3, January 1986.
16. Anderson, J.D, "Modern Compressible Flow With Historical Perspective", McGraw Hill, 1990.
17. Yizheng, Z. and Feng, H., "Analysis of Leakage Characteristics of Labyrinth Seals", Chinese Journal of Aeronautics, V3, Number 4, November, 1990.
18. Morrison, G.L., Rhode, D.L., Cogan, K.C., Chi, D. and Demko, J., "Labyrinth Seals for Incompressible Flow - Final Report", NASA Contract Report CR-170938, November 30, 1983.
19. Miyake, K, and Duh, W.C., "Leakage Characteristics of Labyrinth Seal", Journal of the Chinese Society of Mechanical Engineers, V11, No 4, August, 1990.
20. Komotori, K. and Miyake, K., "Leakage Characteristics of Labyrinth Seals With High Rotating Speed", Presented at the Tokyo Joint Gas Turbine Congress, May 22-27, 1977.

21. Washka, W., Wittig, S., Kim, S., Scherer, T., "Heat Transfer and Leakage in High-Speed Rotating Stepped Labyrinth Seals", AGARD, Heat Transfer and Cooling in Gas Turbines, February, 1993.
22. Stocker, H.L., Cox, D.M. and Holle, G.F., "Aerodynamic Performance of Conventional and Advanced Design Labyrinth Seals with Solid-Smooth, Abradable and Honeycomb lands", NASA Contract Report, CR-135307, November 1977.
23. Liu, J, "Development and Analysis of a Low Speed Particle Image Velocimetry System", Master's Thesis, University of Tennessee, Knoxville, December 1998.
24. Meganathan, A. J., "An Experimental Study of Low Speed Open Cavity Flows", Master's Thesis, University of Tennessee, Knoxville, December 2000.

APPENDICES

APPENDIX A: DETAILED EXPERIMENTAL RESULTS

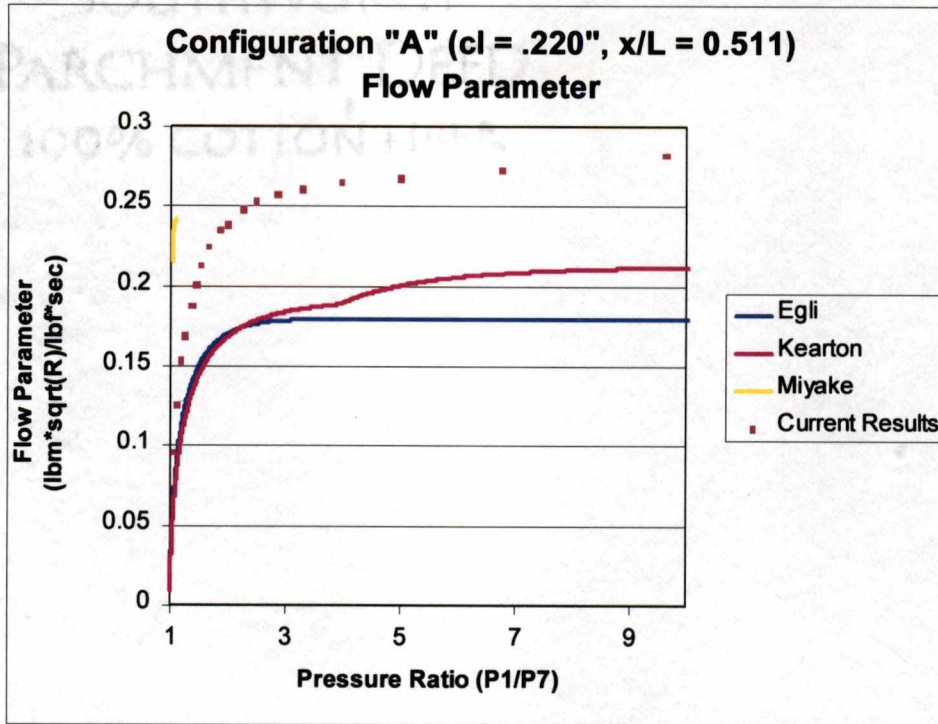


Figure A-1 – Configuration “A” Flow Parameter (cl = .220”, x/L = 0.511)

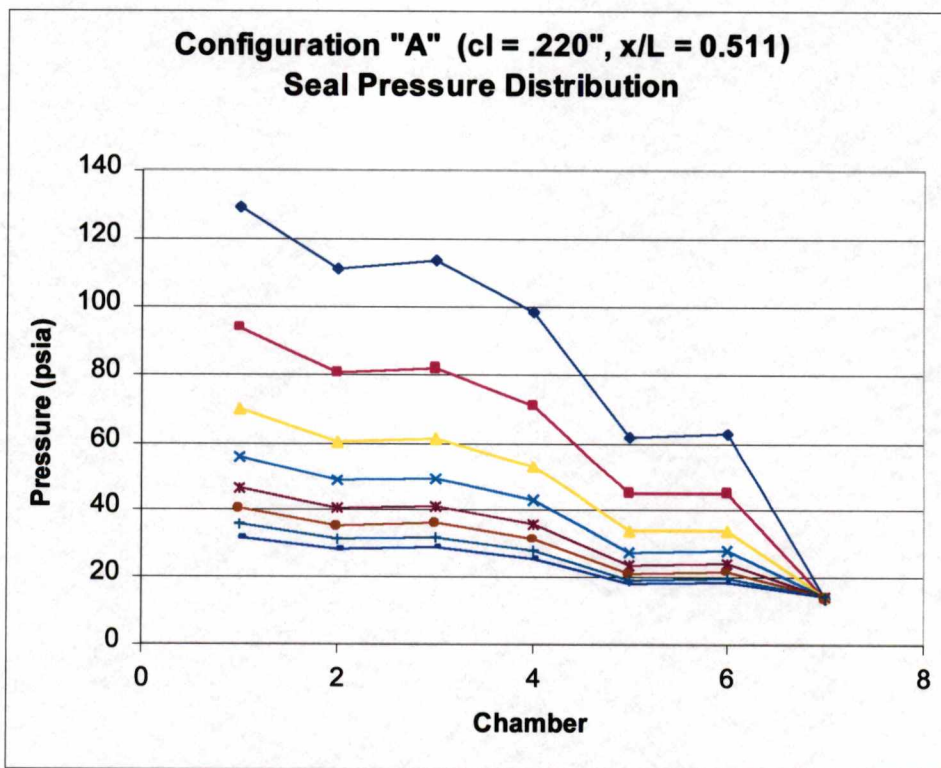


Figure A-2 – Configuration “A” Static Pressure Distribution (cl = .220”, x/L = 0.511)

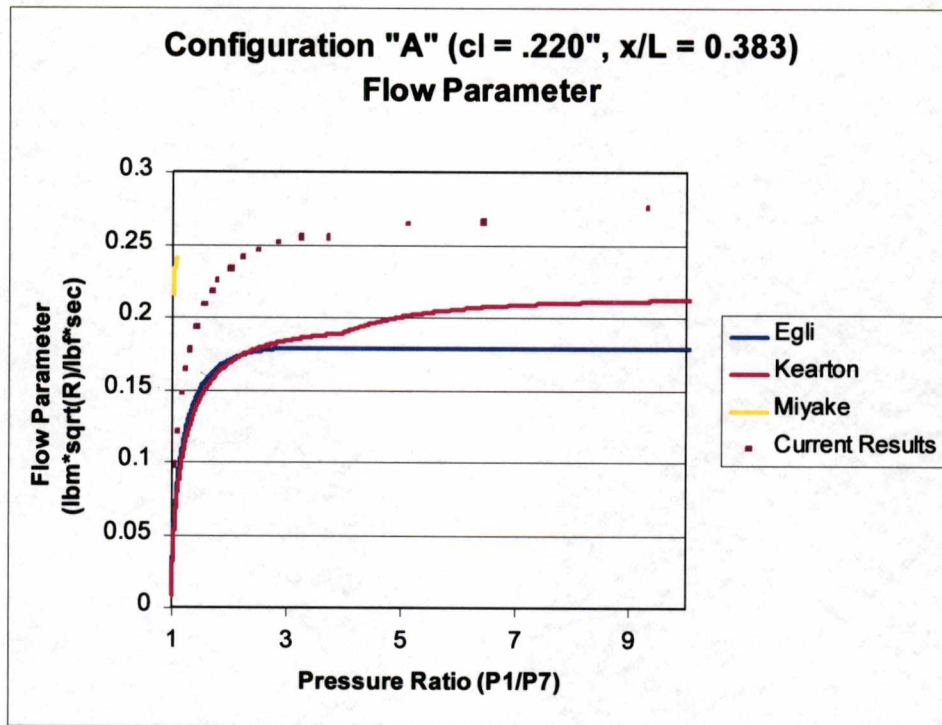


Figure A-3 – Configuration “A” Flow Parameter (cl = .220”, x/L = 0.383)

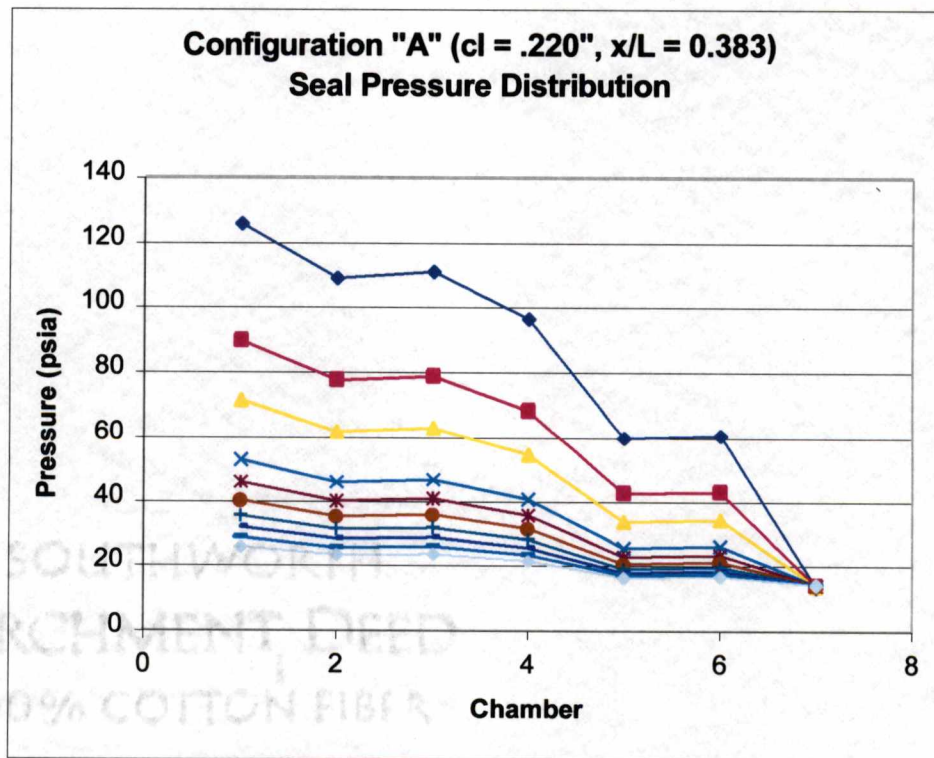


Figure A-4 – Configuration “A” Static Pressure Distribution (cl = .220”, x/L = 0.383)

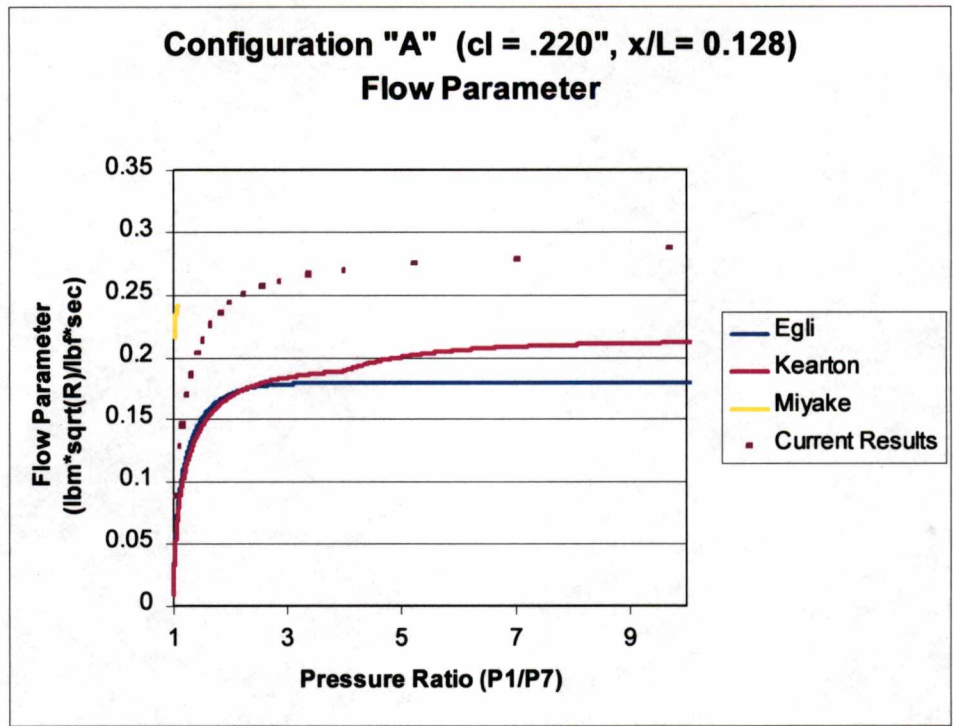


Figure A-5 – Configuration "A" Flow Parameter (cl = .220", x/L = 0.128)

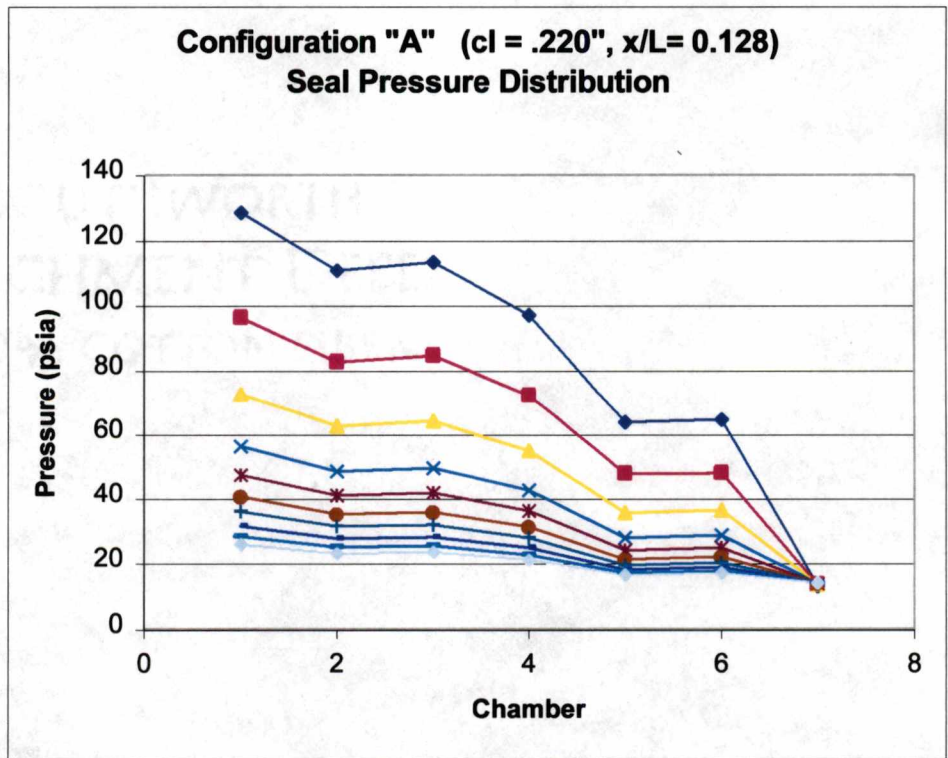


Figure A-6 – Configuration "A" Static Pressure Distribution (cl = .220", x/L = 0.128)

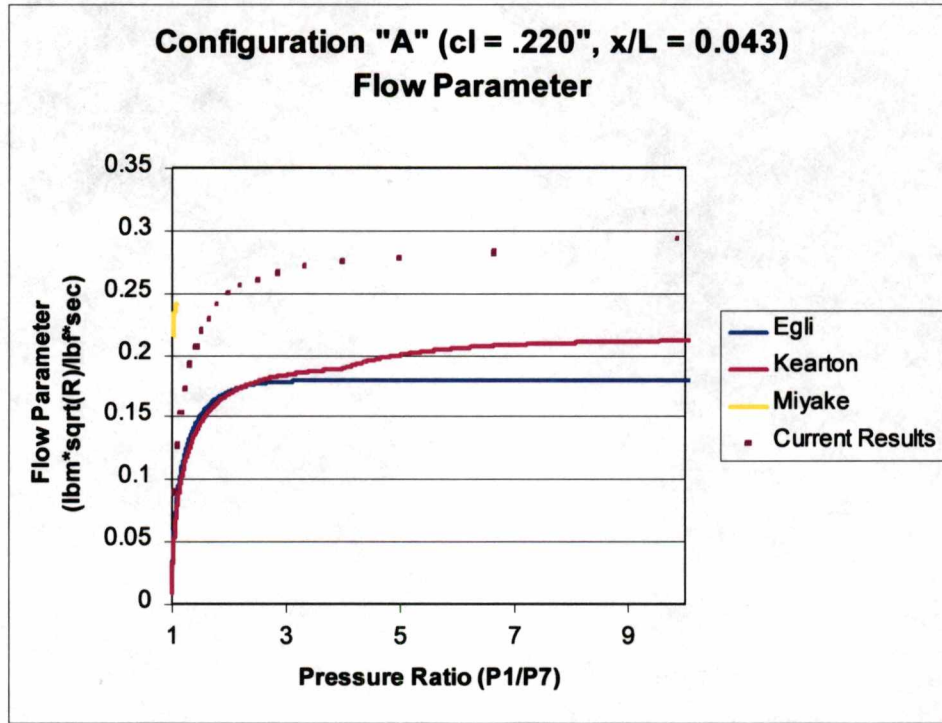


Figure A-7 – Configuration “A” Flow Parameter ($cl = .220"$, $x/L = 0.043$)

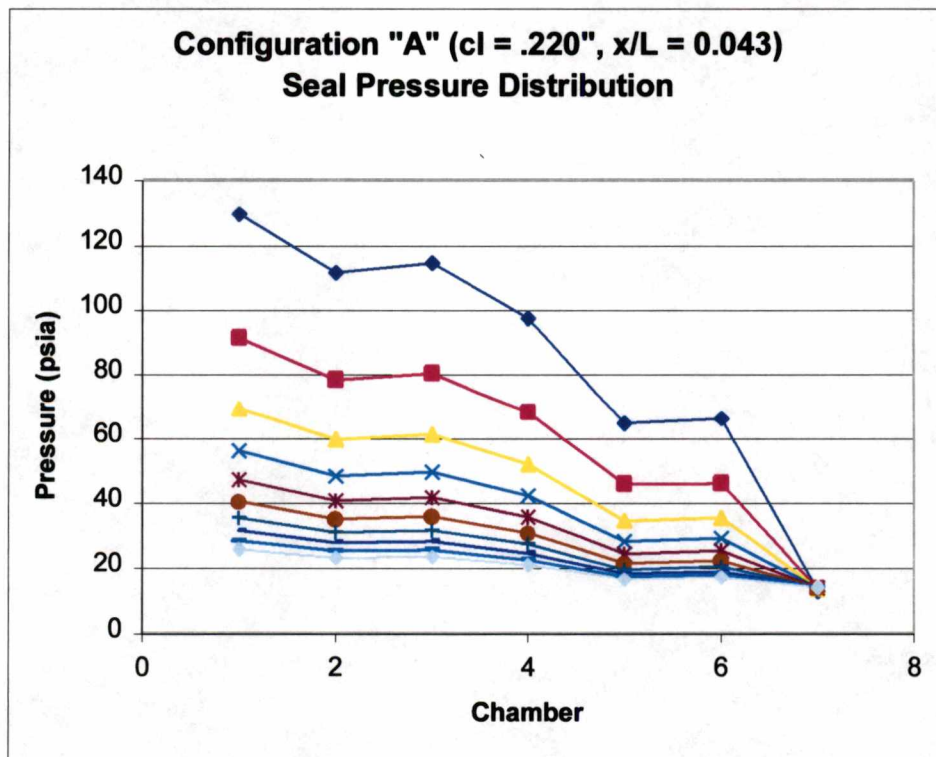


Figure A-8 – Configuration “A” Static Pressure Distribution ($cl = .220"$, $x/L = 0.043$)

SOUTHWORTH
 ARCHMENT DEED
 100% COTTON FIBER

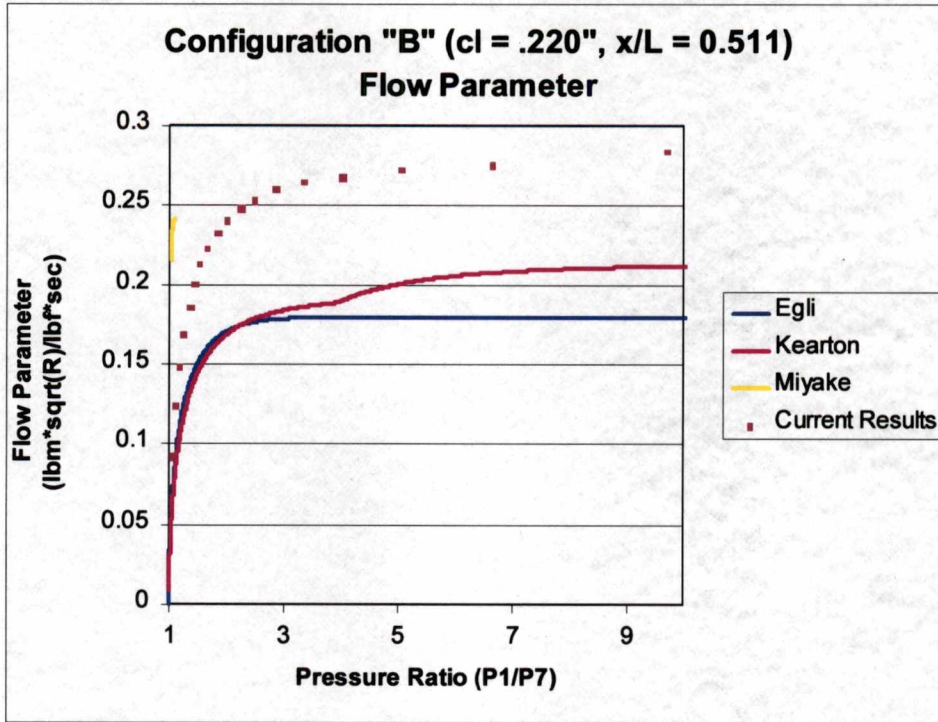


Figure A-9 – Configuration “B” Flow Parameter (cl = .220”, x/L = 0.511)

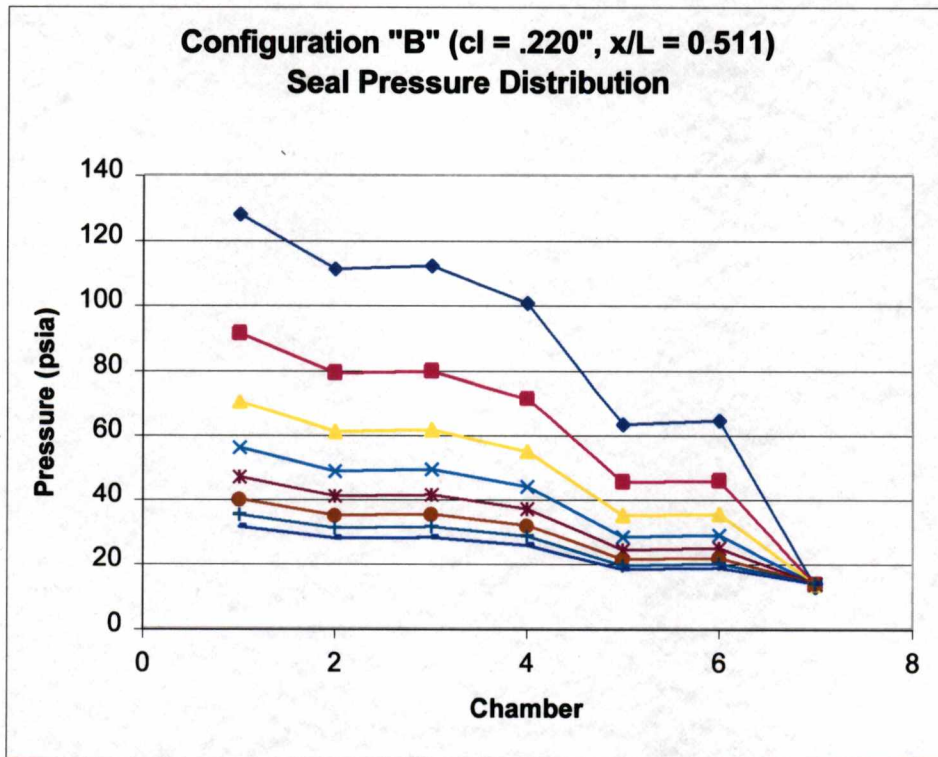


Figure A-10 – Configuration “B” Static Pressure Distribution (cl = .220”, x/L = 0.511)

SOUTHWORTH

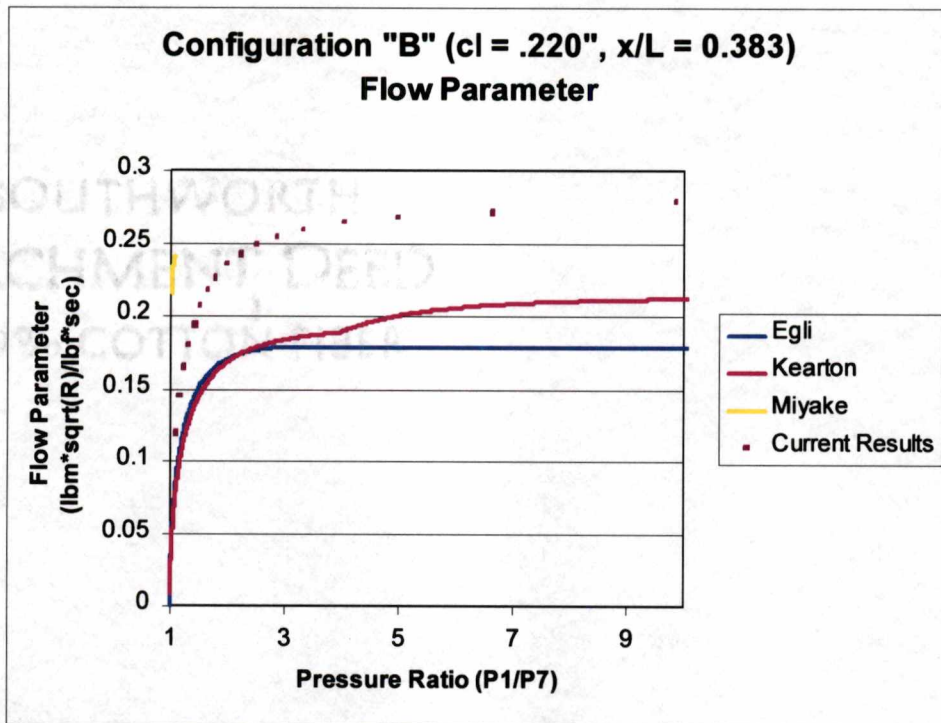


Figure A-11 – Configuration "B" Flow Parameter ($c_l = .220$ ", $x/L = 0.383$)

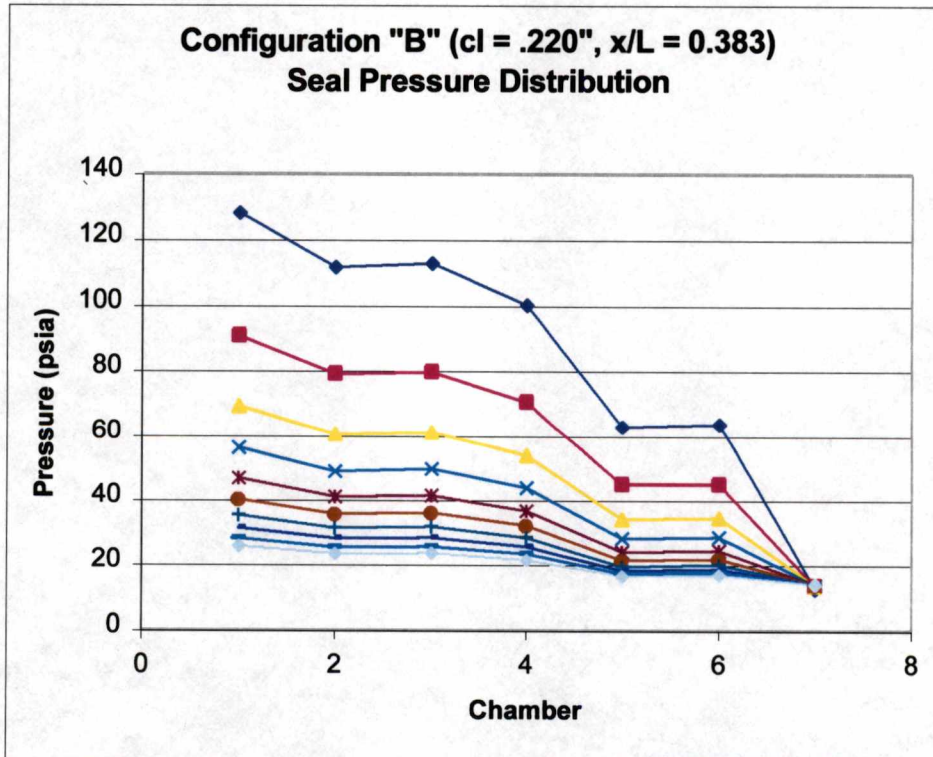


Figure A-12 – Configuration "B" Static Pressure Distribution ($c_l = .220$ ", $x/L = 0.383$)

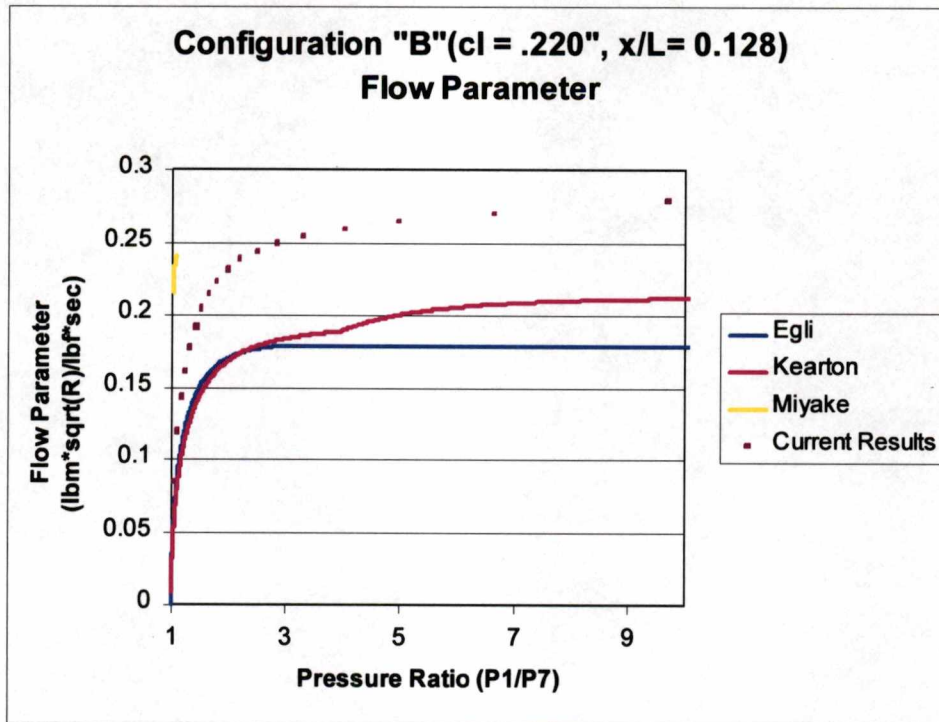


Figure A-13 – Configuration "B" Flow Parameter (cl = .220", x/L = 0.128)

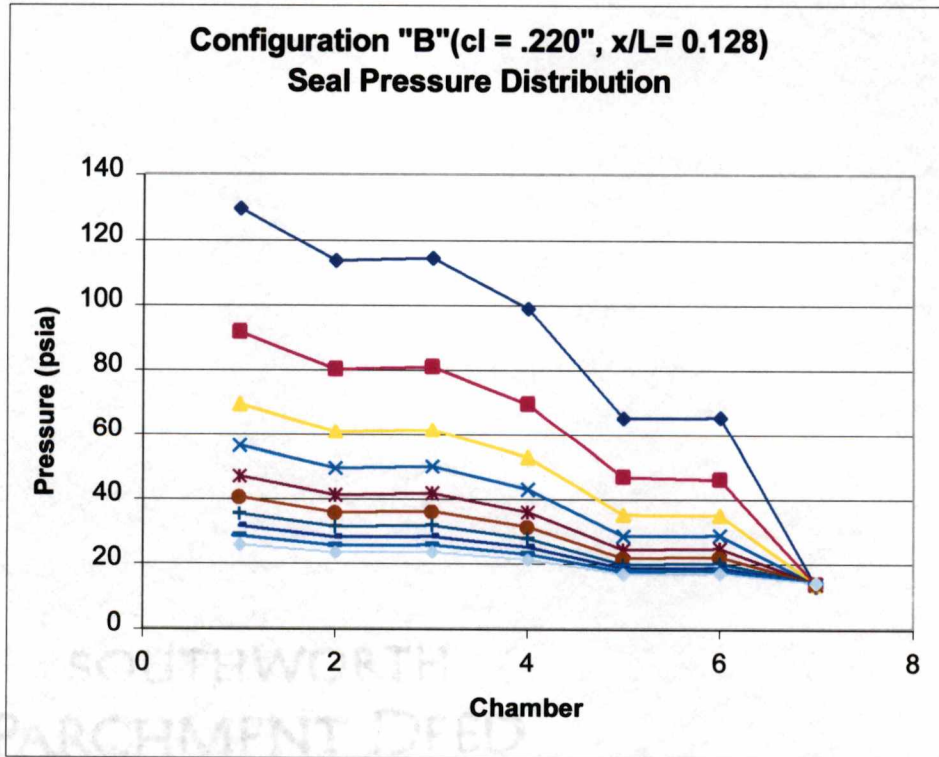


Figure A-14 – Configuration "B" Static Pressure Distribution (cl = .220", x/L = 0.128)

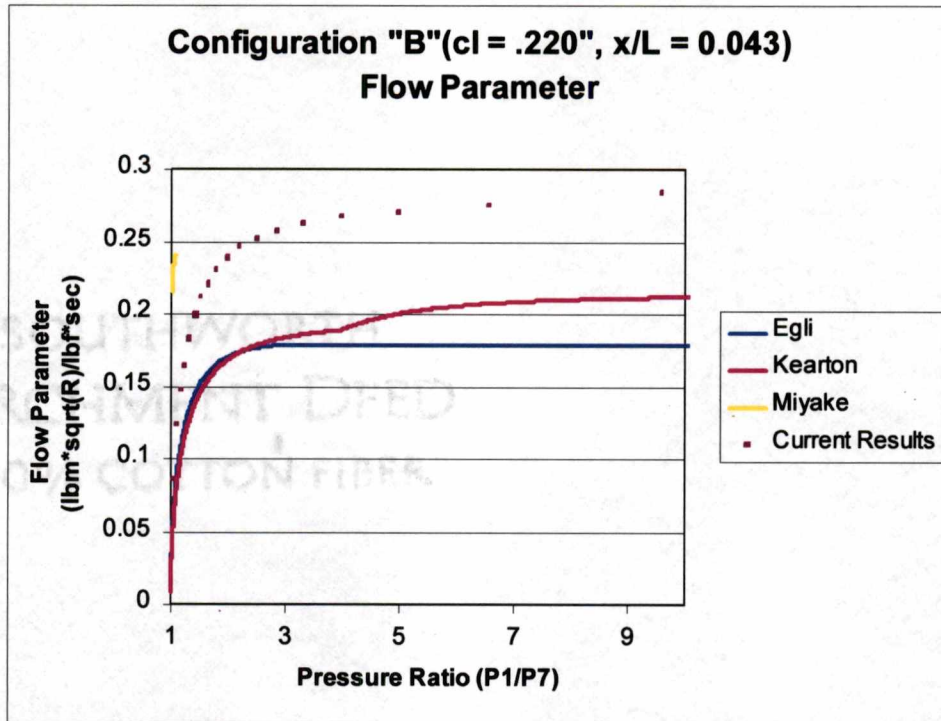


Figure A-15 – Configuration "B" Flow Parameter (cl = .220", x/L = 0.043)

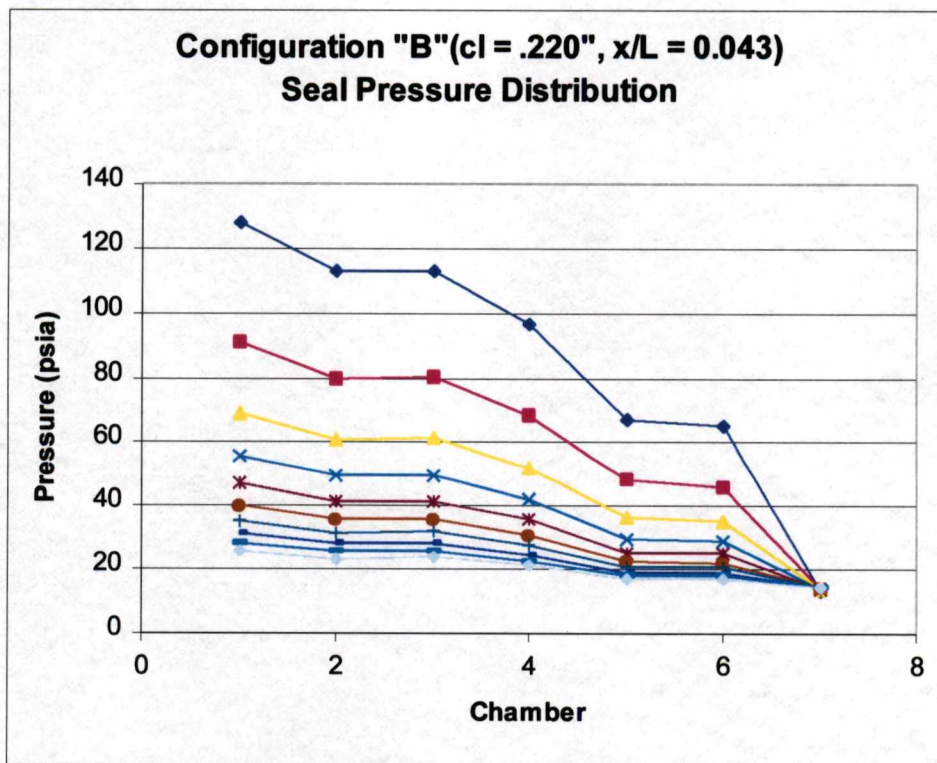


Figure A-16 – Configuration "B" Static Pressure Distribution (cl = .220", x/L = 0.043)

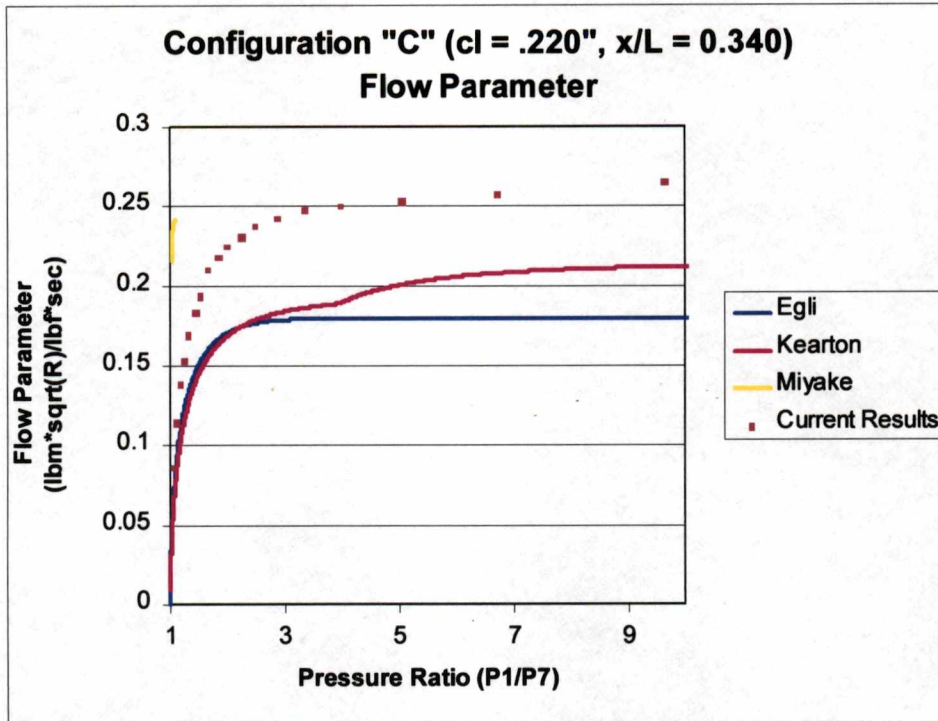


Figure A-17 – Configuration "C" Flow Parameter (cl = .220", x/L = 0.340)

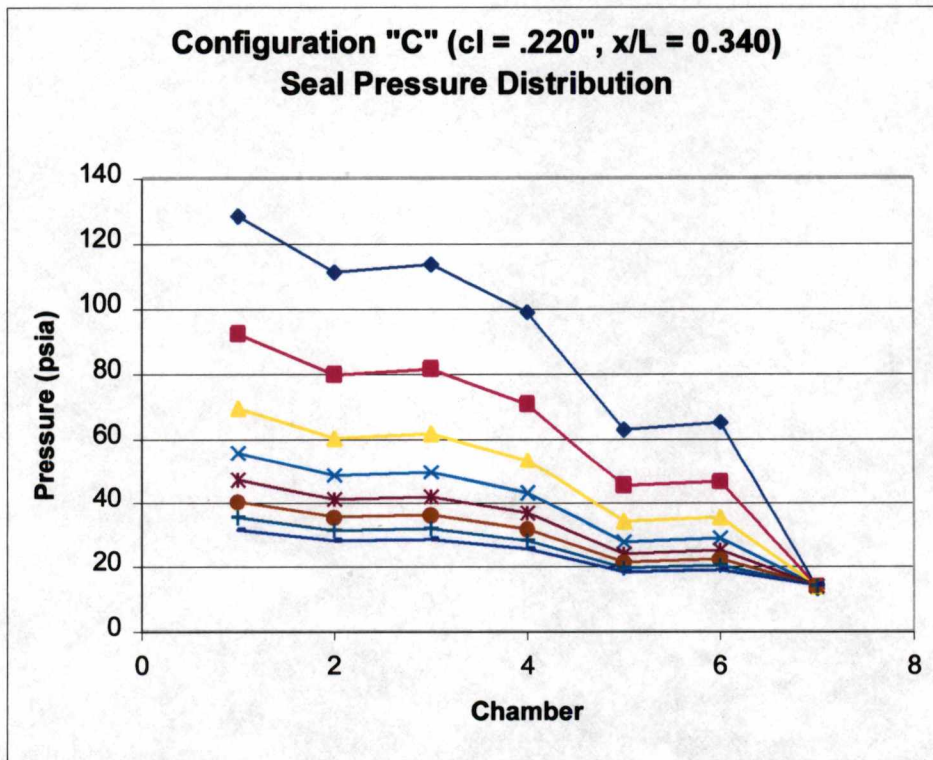


Figure A-18 – Configuration "C" Static Pressure Distribution (cl = .220", x/L = 0.340)

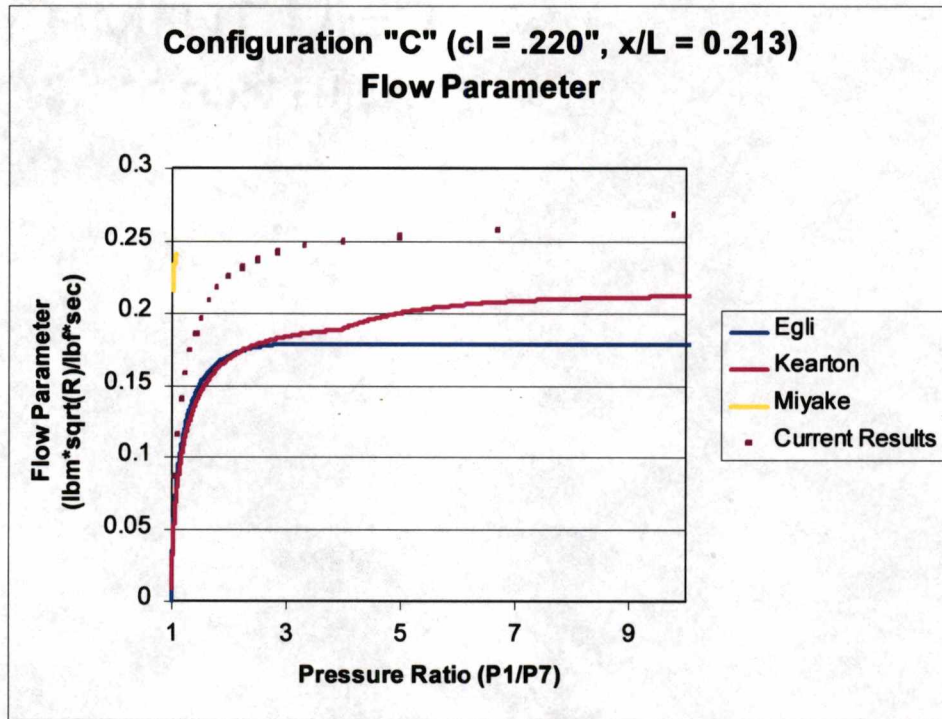


Figure A-19 – Configuration "C" Flow Parameter (cl = .220", x/L = 0.213)

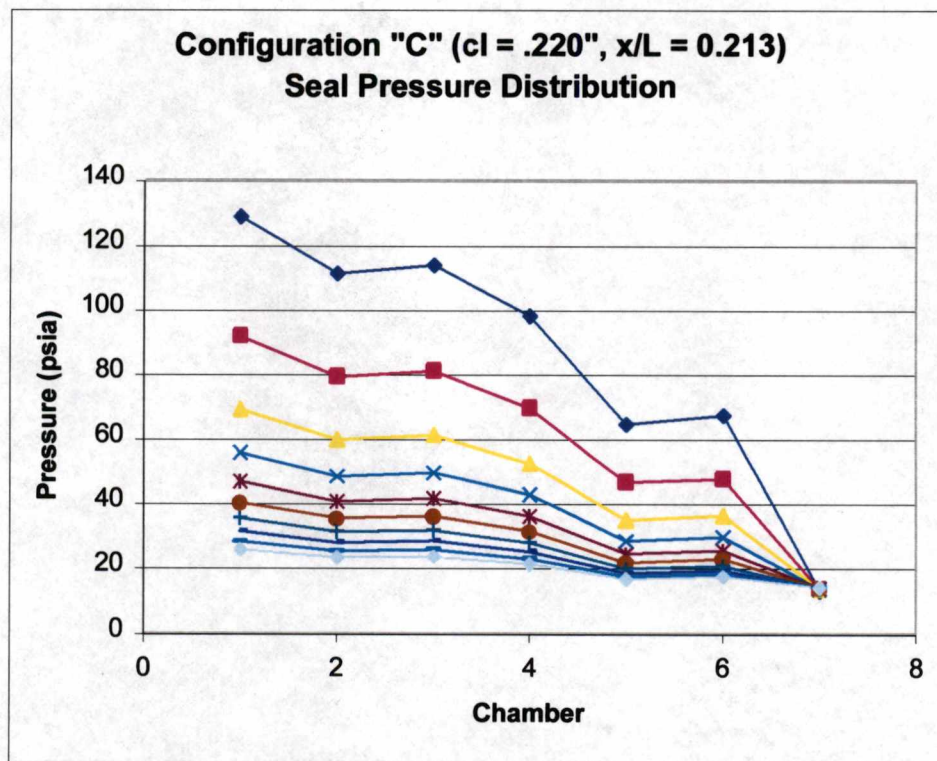


Figure A-20 – Configuration "C" Static Pressure Distribution (cl = .220", x/L = 0.213)

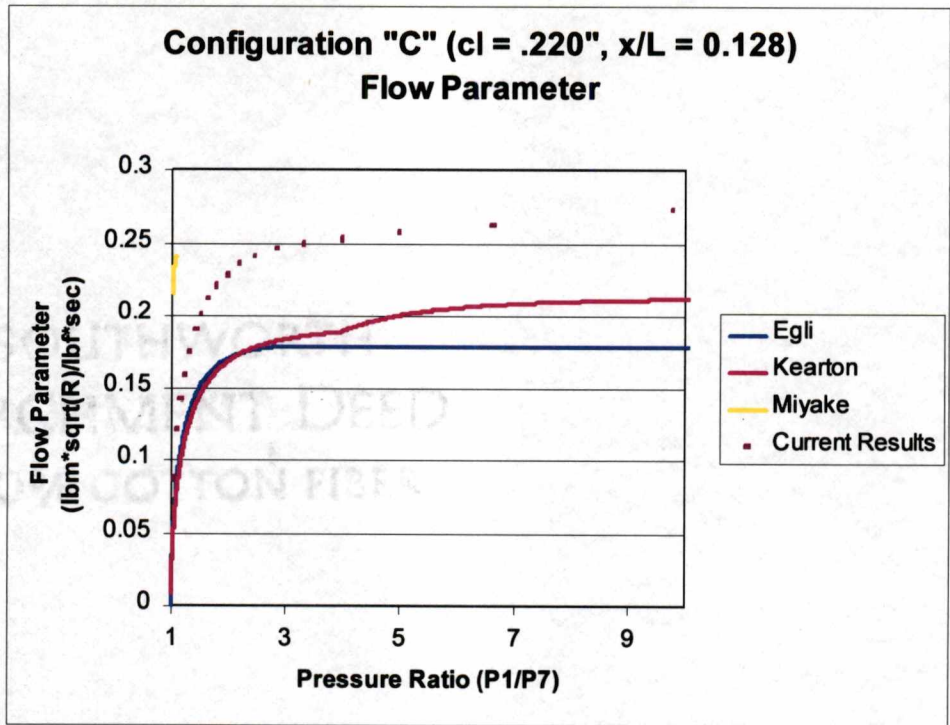


Figure A-21 – Configuration “C” Flow Parameter (cl = .220”, x/L = 0.128)

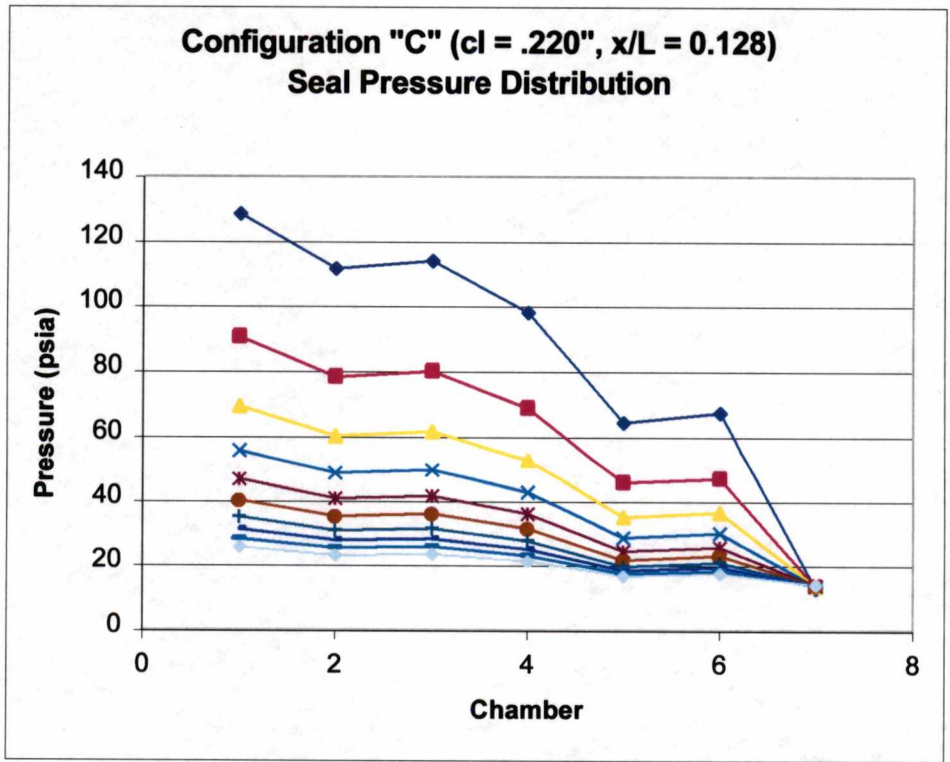


Figure A-22 – Configuration “C” Static Pressure Distribution (cl = .220”, x/L = 0.128)

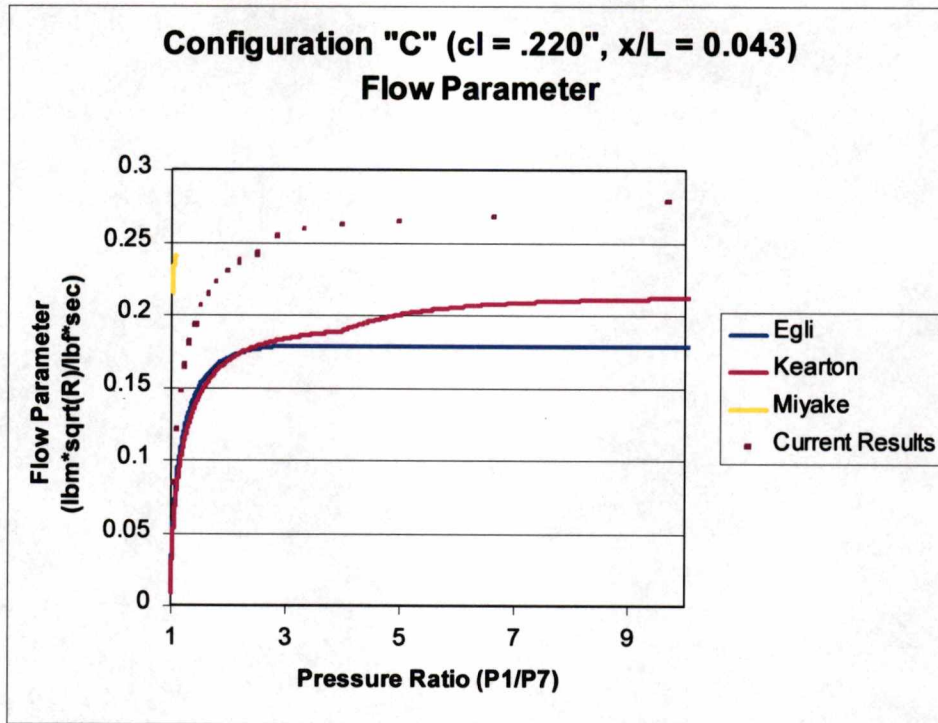


Figure A-23 – Configuration "C" Flow Parameter (cl = .220", x/L = 0.043)

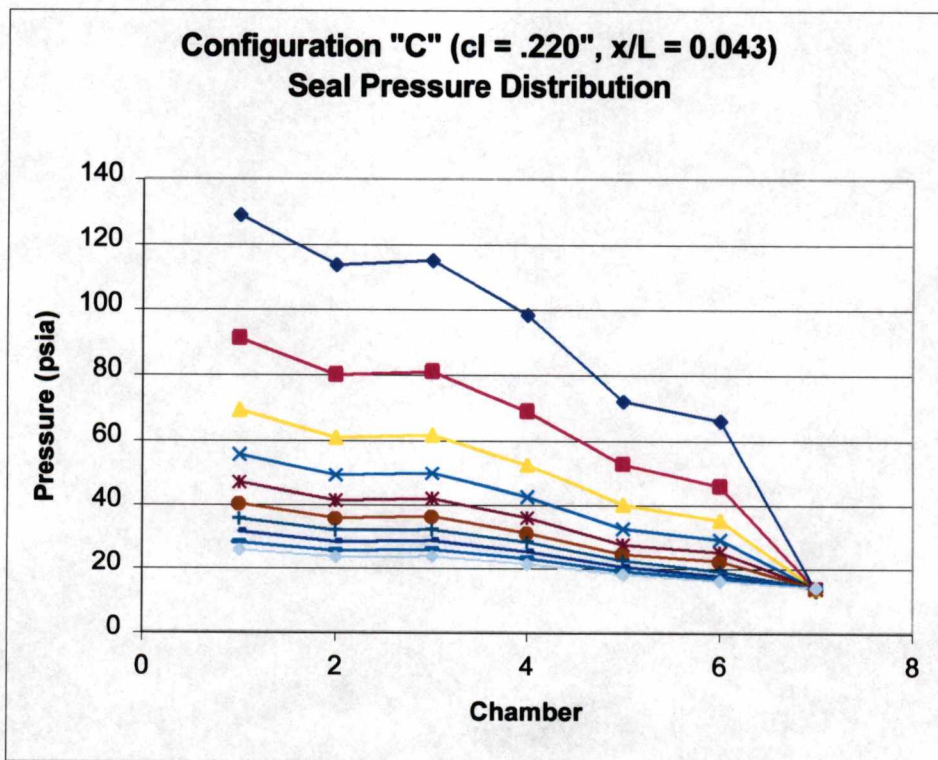


Figure A-24 – Configuration "C" Static Pressure Distribution (cl = .220", x/L = 0.043)

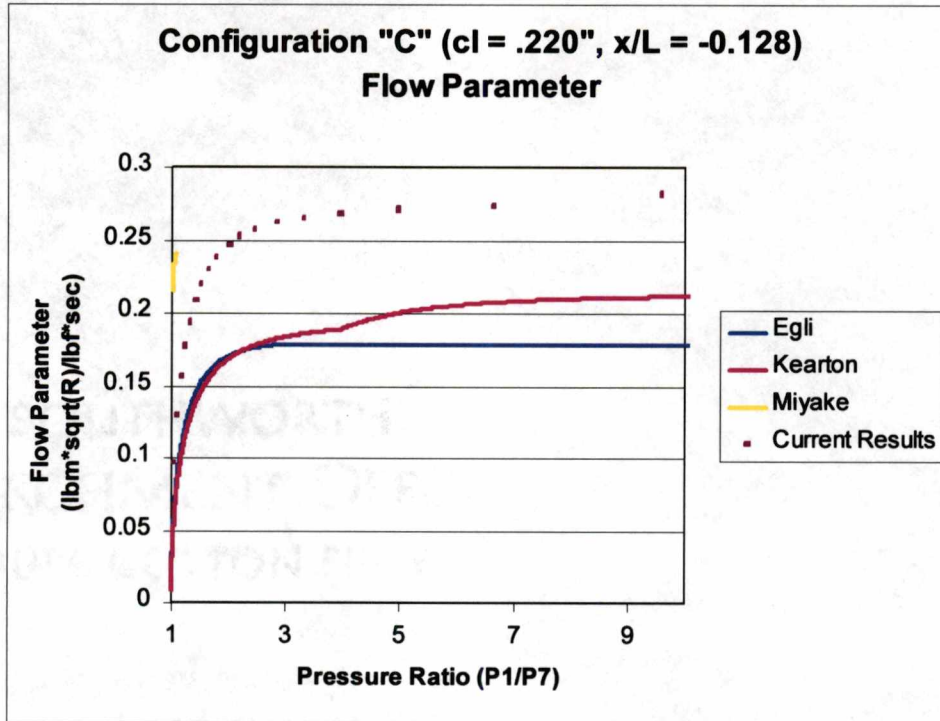


Figure A-25 – Configuration "C" Flow Parameter (cl = .220", x/L = -0.128)

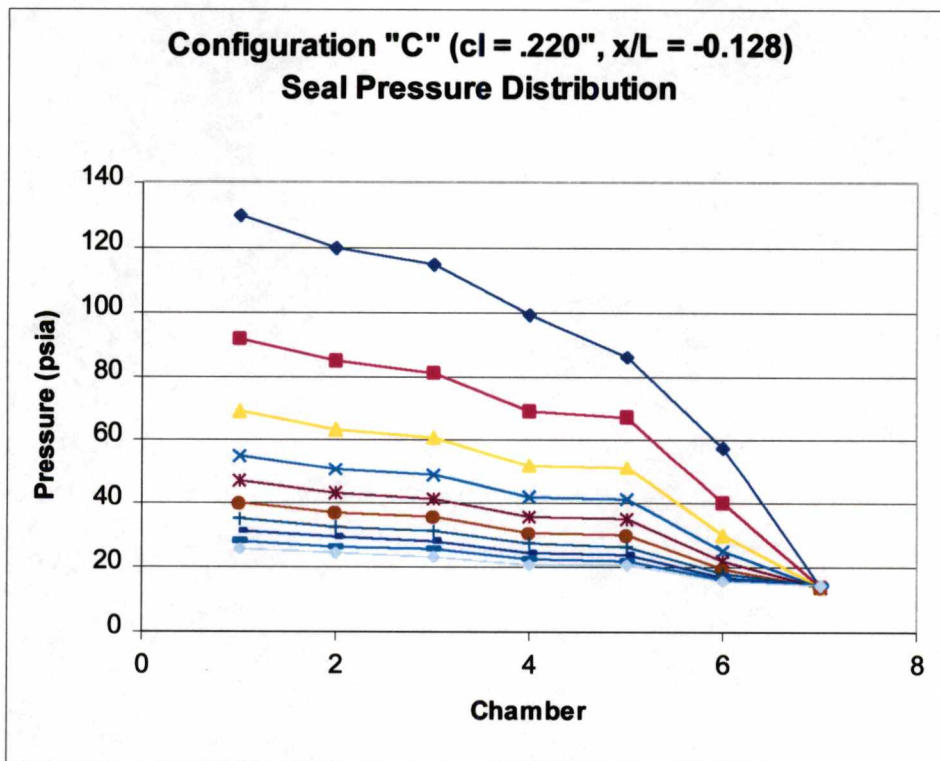


Figure A-26 – Configuration "C" Static Pressure Distribution (cl = .220", x/L = -0.128)

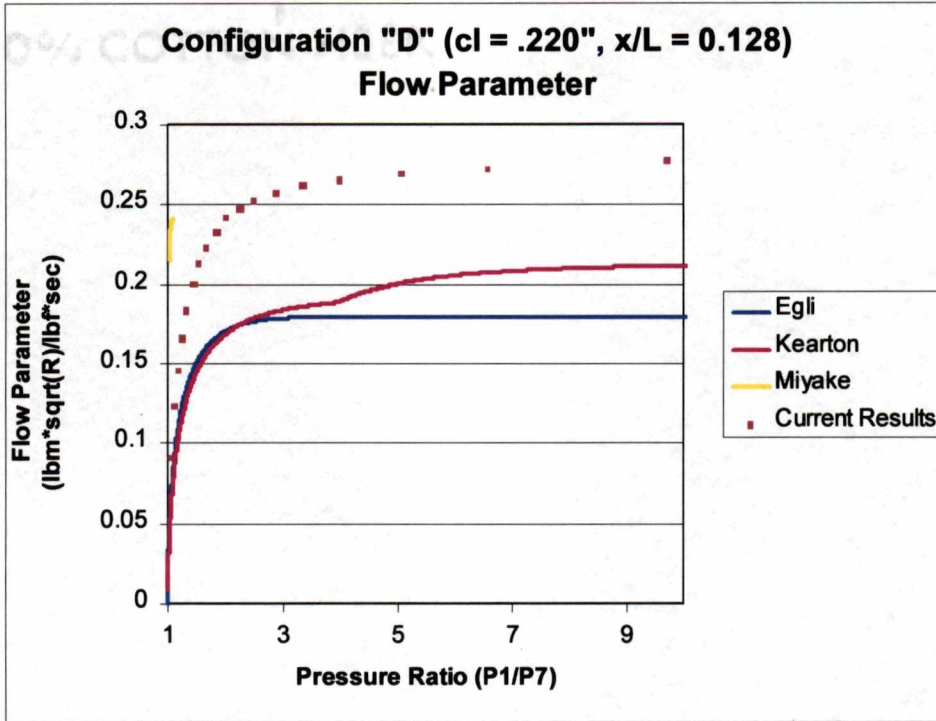


Figure A-27 – Configuration “D” Flow Parameter (cl = .220”, x/L = 0.128)

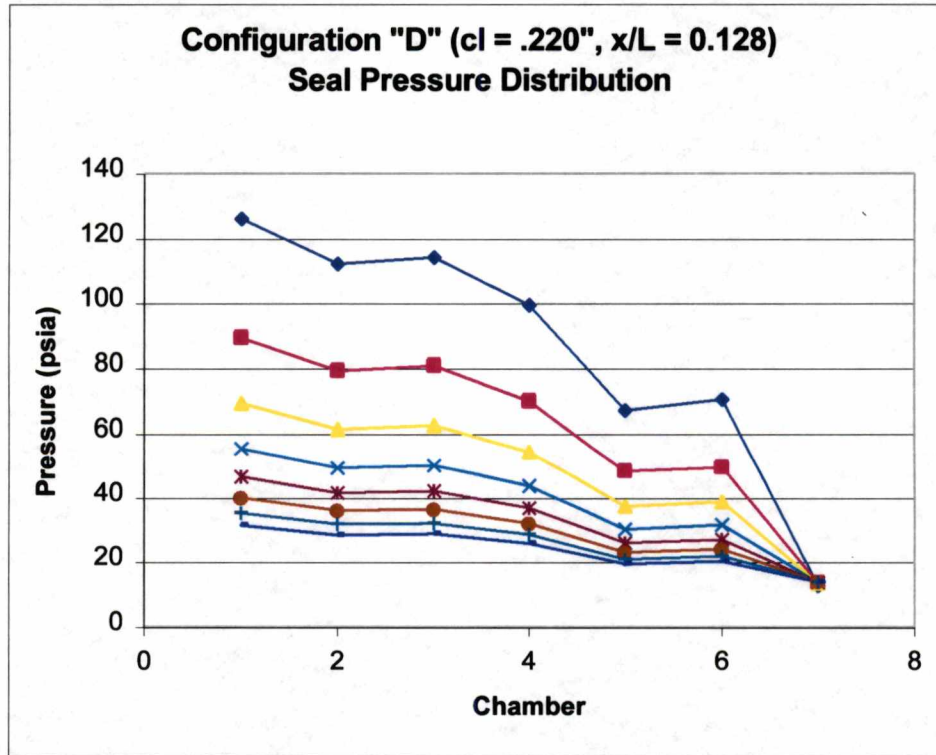


Figure A-28 – Configuration “D” Static Pressure Distribution (cl = .220”, x/L = 0.128)

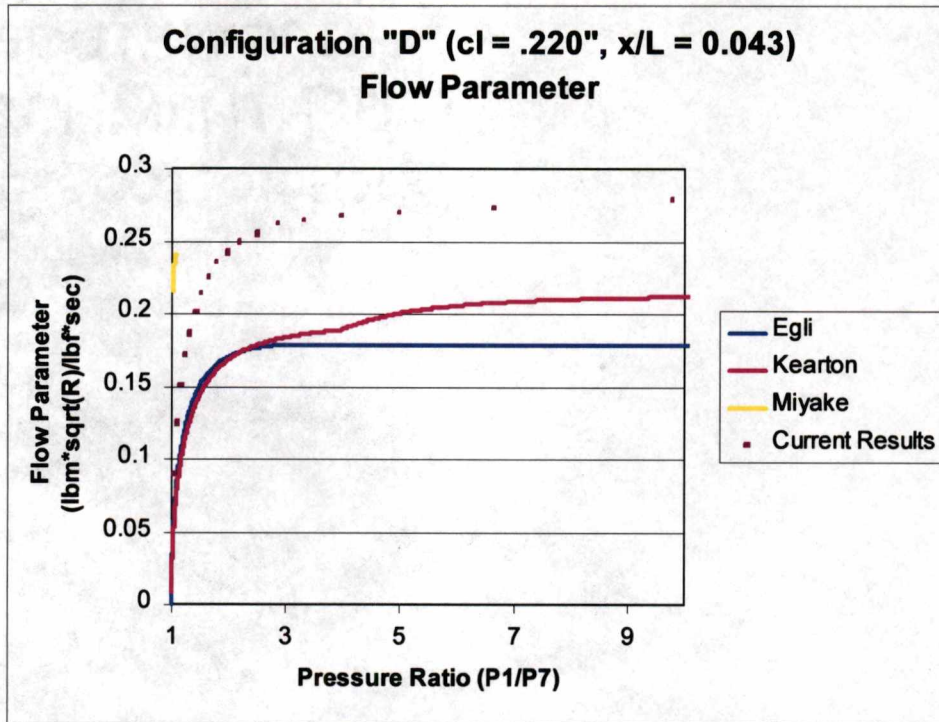


Figure A-29 – Configuration "D" Flow Parameter (cl = .220", x/L = 0.043)

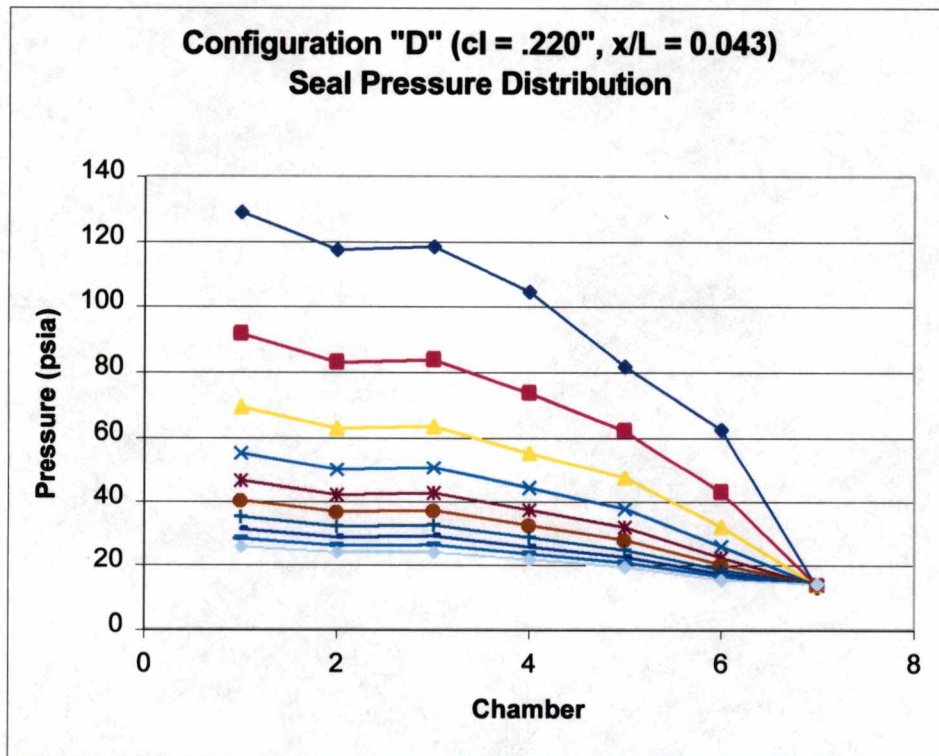


Figure A-30 – Configuration "D" Static Pressure Distribution (cl = .220", x/L = 0.043)

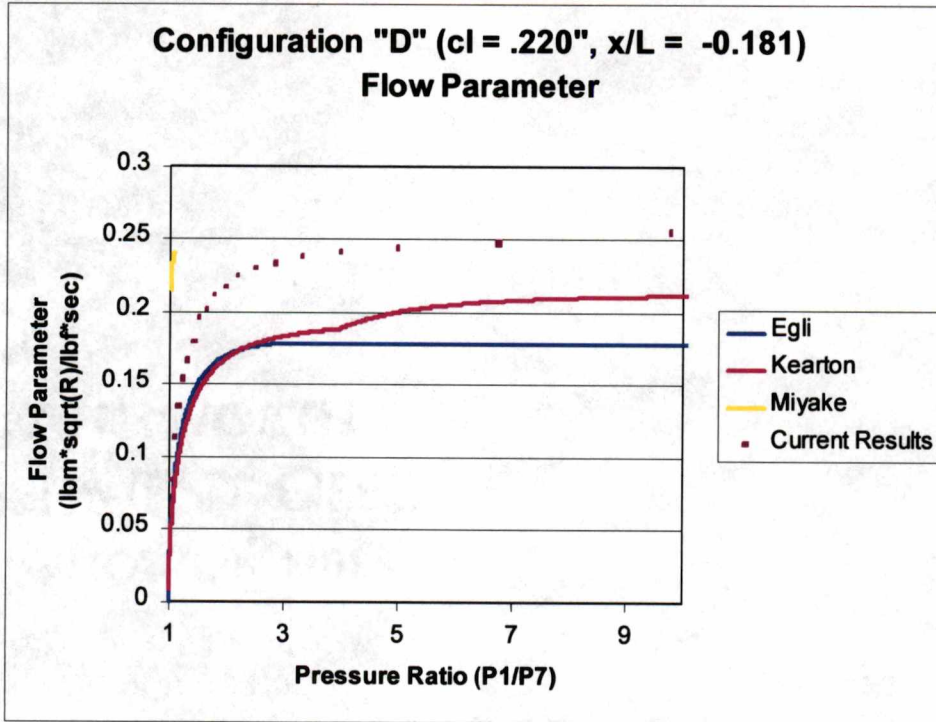


Figure A-31 – Configuration “D” Flow Parameter (cl = .220”, x/L = -0.181)

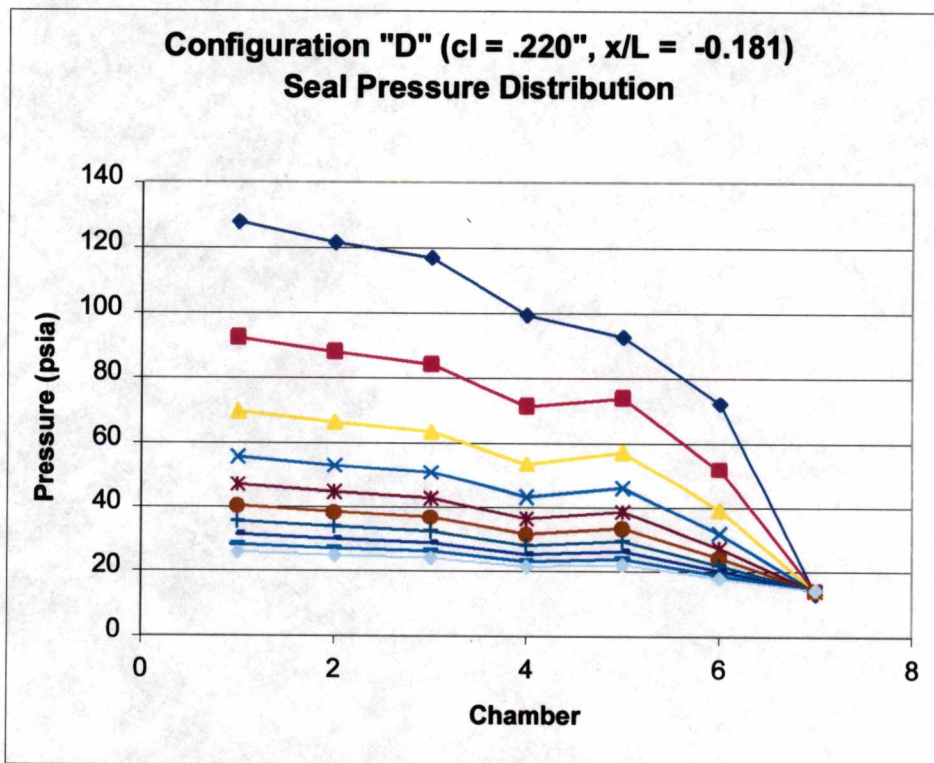


Figure A-32 – Configuration “D” Static Pressure Distribution (cl = .220”, x/L = -0.181)

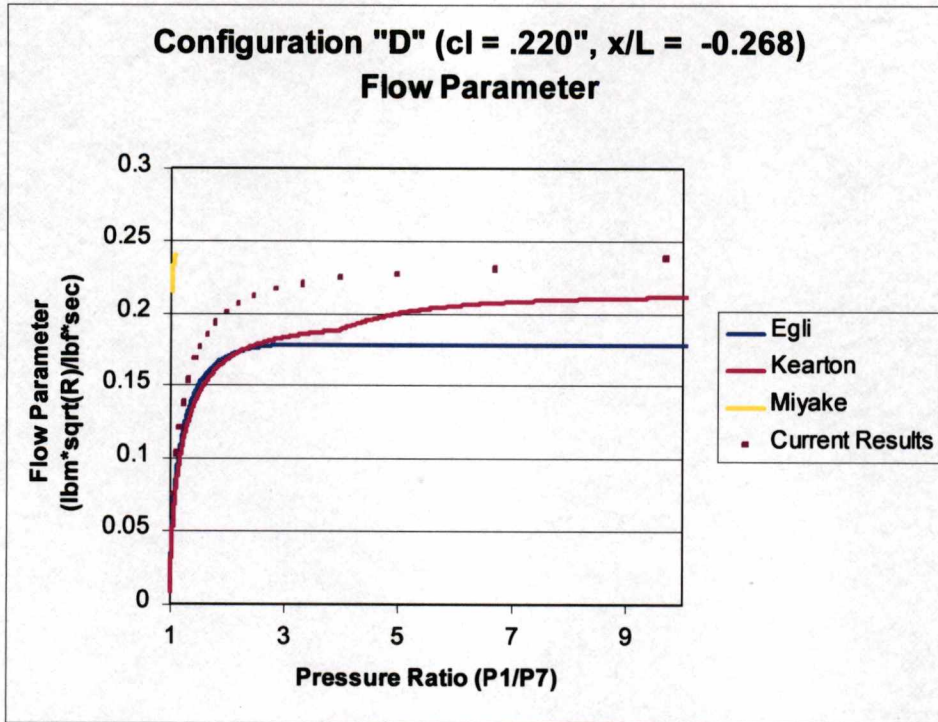


Figure A-33 – Configuration “D” Flow Parameter (cl = .220”, x/L = -0.268)

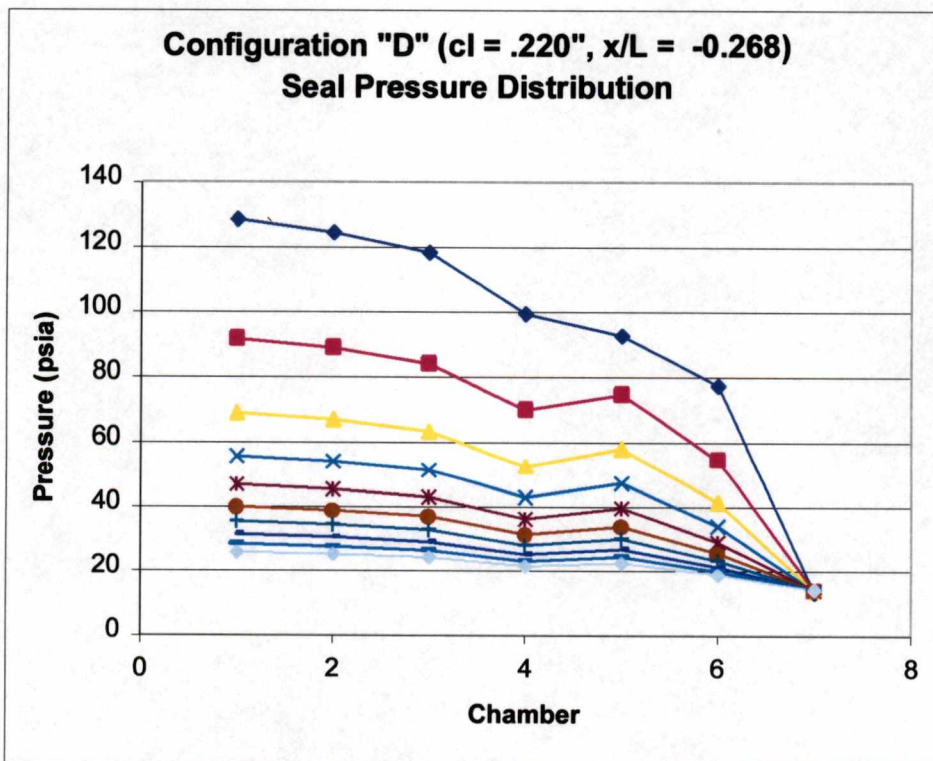


Figure A-34 – Configuration “D” Static Pressure Distribution (cl = .220”, x/L = -0.268)

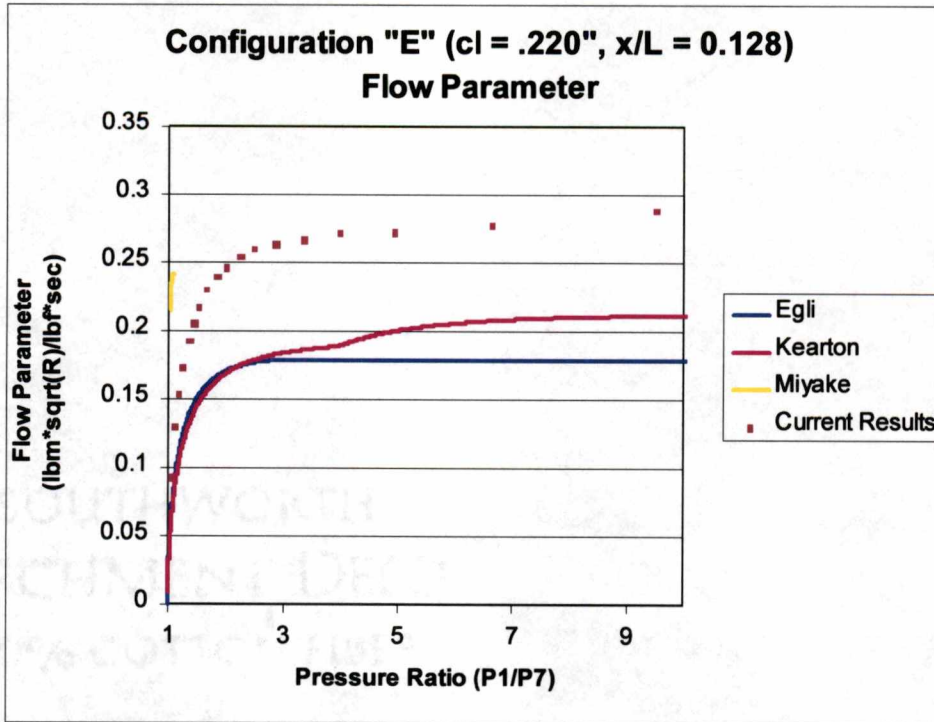


Figure A-35 – Configuration "E" Flow Parameter (cl = .220", x/L = 0.128)

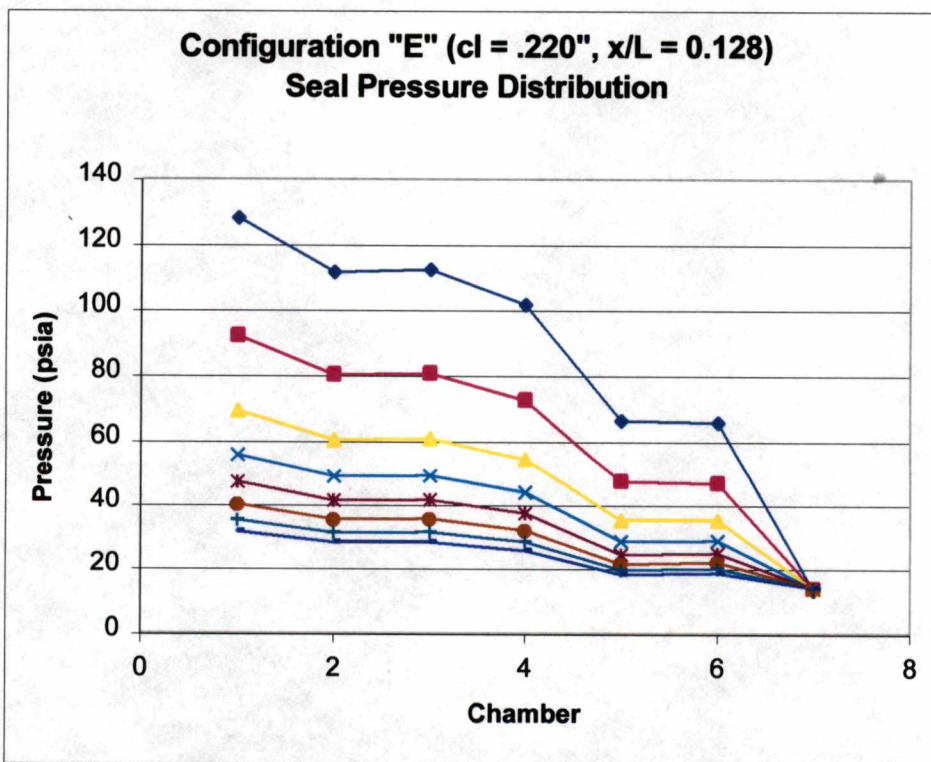


Figure A-36 – Configuration "E" Static Pressure Distribution (cl = .220", x/L = 0.128)

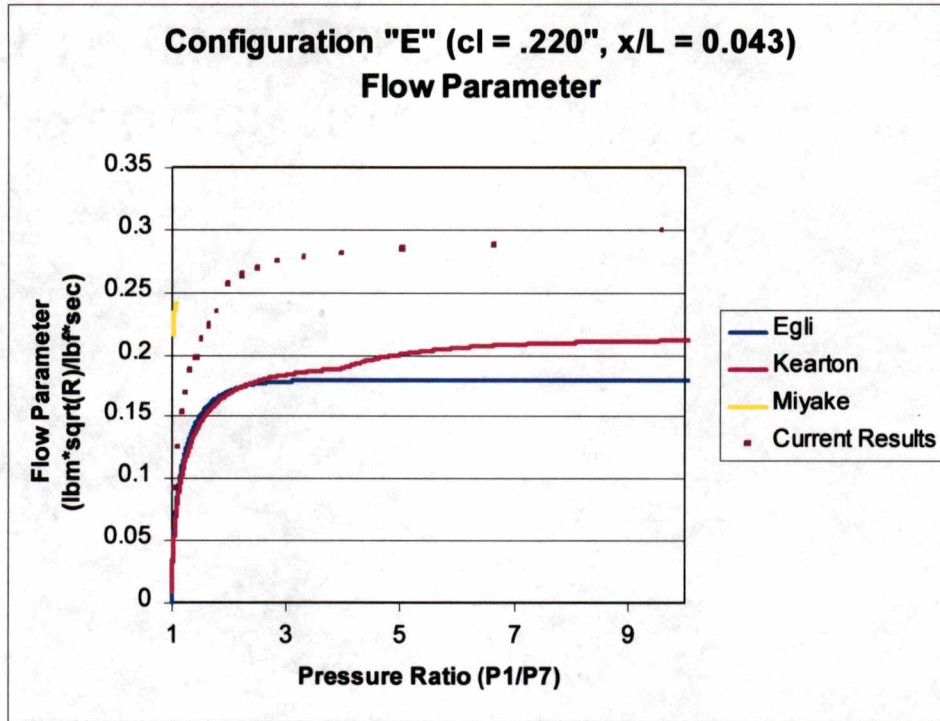


Figure A-37 – Configuration "E" Flow Parameter ($cl = .220$ ", $x/L = 0.043$)

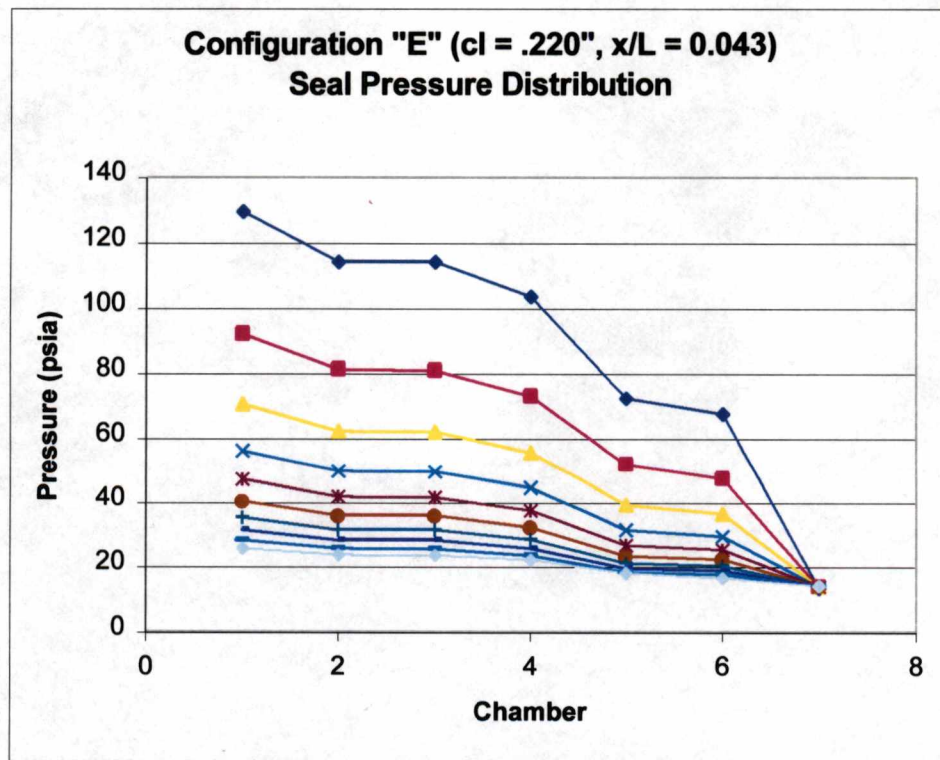


Figure A-38 – Configuration "E" Static Pressure Distribution ($cl = .220$ ", $x/L = 0.043$)

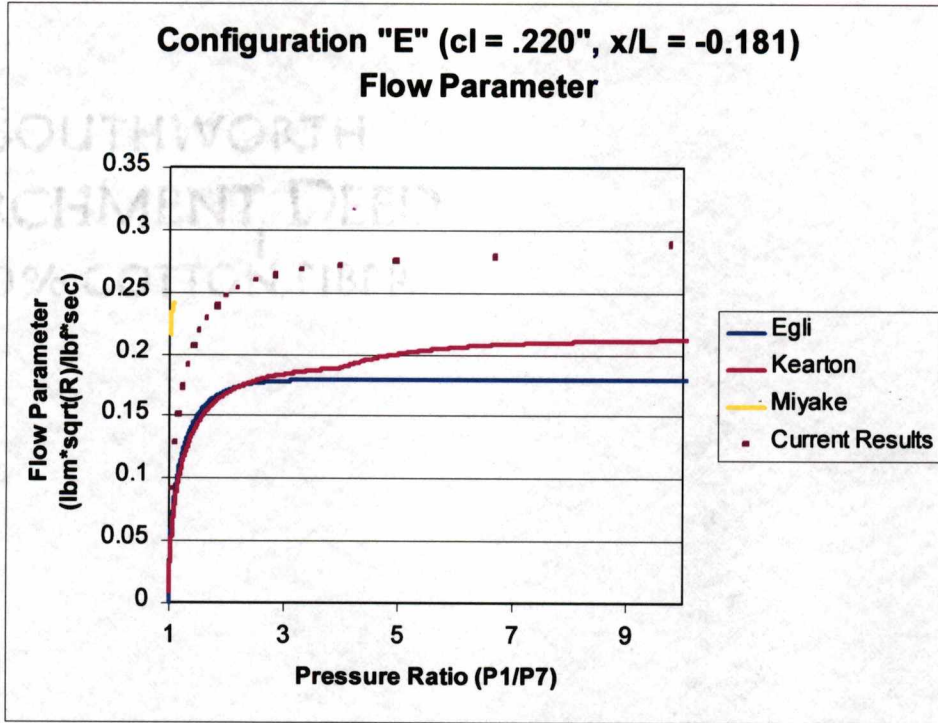


Figure A-39 – Configuration “E” Flow Parameter (cl = .220”, x/L = -0.181)

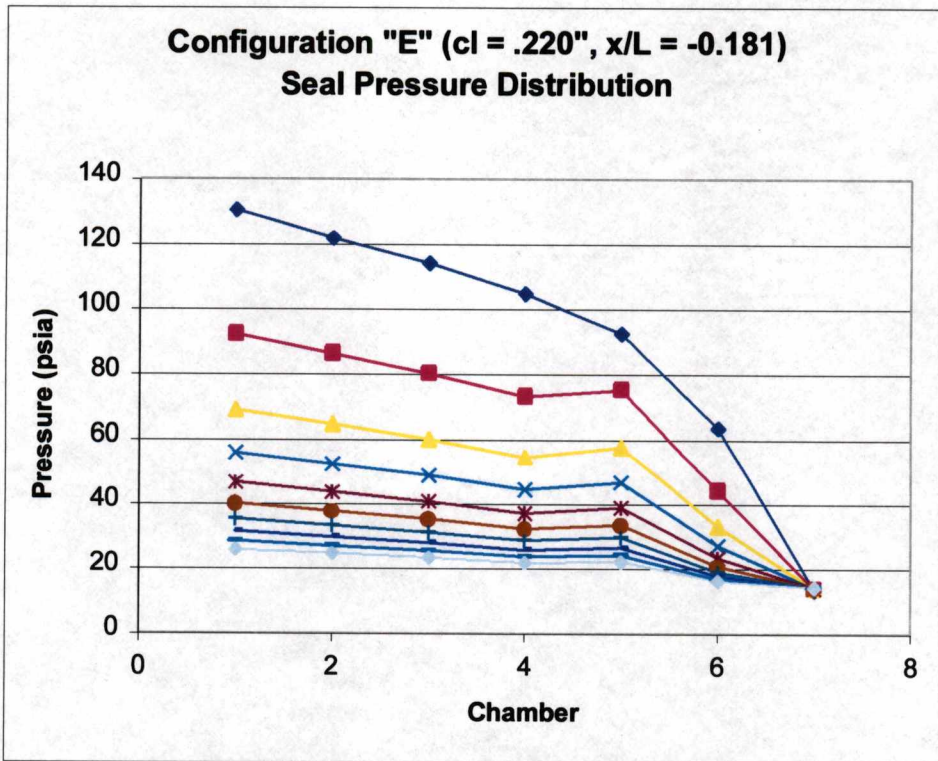


Figure A-40 – Configuration “E” Static Pressure Distribution (cl = .220”, x/L = -0.181)

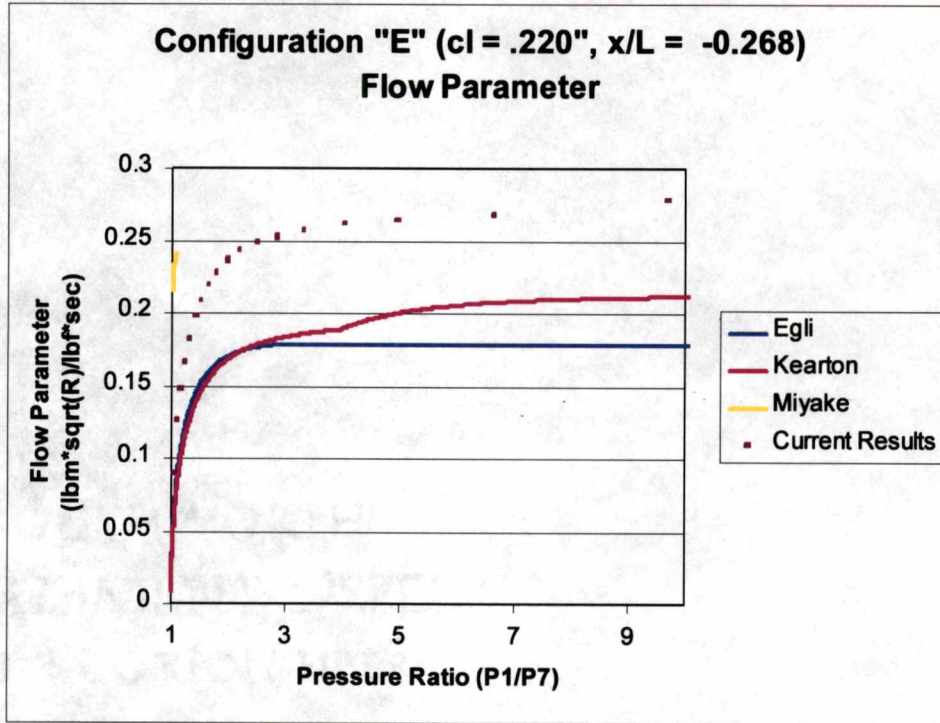


Figure A-41 – Configuration "E" Flow Parameter (cl = .220", x/L = -0.268)

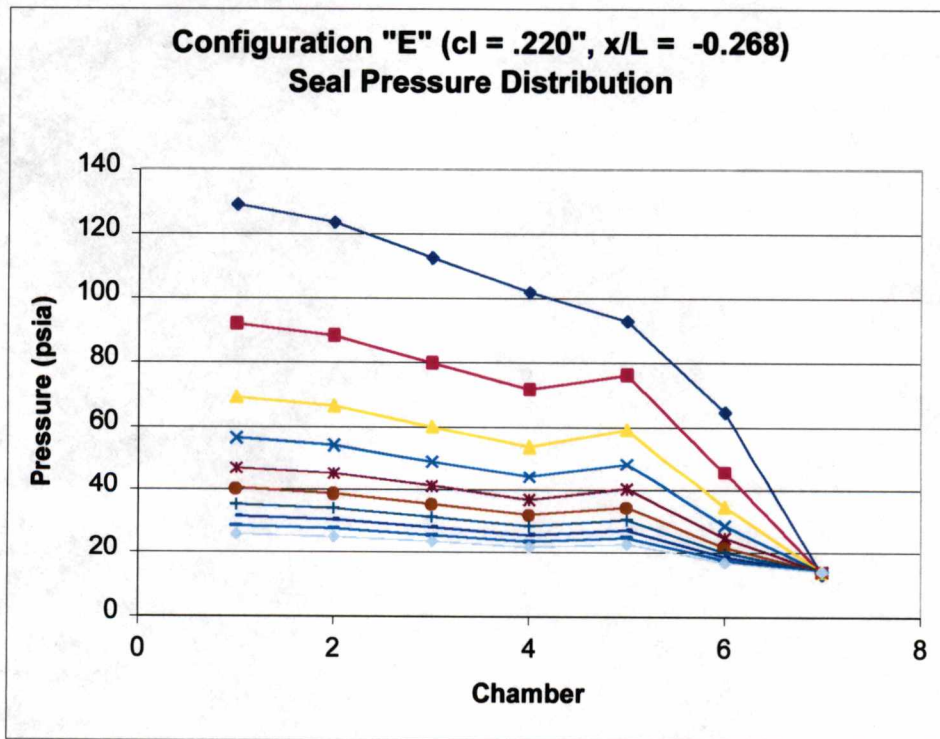


Figure A-42 – Configuration "E" Static Pressure Distribution (cl = .220", x/L = -0.268)

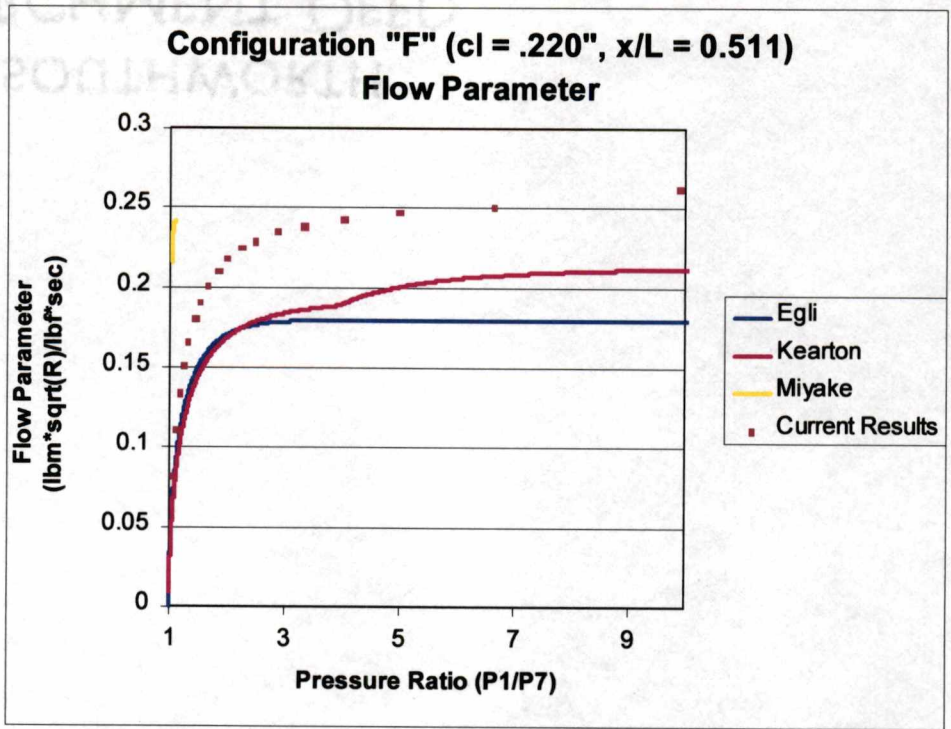


Figure A-43 – Configuration "F" Flow Parameter ($c_l = .220$ ", $x/L = 0.511$)

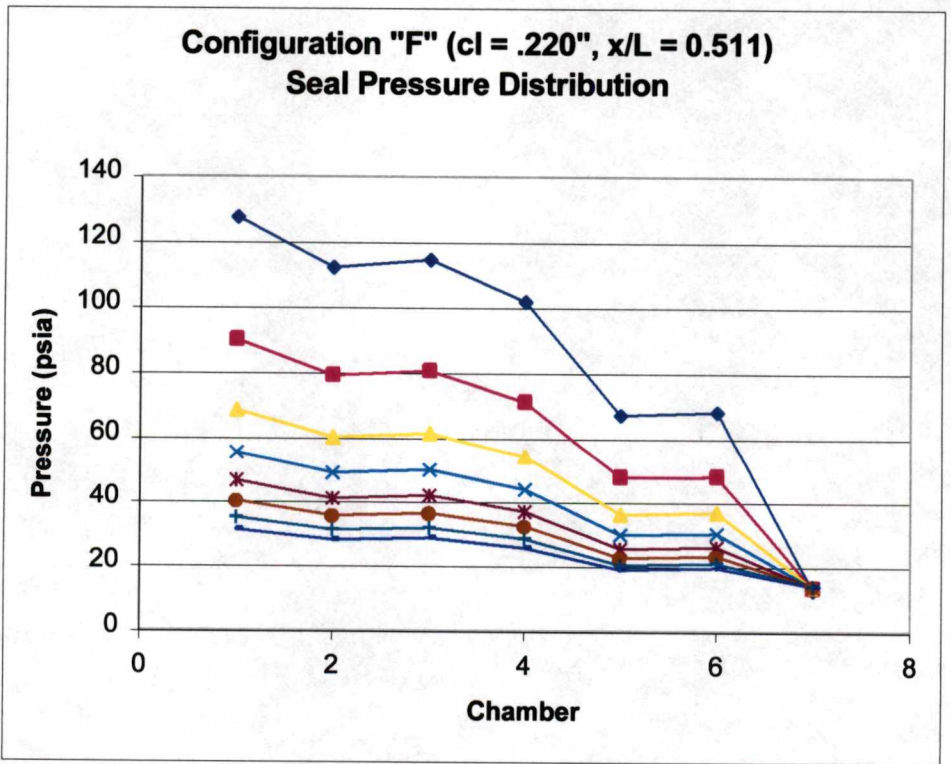


Figure A-44 – Configuration "F" Static Pressure Distribution ($c_l = .220$ ", $x/L = 0.511$)

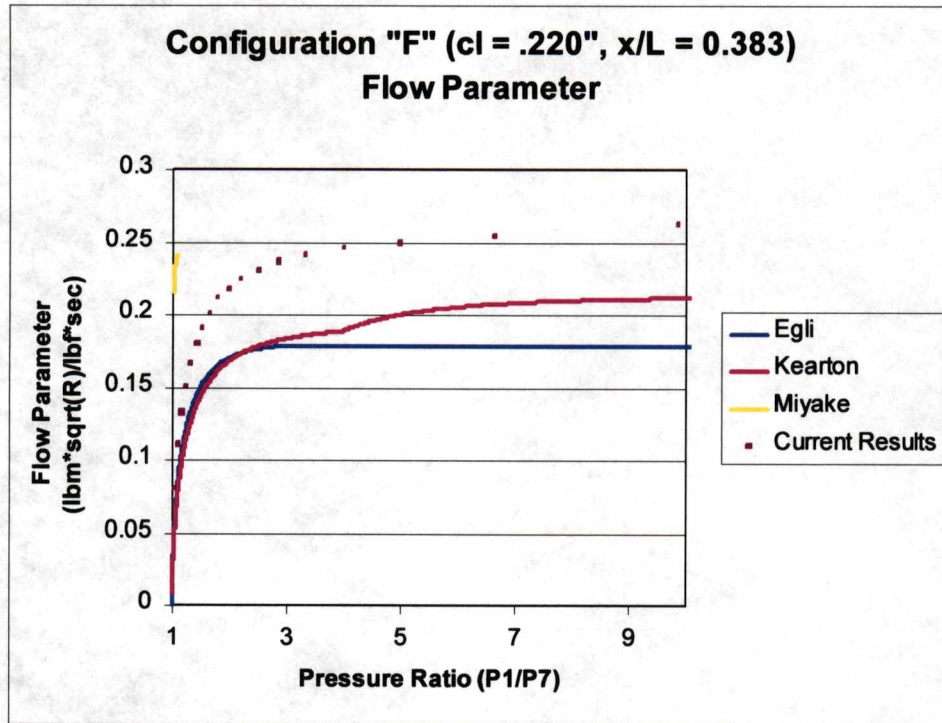


Figure A-45 – Configuration "F" Flow Parameter (cl = .220", x/L = 0.383)

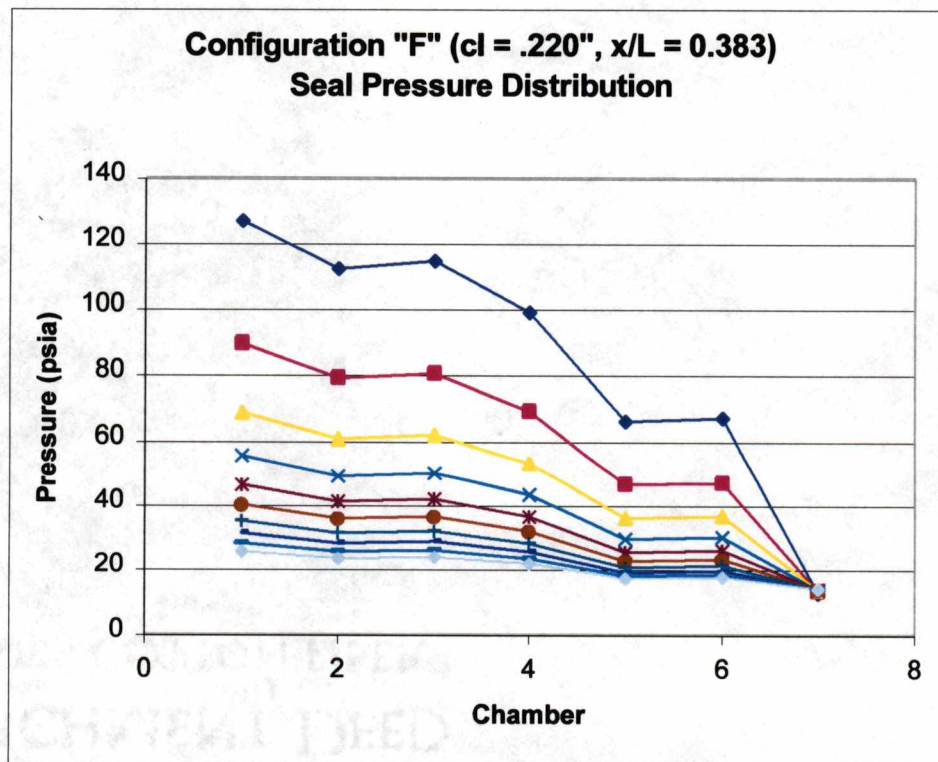


Figure A-46 – Configuration "F" Static Pressure Distribution (cl = .220", x/L = 0.383)

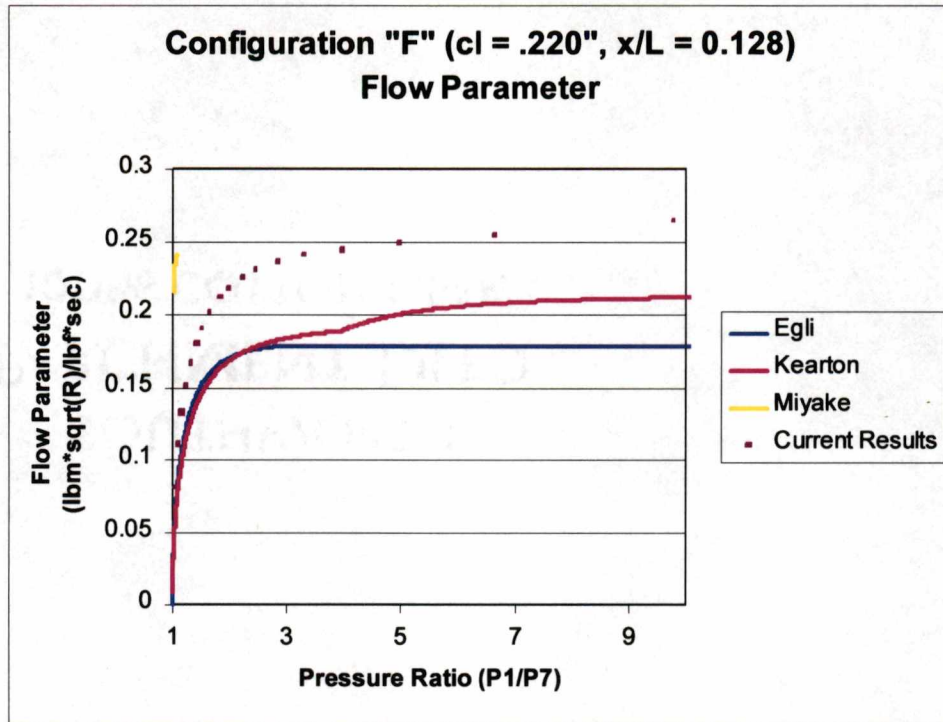


Figure A-47 – Configuration "F" Flow Parameter ($c_l = .220"$, $x/L = 0.128$)

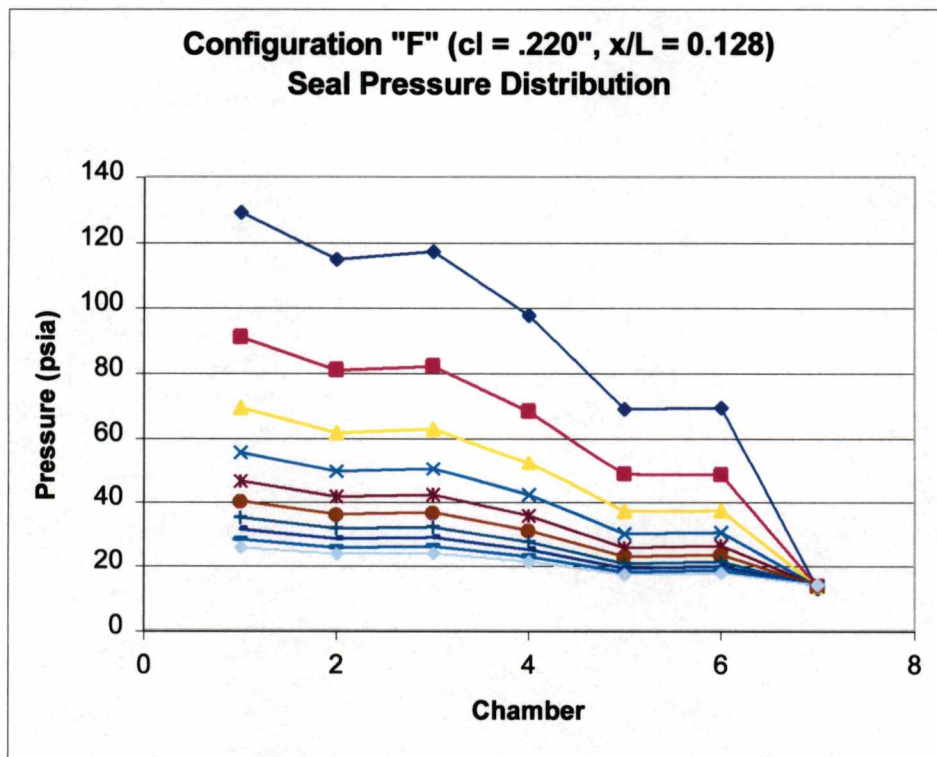


Figure A-48 – Configuration "F" Static Pressure Distribution ($c_l = .220"$, $x/L = 0.128$)

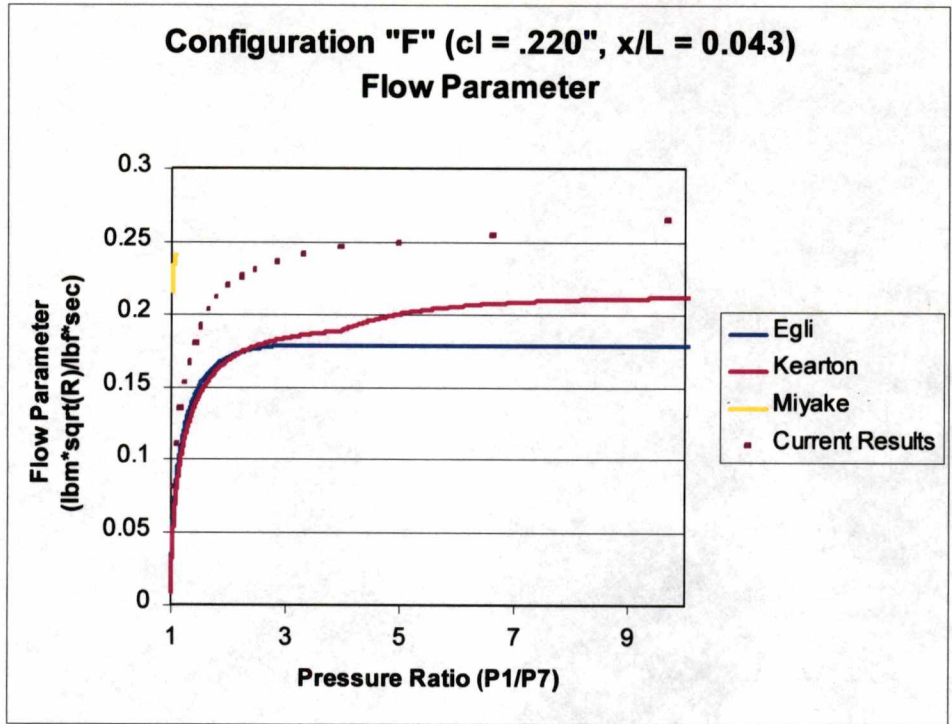


Figure A-49 – Configuration "F" Flow Parameter (cl = .220", x/L = 0.043)

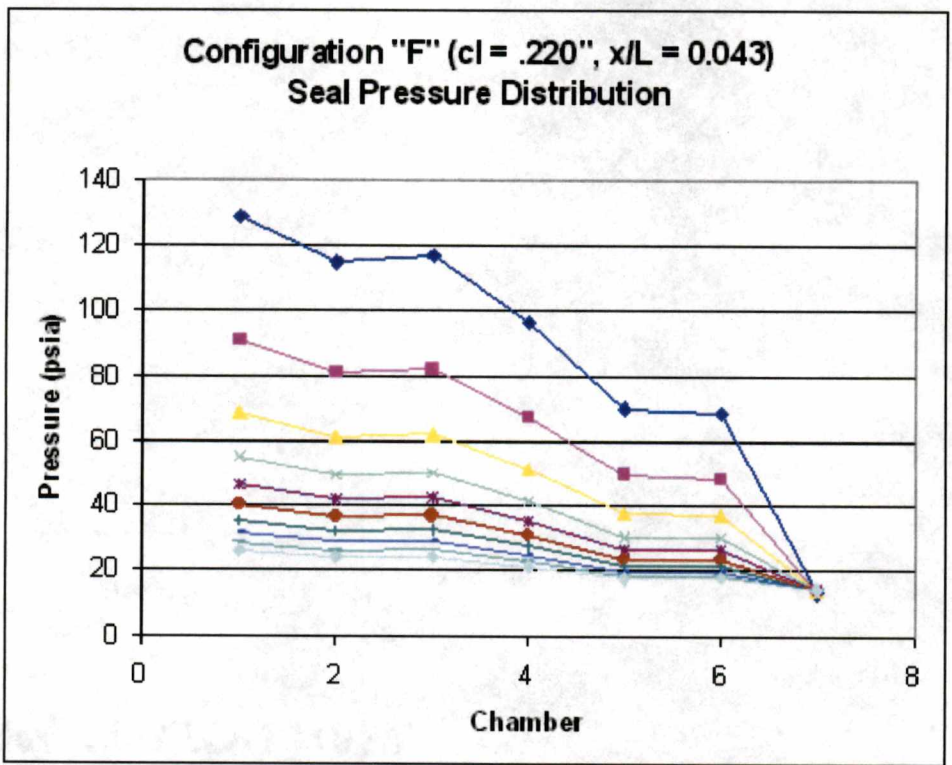


Figure A-50 – Configuration "F" Static Pressure Distribution (cl = .220", x/L = 0.043)

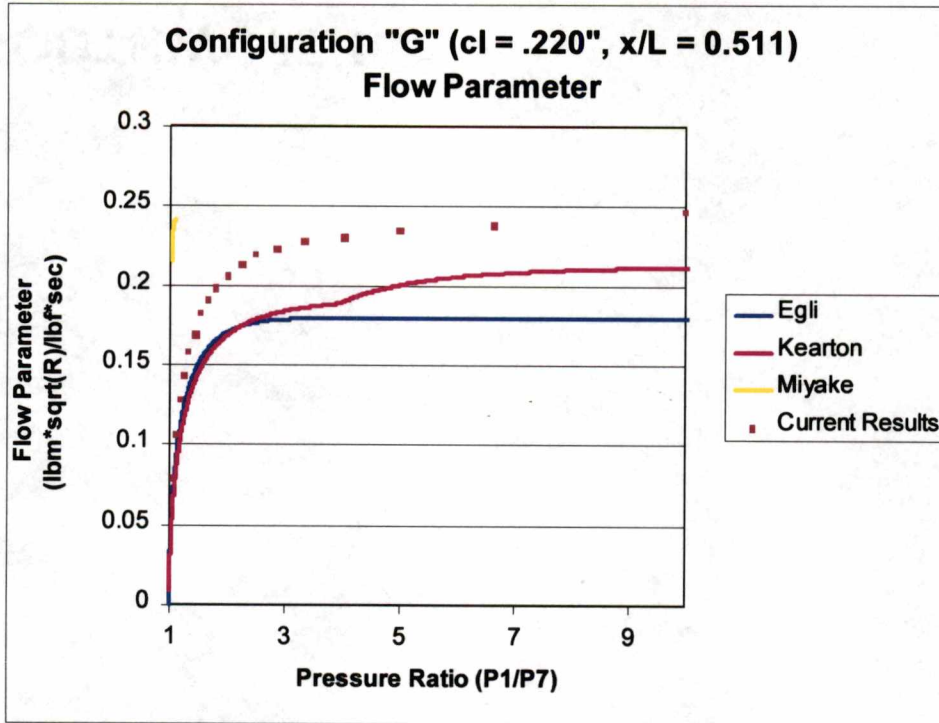


Figure A-51 – Configuration “G” Flow Parameter (cl = .220”, x/L = 0.511)

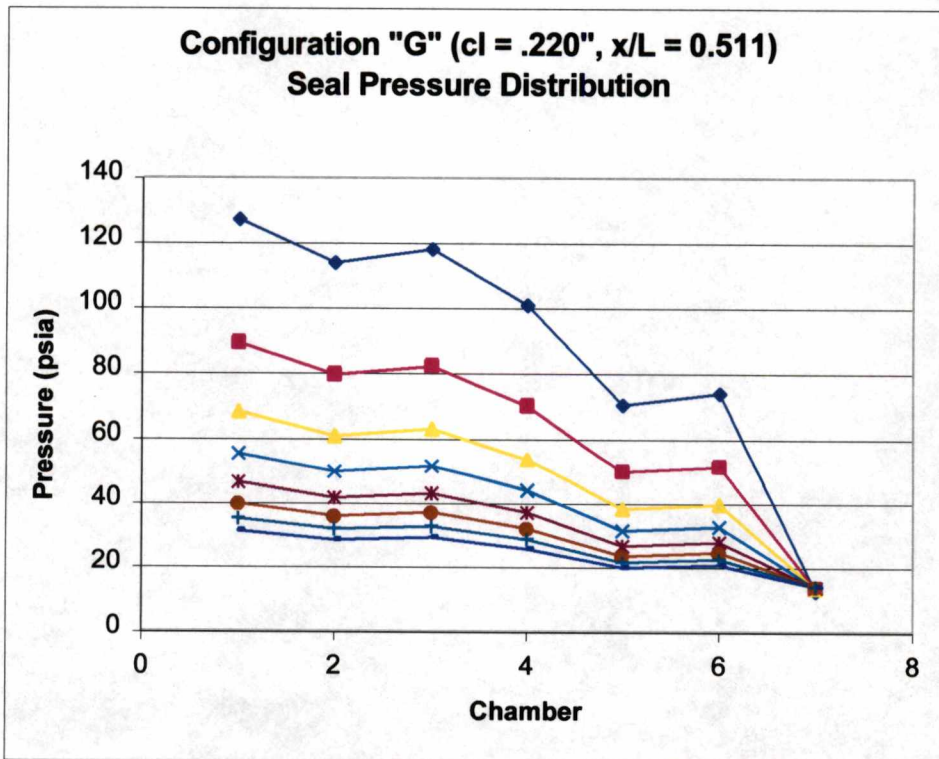


Figure A-52 – Configuration “G” Static Pressure Distribution (cl = .220”, x/L = 0.511)

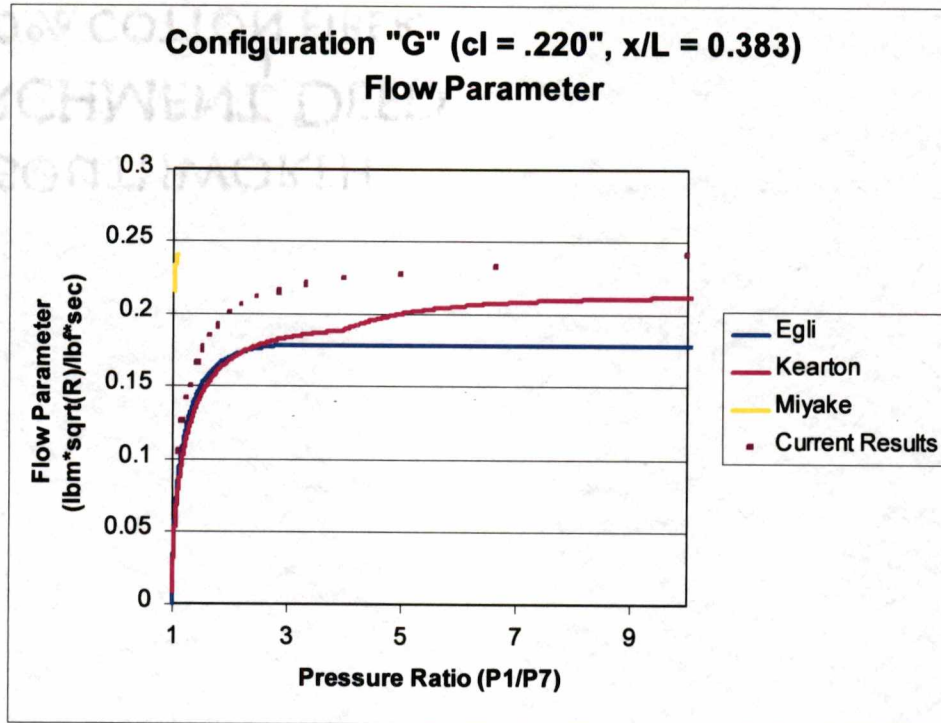


Figure A-53 – Configuration "G" Flow Parameter ($c_l = .220$ ", $x/L = 0.383$)

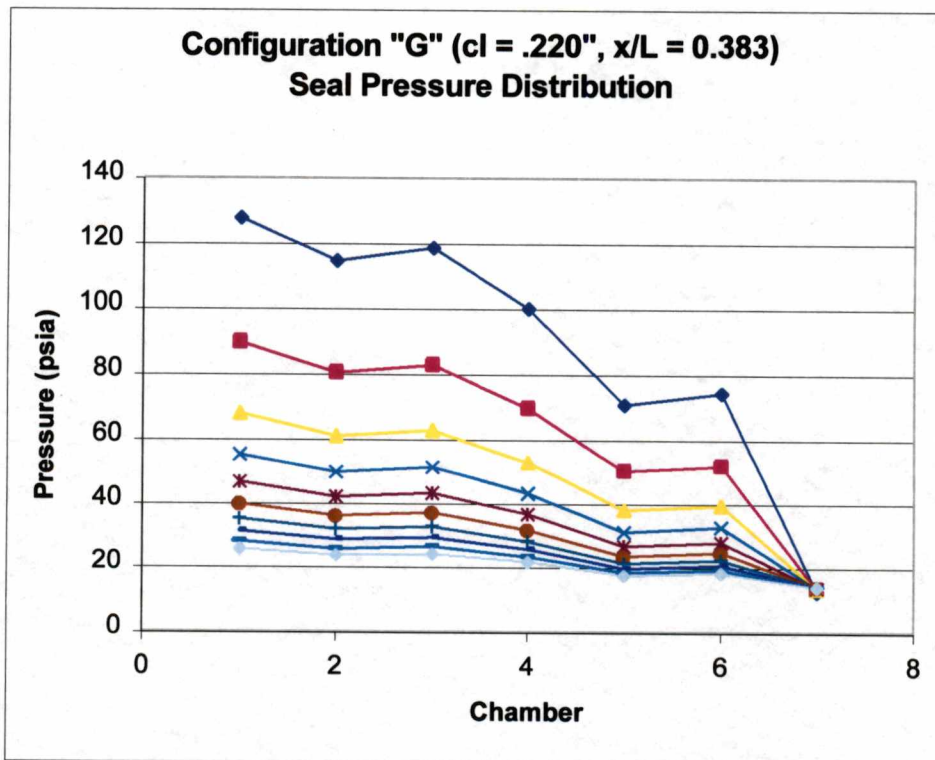


Figure A-54 – Configuration "G" Static Pressure Distribution ($c_l = .220$ ", $x/L = 0.383$)

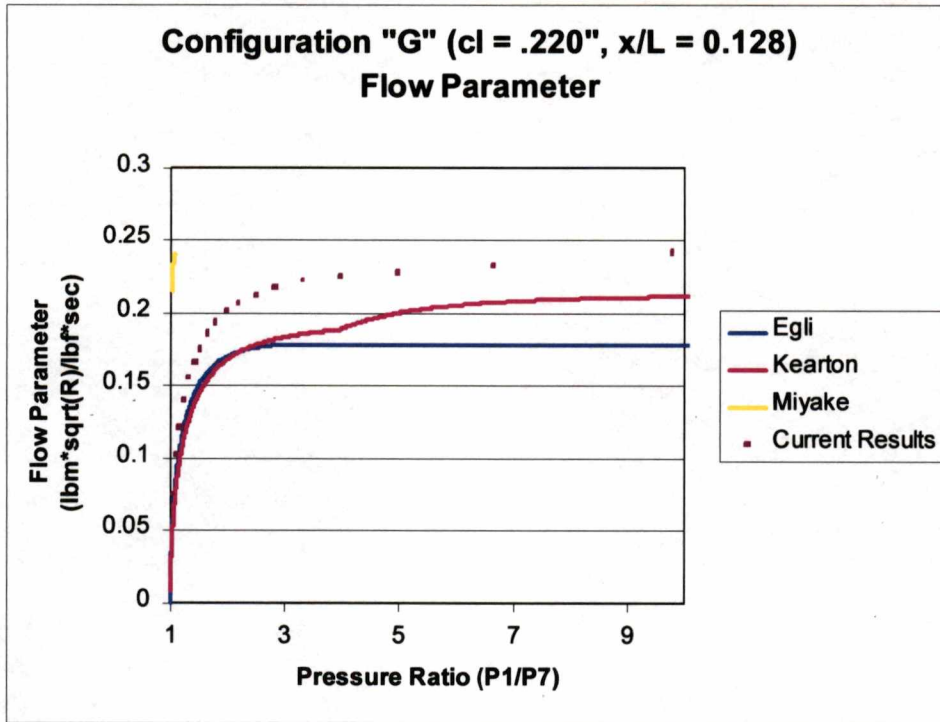


Figure A-55 – Configuration "G" Flow Parameter (cl = .220", x/L = 0.128)

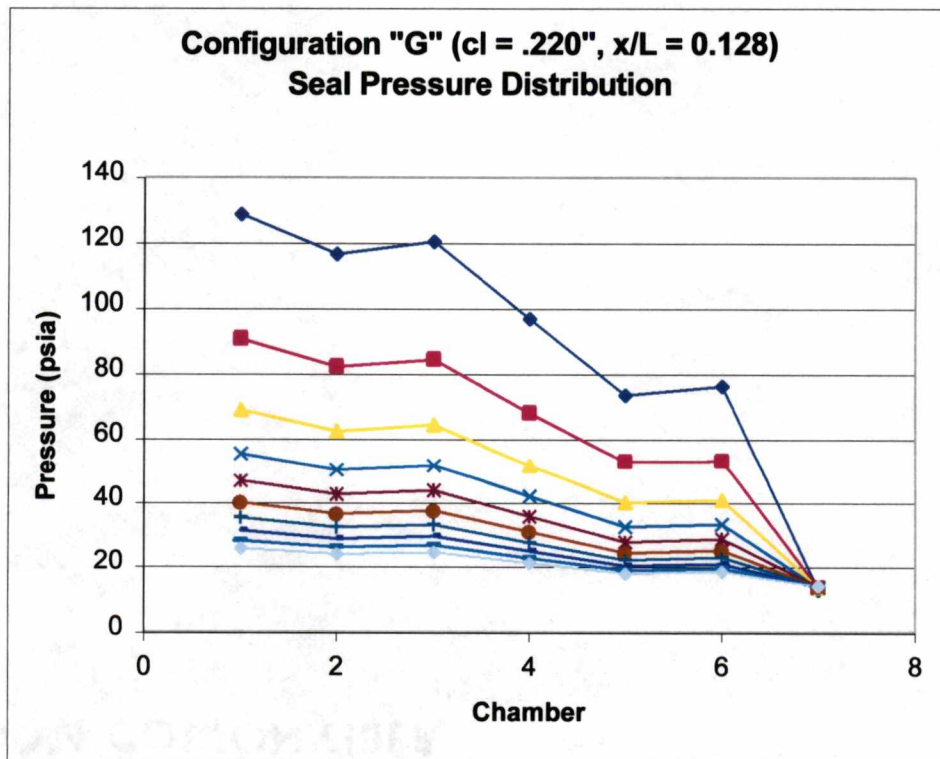


Figure A-56 – Configuration "G" Static Pressure Distribution (cl = .220", x/L = 0.128)

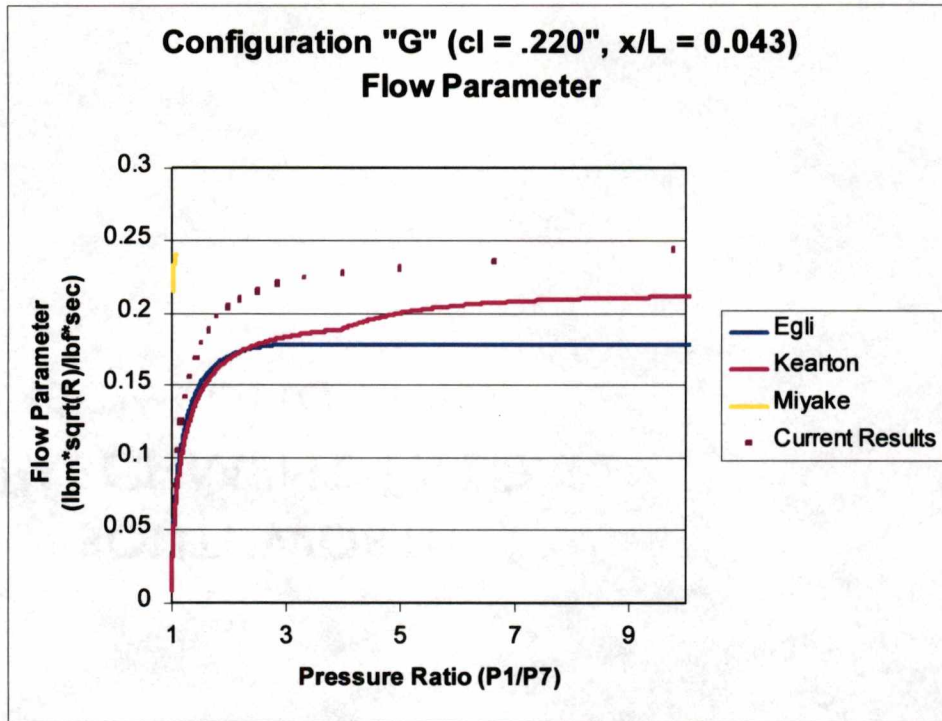


Figure A-57 – Configuration "G" Flow Parameter (cl = .220", x/L = 0.043)

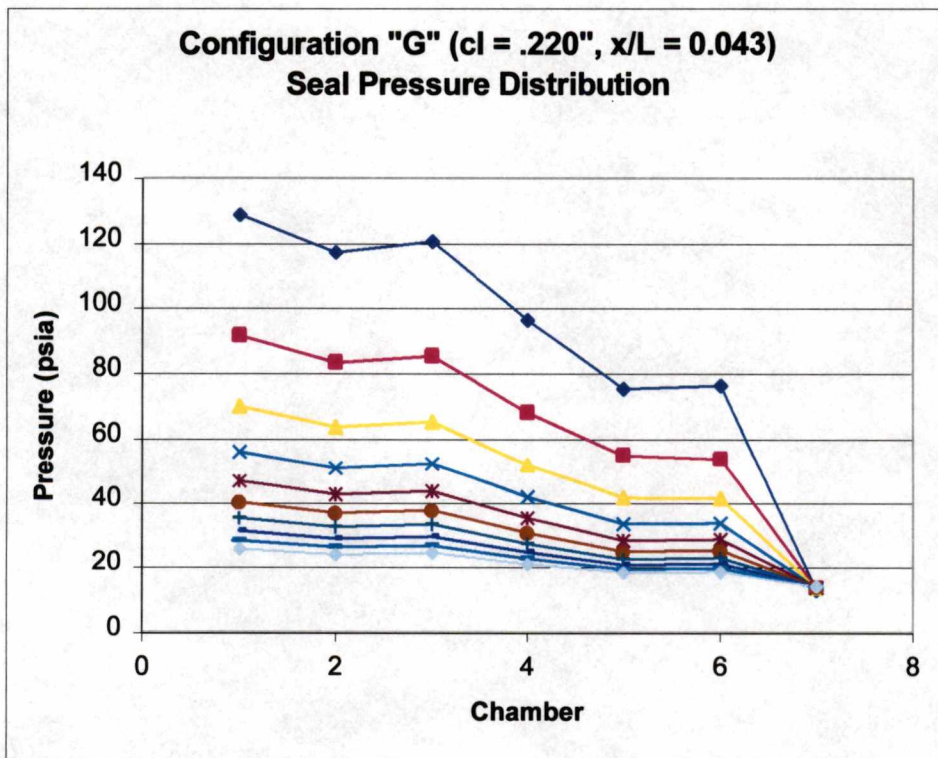


Figure A-58 – Configuration "G" Static Pressure Distribution (cl = .220", x/L = 0.043)

**APPENDIX B: SAMPLE MATHCAD™ CALCULATIONS FOR EGLI,
KEARTON & KEH AND MIYAKE & DUH METHODS**

The following calculations provide estimates for leakage through the TVA/UTSI labyrinth seal air model using three methods available in the open literature.

$k := 1.4$	Ratio of specific heats for air
$\text{clearance} := 0.220\text{-in}$	Throttle clearance in the model (may be varied)
$\text{width} := 4\text{-in}$	Seal model width
$A := \text{clearance} \cdot \text{width}$	Geometric throttling area
$T_o := 511\text{-R}$	Ambient temp (upstream)
$T_n := 519\text{-R}$	Ambient temp (downstream)
$\text{gas_const} := \frac{53.18\text{-ft}\cdot\text{lb}}{\text{lb}\cdot\text{R}}$	Ideal gas const
$n := 6$	Number of stages in the seal
$\alpha := .67$	Assumed sharp edged throttlings

A vector of pressure ratios is created so that seal leakage can be estimated over a range of seal pressure ratios from 0 to 1.

$i := 1..1000$	Define size of array. Can be varied but this size provides reasonable accuracy	
$P_o := 125 \cdot \frac{\text{lb}}{\text{in}^2}$	Upstream pressure	
$P_{n_i} := P_o \cdot \frac{i}{1000}$	Pressure after the last throttling	
$\rho_o := \frac{P_o}{\text{gas_const} \cdot T_o}$	Upstream air density at STP	$\rho_o = 10.61 \frac{\text{kg}}{\text{m}^3}$
$v_o := \frac{1}{\rho_o}$	Specific volume for air at STP	$v_o = 48.574 \frac{\text{ft}^3}{\text{slug}}$
$\rho_n := \frac{P_n}{\text{gas_const} \cdot T_n}$	Downstream air density	

$$\mu_o := 2.85 \cdot \left[\frac{(T_o)}{R} \right]^{.68} \cdot 10^{-5} \cdot \frac{\text{lb}}{\text{ft}\cdot\text{sec}}$$

Calculates air viscosity as a function of temperature. Based on data from "Basic Turbine design".

$$\mu_o = 1.009 \times 10^{-6} \frac{\text{lb}}{\text{in}\cdot\text{sec}}$$

$$v_o := \frac{\mu_o}{\rho_o}$$

Calculates upstream kinematic viscosity

$$v_o = 1.828 \times 10^{-5} \frac{\text{ft}^2}{\text{sec}}$$

$$v_n := 1.8 \cdot 10^{-5} \frac{\text{m}^2}{\text{sec}}$$

Provides a value for exit viscosity (air at STP)

$$v := \frac{v_n + v_o}{2}$$

Average kinematic viscosity of air in seal (rough estimate as I'm not yet sure what temps will be)

$$v = 9.849 \times 10^{-6} \frac{\text{m}^2}{\text{s}}$$

Egli's Method

For the case of a ideal labyrinth with n throttles, as described in Egli's paper

$$\phi_i := \sqrt{\frac{1 - \left(\frac{P_{n_i}}{P_o} \right)^2}{n + \frac{2}{k} \ln \left(\frac{P_o}{P_{n_i}} \right)}}$$

$$i := 2..1000$$

$$\phi_{v_E_i} := \begin{cases} \max(\phi) & \text{if } \phi_i < \max(\phi) \wedge \phi_i - \phi_{i-1} > 0 \\ \phi_i & \text{otherwise} \end{cases}$$

Determines if flow is choked

$$G_Eg_{l_i} := \phi_{v_E_i} \cdot \alpha \cdot A \cdot \sqrt{g \cdot \frac{P_o^2}{\text{gas_const} \cdot T_o}}$$

This calculates the leakage mass flow rate (lb/sec) according to Egli's method

Kearton and Keh Method

Kearton and Keh analyzed leakage flows through staggered labyrinth seals. Although the geometry differs from stepped seals, the literature suggests that leakage rates are similar to stepped seals with the same clearances and number of stages. Their method combines a theoretical analysis based on isentropic expansions through the seal throttlings with empirical data for flows past sharp edged throttlings. They use empirical data to estimate the point where the seal will choke.

$$P_{ncrit} := (.5631 \cdot n^{-.4487}) \cdot P_o$$

$$P_{ncrit-g} = 31.502 \text{ psi}$$

$$crit_ratio := .528$$

This calculates a value of P_n/P_o where the last throttling in the seal will be choked. Based on experimental data from Kearton and Keh, it allows a choked/not choked estimate to be made. Although this data was obtained from staggered seals rather than the TVA stepped type seal, this should be useful as a first estimate

For an "n" stage seal, this pressure ratio should cause choking

Choking Pressure ratio for air

$$P_{2nd_last_crit} := \frac{P_{ncrit}}{crit_ratio}$$

$$P_{2nd_last} := \frac{P_o}{.9372 \cdot n^{.4485}}$$

From Kearton and Keh

$$C1 := .67$$

$$C2_i := -.6017 \cdot \left(\frac{P_{n_i}}{P_{2nd_last_crit}} \right)^2 + .1647 \cdot \frac{P_{n_i}}{P_{2nd_last_crit}} + .826$$

Formula is from a curve fit of empirical data from Keartyon and Keh

$$f := 0.84$$

The below formula calculates the leakage mass flow rate based on Kearton and Keh's work

$$G_{Kearton_i} := \begin{cases} A \sqrt{15} \cdot \frac{\text{ft}}{\sqrt{\text{sec}^2}} (C2)_i \cdot \frac{P_{2nd_last}}{\sqrt{\text{gas_const} \cdot T_o}} & \text{if } P_{n_i} < P_{ncrit} & \text{If flow is choked} \\ A \cdot C1 \cdot \frac{\sqrt{f \cdot g \cdot [(P_o)^2 - (P_{n_i})^2]}}{n \cdot \text{gas_const} \cdot T_o} & \text{otherwise} & \text{If flow is not choked} \end{cases}$$

Miyake and Duh Empirical Equation

Below is a prototype calculation for stepped labyrinth seal leakage using the methods outlined in Miyake and Duh's paper :

DTC := 1·in Distance to contact for the TVA model

p := 1.315·in Pitch (distance between knives) for TVA model

From equation (9) in the paper, leakage, $G = A \cdot \phi v \cdot \sqrt{g \cdot \frac{P_o}{v_0}}$

Miyake and Duh propose an empirical formula for calculating ϕv :

$$\phi v = 117 \cdot \sqrt{\left[\text{Re}^{\frac{-0.8}{1.2}} - 6.14 \cdot \text{Re}^{\frac{-1.1}{1.2}} \right]} \cdot \left(\frac{\text{DTC}}{p} \right)^3 \cdot n^{-0.55}$$

This is valid only between $.42 \leq \frac{\text{DTC}}{p} \leq .87$ $\frac{\text{DTC}}{p} = 0.76$

$$\text{Re} = p \cdot \sqrt{\frac{dP}{\rho}} \quad \text{so,} \quad \text{Re}_i := p \cdot \sqrt{\frac{(P_o - P_{n_i}) \cdot g}{\rho n_i}}$$

$$\text{Re}_1 := \text{Re}_2$$

$$\text{Re}_{1000} := \text{Re}_{999}$$

This corrects the Re values at extremes of pressure ratio to prevent singularities in the function

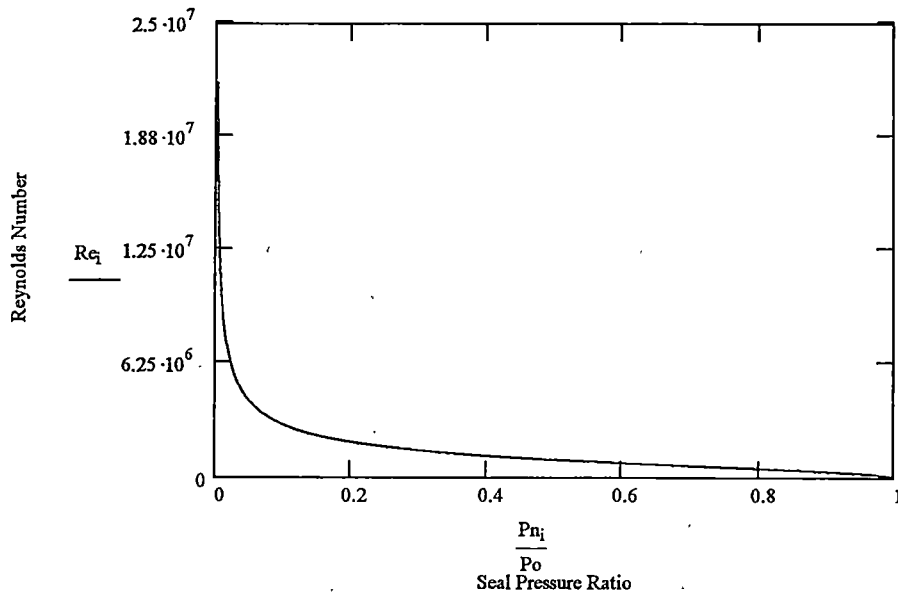


Figure B-1 - Seal Reynolds Number

$$\phi v_{M_i} := 117 \cdot \sqrt{\left(Re_i \right)^{-0.8} - 6.14 \cdot \left(Re_i \right)^{-1.2} \cdot \left(\frac{DTC}{p} \right)^3} \cdot n^{-0.55}$$

$$G_{Miyake} := A \cdot \phi v_{M_i} \cdot \sqrt{g \frac{P_o}{v_o}}$$

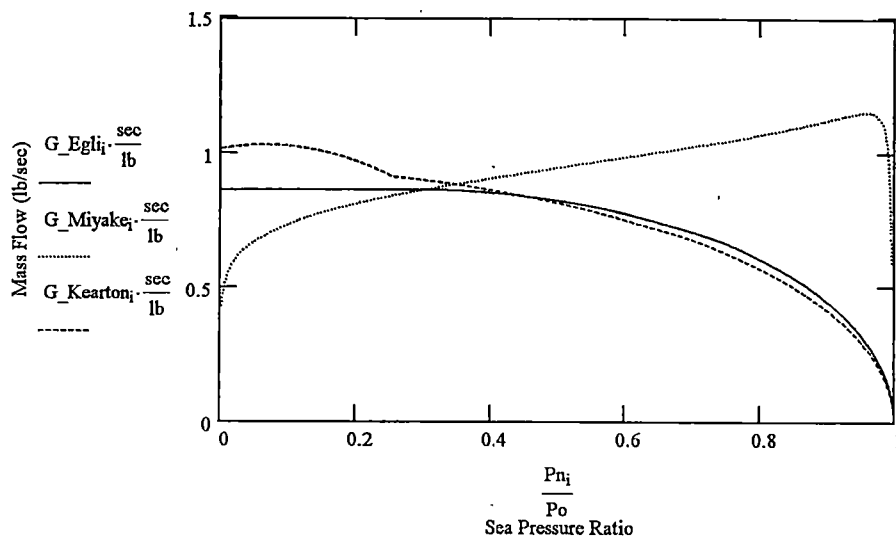


Figure B-2 - Predicted Mass Flow

The Miyake formula does not appear to provide a reasonably shaped function for this geometry, ie the curve shows decreasing flow with decreasing pressure ratio. The Miyake paper shows results over only a very limited range of Reynolds number, ie $.8E5 < Re < 1.95E5$ while in the seal model application the value of Re varies from:

$$Re_1 = 2.176 \times 10^7 \quad \text{to} \quad Re_{1000} = 3.082 \times 10^4$$

If we limit the range of Reynolds numbers to approximately those tested by Miyake, ie

$$Re_{992} = 8.748 \times 10^4$$

$$Re_{962} = 1.936 \times 10^5$$

And define a new index variable as such $j := 962..992$

We see that within the range of Reynolds numbers examined, the function takes a more reasonable shape and can be compared to the Egli and Kearton and Keh methods although it predicts significantly greater leakage.

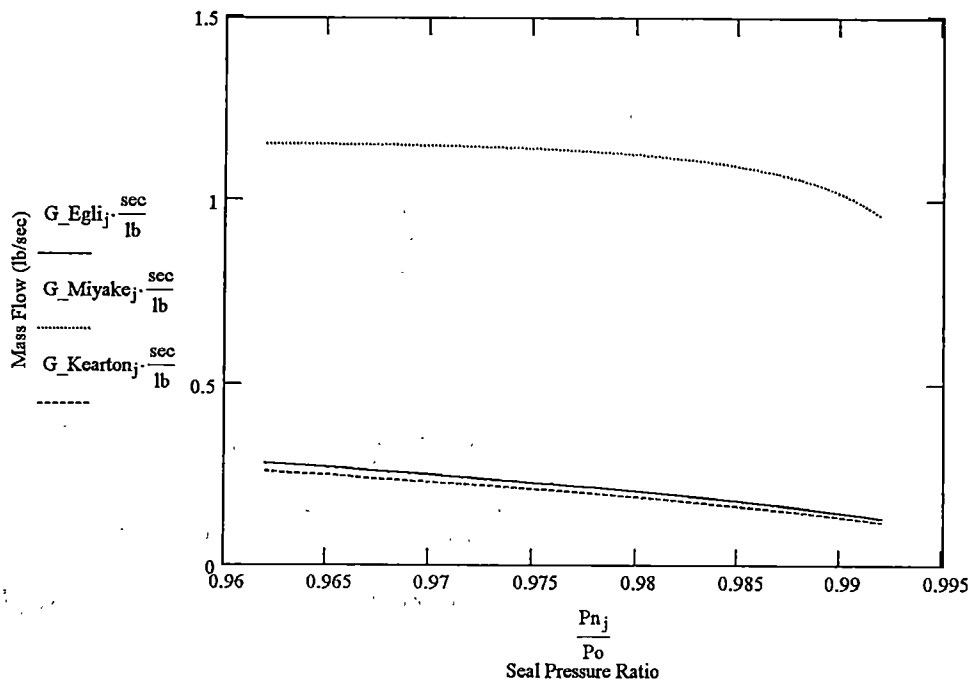


Figure B-3 - Predicted Mass Flow (lb/s)

Ideal Nozzle Flow Through A Single Clearance

Calculate Isentropic mass flow through one clearance area - to be used to non-dimensionalize results.

$A_{model} := 4\text{-in} \cdot 1.638\text{-in}$ total test section area

$$m_{isen_i} := A \cdot \sqrt{g \cdot P_o \cdot \rho_o} \cdot \sqrt{\frac{\frac{2 \cdot k}{k-1} \cdot \left(\frac{P_{n_i}}{P_o}\right)^{\frac{2}{k}} \cdot \left[1 - \left(\frac{P_{n_i}}{P_o}\right)^{\frac{k-1}{k}}\right]}{1 - \left(\frac{P_{n_i}}{P_o}\right)^{\frac{2}{k}} \cdot \left(\frac{A}{A_{model}}\right)^2}}$$

To calculate choked flow,

$i := 2..1000$

$mass_i := \begin{cases} \max(m_{isen}) & \text{if } m_{isen_i} < \max(m_{isen}) \wedge m_{isen_i} - m_{isen_{i-1}} > 0 \\ m_{isen_i} & \text{otherwise} \end{cases}$

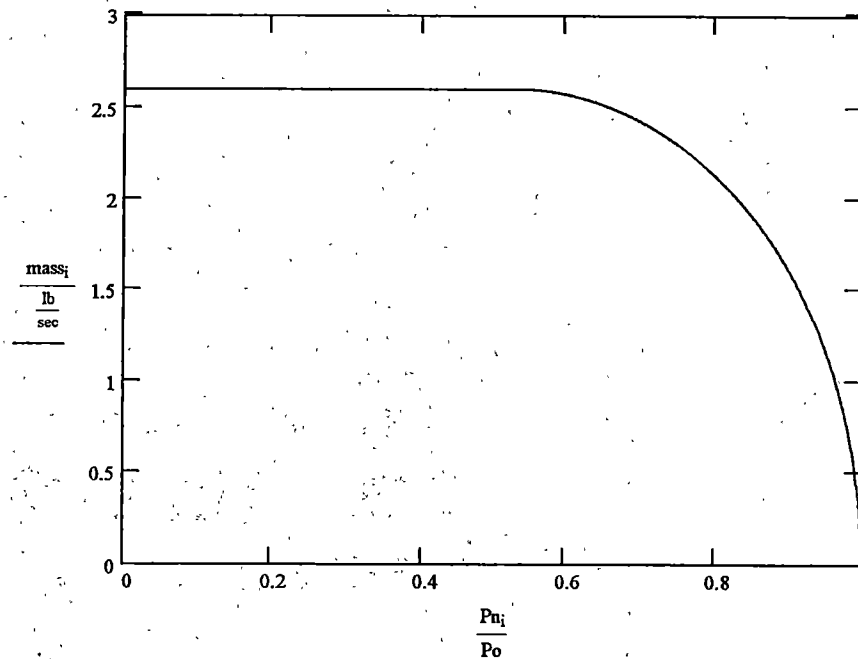


Figure B-4 - Ideal Flow (Single Orifice)

VITA

Michael Andrew Michaud was born on 18 December 1963 in Halifax, Nova Scotia. He attended various schools in the Canadian provinces of Ontario and Quebec, ultimately graduating with a High School Diploma from Laval Catholic High School in Laval, Quebec in May, 1981. In 1985 he joined the Canadian Armed Forces as an Airframe Technician, and, following initial trades training, returned to beautiful Nova Scotia, Canada to serve as an aircraft technician with Canada's venerable fleet of CH124 Sea King helicopters at Canadian Forces Base (CFB) Shearwater. Selected for commissioning in 1990, then-Cpl Michaud attended Saint Mary's University and the Technical University of Nova Scotia in Halifax where he earned a Bachelor of Mechanical Engineering Degree in 1994. Following classification training as an Aerospace Engineering Officer in 1995/96 at CFB Borden, Ontario, he returned to Shearwater, Nova Scotia where he served in 12 Air Maintenance Squadron as the Mechanical Support Officer (1996-97) and the Aircraft Servicing Officer at 406 Helicopter Operational Training Squadron (1998-1999).

In 1999, Captain Michaud was selected to attend UTSI under the auspices of the Canadian Forces Post-Graduate Training Program, and graduated in 2001 with an MS degree in Aerospace Engineering. He is planning to enroll in the PhD program at UTSI, and hopes to complete the requirements for his PhD in Aerospace Engineering in 2005.

Captain Michaud is a registered Professional Engineer (PEng) with the Association of Professional Engineers of Nova Scotia. He is a member of the American Helicopter Society (AHS) and the American Society of Mechanical Engineers (ASME). Captain Michaud has had the pleasure of serving as the Chairperson of the Canadian Aeronautics and Space Institute (CASI) Flight Operations Section (1997/98) and the CASI Atlantic Region Branch President (1998/99).